

Doctorate Dissertation (Censored)

博士論文 (要約)

CRISPR-mediated establishment and analyses of novel
Drosophila cell lines for investigation of the piRNA pathway

(piRNA 機構の解明を目指したゲノム編集による

新規細胞株の樹立とその解析)

A Dissertation Submitted for Degree of Doctor of Philosophy

December 2018

平成 30 年 12 月博士 (理学) 申請

Department of Biological Sciences, Graduate School of
Science,

The University of Tokyo

東京大学大学院理学系研究科生物科学専攻

Tetsutaro Sumiyoshi

住吉 哲太郎

Contetnts

Abstract	4
Abbreviations	9
Introduction	12
<i>RNA silencing</i>	13
<i>Argonaute family of proteins and small RNAs</i>	14
<i>piRNAs: functions and biogenesis</i>	15
<i>Cultured cells for piRNA biogenesis study</i>	16
<i>Biogenesis of piRNAs in Drosophila ovarian somatic cells</i>	17
<i>Biogenesis of piRNAs in Drosophila ovarian germ cells</i>	18
<i>Biogenesis of phased piRNAs and Zucchini</i>	20
<i>TUDOR domain-containing piRNA factors</i>	21
<i>Vasa, a principal nuage component</i>	22
<i>The CRISPR-Cas9 system</i>	23
<i>l(3)mbt, a repressor of piRNA biogenesis factors</i>	24
<i>The aim of this study</i>	25
<i>Summery of this study</i>	27
Materials and Methods	29
<i>Fly stock, cell culture and RNAi</i>	30
<i>Plasmid constructs and OSCs transfection</i>	31
<i>Establishment of cultured Δmbt-OSCs and Zuc-FLAG OSC</i>	33
<i>Immunoprecipitation</i>	35

<i>Western blotting</i>	36
<i>Immunofluorescence</i>	38
<i>qRT-PCR</i>	39
<i>Visualization of small RNAs</i>	39
<i>Preparation of total RNA libraries and bioinformatic analysis</i>	40
<i>Preparation of small RNA libraries and bioinformatic analysis</i>	41
<i>Co-Immunoprecipitation and Silver Stain</i>	42
<i>RNA UV-crosslink for iCLIP and bioinformatic analysis</i>	42
Results	45
1.1 <i>Loss of <i>l(3)mbt</i> leads to ectopic expression of ping-pong factors in OSCs</i>	46
1.2 <i>Loss of <i>l(3)mbt</i> activates the ping-pong pathway in OSCs</i>	48
1.3 <i>Appearance of perinuclear granules resembling nuage in Δ<i>mbt</i>-OSCs</i>	51
1.4 <i>The ping-pong pathway in Δ<i>mbt</i>-OSCs</i>	52
1.5 <i>Loss of <i>l(3)mbt</i> fails to activate the ping-pong pathway in S2 cells</i>	53
1.6 <i>Piwi-piRNAs in Δ<i>mbt</i>-OSCs</i>	53
2.1 <i>Vasa function in nuage-like granules formation</i>	55
2.2 <i>Vasa function in the ping-pong pathway</i>	58

3.1 <i>Establishment of Zuc-FLAG OSCs using the CRISPR/Cas9 system</i>	60
Discussion	61
1.1 <i>Δmbt-OSC accommodates the ping-pong pathway</i>	62
1.2 <i>Transcription of the piRNA factors driven by I(3)mbt</i>	62
1.3 <i>Dual-strand clusters expression in Δmbt-OSCs</i>	63
1.4 <i>AGO3 piRNA derivation in Δmbt-OSCs</i>	63
1.5 <i>sDMA modification regulator of AGO3</i>	64
1.6 <i>piRNA factors localization</i>	65
2.1 <i>Factor(s) transferring Vasa to nuage</i>	65
2.2 <i>The role of Vasa helicase activity in localization</i>	66
2.3 <i>The beginning of RNAs unwinding by Vasa in the ping-pong pathway</i>	66
3.1 <i>Zuc-FLAG OSC, a helpful for Zuc study cell line</i>	67
3.2 <i>The method of genome editing using the CRISPR/Cas9 system</i> ...67	
References	69
Figures	82
Tables	128
Acknowledgement	131

Abstract

piRNA 機構の解明を目指したゲノム編集による新規細胞株の樹立とその解析

住吉哲太郎

○背景・目的

PIWI-interacting RNA (piRNA) は、主に生殖組織特異的な小分子 RNA である。piRNA は PIWI タンパク質と複合体を形成し、トランスポゾンの発現を抑制することによって、生殖細胞ゲノムをトランスポゾンによる DNA 損傷から保護する。生殖細胞の保護に重要な piRNA は、有性生殖を行う多くの生物で保存されている。piRNA の欠損は、生殖組織の発生・分化を阻害し、その個体は不妊となる。近年は、piRNA が幹細胞やがん細胞などの体細胞においてもごく微量ながら発現することが明らかとなった。piRNA は、体細胞においても、トランスポゾンの抑制などによって、細胞の状態の維持に働くと考えられている。

piRNA の生合成の分子メカニズムは十分な理解が進んでいない。その一因として、piRNA が多量に発現する生殖系列由来の培養細胞株は極めて少なく、生化学的解析が困難であることが挙げられる。ping-pong 機構は哺乳類から無脊椎動物まで生物間に広く保存されている重要な piRNA 生合成機構の一つである。しかし、ping-pong 機構を有し、容易な生化学的解析が可能な細胞株は存在しないため、ping-pong 機構の分子メカニズム解明は進んでいなかった。ping-pong 経路に必須の RNA ヘリカーゼタンパク質である Vasa は、ping-pong 経路の場である核膜近傍に局在する細胞質顆粒、nuage の形成において中核を担い、Vasa を足場にして他の ping-pong 関連因子が集積すると示唆されている。nuage 形成に関連して、マウスの Vasa ホモログを用いた先行研究より、N 末に存在する disorder 領域が相分離を起こし、顆粒を形成すると報告がある。さらに、Vasa は ping-pong 機構に使用する RNA を nuage で受け取る役割があり、受け渡しを契機に nuage を形成すると示唆する報告もある。また、Vasa が標的 RNA をどのように認識し、乖離するか、その詳細な分子機構も不明である。

本研究では、ショウジョウバエ卵巢由来の培養細胞株、OSC の遺伝子編集により ping-pong 経路の機能する細胞株を樹立した。また、その細胞株を用いて、nuage 形成及び、ping-pong 経路における Vasa の生化学的な機能解析を行った。

○方法・結果・考察

1) Δmbt -OSC の樹立

ping-pong 機構を有するショウジョウバエ由来細胞株の樹立にあたり、先行研究で報告された *l(3)mbt* 遺伝子に着目した。*l(3)mbt* は転写抑制因子であり、その変異体は脳腫瘍を誘発する。*l(3)mbt* 変異体の脳腫瘍で発現上昇する遺伝子の解析から、複数の生殖細胞特異的遺伝子が異所的に発現すること、またそれらには ping-pong 機構の主要因子が多く含まれることが示された。よって体細胞株の *l(3)mbt* を欠失させれば、ping-pong 機構に関与する因子

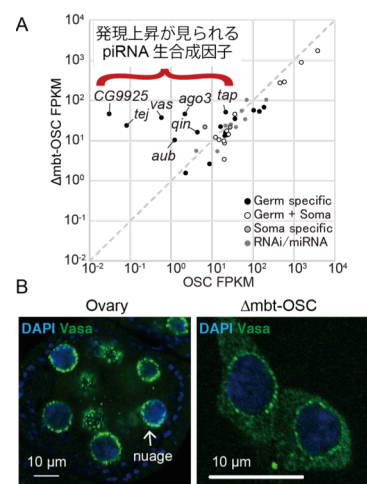


図 1 *l(3)mbt* の欠失は体細胞 OSC に生殖細胞様の性質をもたらす (A) Δmbt -OSC における、トランスクリプトーム解析。 (B) 生殖細胞(Ovary)と Δmbt -OSC の Vasa 免疫染色。緑色が Vasa であり、核周辺の緑色の顆粒が nuage である(白矢印)。

が発現し、体細胞株が ping-pong 機構を獲得するのではないかと着想した。そこで CRISPR/Cas9 システムによるゲノム編集を用いて、ショウジョウバエ卵巣体細胞由来培養細胞株 OSC の I(3)mbt を恒常的に欠失した株の確立を試みた。OSC を用いたゲノム編集は前例がなかったため、OSC に適した条件の検討を行った。その結果 50 株から 2 株程度、新規細胞株 Δ mbt-OSC を樹立することに成功した。 Δ mbt-OSC を用いたトランスクリプトーム解析等の結果より、 Δ mbt-OSC では Aub や AGO3、Vasa などの ping-pong 機構に必要な因子の発現が見られた (図 1A)。 Δ mbt-OSC は ping-pong 機構が生じる場である nuage を有した (図 1B)。さらに、piRNA のシーケンス解析を行うと、 Δ mbt-OSC の piRNA には、ping-pong 機構特異的な特徴がみられた。また、ping-pong 機構に必須の因子を発現抑制したところ、ping-pong 機構に依存する piRNA が失われた。これらの結果から、私は Δ mbt-OSC が ping-pong 機構を獲得したことを示した。私が樹立した Δ mbt-OSC は ping-pong 機構を有する唯一のショウジョウバエ由来細胞株である。

2) Vasa の分子動態の解明

樹立した Δ mbt-OSC では、nuage の形成が確認された。そこで、nuage が形成される機構を解析した。Vasa は ping-pong 機構に必要なヘリカーゼタンパク質であり、ping-pong 機構の場である nuage 形成においても必須の因子である。そこで、Vasa の nuage 形成に必要な条件の解析を行った。まず OSC やショウジョウバエ体細胞由来の細胞株である S2 細胞に Vasa を強制発現させた。すると S2 細胞では nuage が形成されなかったが、OSC には nuage 様の顆粒が観察された。 Δ mbt-OSC においても、強制発現した Vasa は nuage を形成するが、安定した nuage の観察が困難であった。そこで強制発現を行う系では、S2 細胞と OSC を用いることにした。Vasa は N 末端側に disorder 領域をもち、C 末側にヘリカーゼ活性をもつ部分が存在する。Vasa のヒトホモログである DDX4 は、N 末端側の領域が顆粒形成において重要であるという先行研究がある。Vasa の nuage 形成に必要な部分を検証するために、Vasa を disorder 領域と helicase 領域の二つに分割した欠損変異体を作製した。2 つの Vasa を強制発現させたところ、意外にも helicase 領域のみが nuage 様の顆粒を形成した(図 2A)。先行研究と異なる結果が得られたが、この結果は Vasa においては、ヘリカーゼ活性に関する部分が nuage 様顆粒の形成に重要であることを示唆した。Vasa は、RNA と結合し、ATP を加水分解して、二本鎖になった RNA を乖離させる。そこで、Vasa の点変異体 RNA 結合変異体(R528A)を作成し、nuage 形成を観察した。その結果、R528A 変異体において nuage 様の顆粒が見られなかった(図 2A)。この結果は、Vasa が nuage

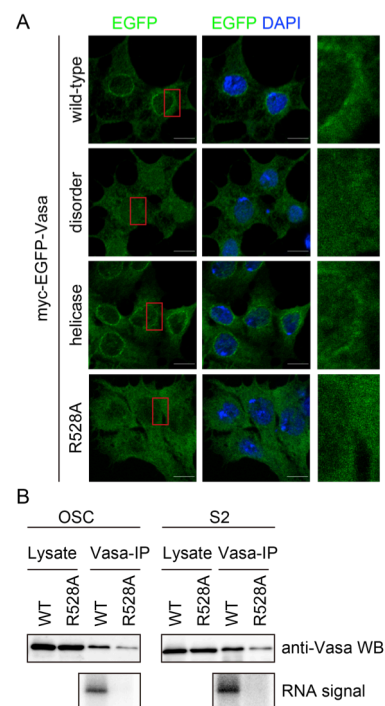


図 2 Vasa の nuage 形成アッセイ(A) Vasa 変異体の局在。右端の図は、左端の赤枠拡大図を示す。disorder が disorder 領域を、helicase が helicase 領域を、R528A が R528A 変異体を示す。(B) RNA 結合アッセイ。2 段目の RNA signal が RI ラベルされた RNA シグナルを示す。

は、RNA と結合し、ATP を加水分解して、二本鎖になった RNA を乖離させる。そこで、Vasa の点変異体 RNA 結合変異体(R528A)を作成し、nuage 形成を観察した。その結果、R528A 変異体において nuage 様の顆粒が見られなかった(図 2A)。この結果は、Vasa が nuage

を形成するには、Vasa の RNA 結合能が必要であると示唆する。しかし、顆粒を形成する OSC 細胞と顆粒を形成しない S2 細胞において、UV クロスリンクを用いた Vasa の RNA 結合アッセイを行ったところ、いずれの細胞株においても、RNA 結合シグナルが観察された(図 2B)。Vasa が nuage 様の顆粒を形成するには、RNA に結合するだけでなく、他の要素も必要であると考えられる。Δmbt-OSC において RNA 存在、非存在下で Vasa 結合タンパク質を比較したところ、いくつか結合量が異なるタンパク質がみられた。CG7194 は、MS 解析によって RNA 非存在下で、Vasa との結合が著しく低下する因子である。しかし、CG7194 の発現減少は Vasa の局在に影響を与えなかった。したがって、CG7194 とは異なる未知因子が要求されることが考えられる。

Vasa 結合 RNA は、UV クロスリンクによって取得することが可能である。そこで、Δmbt-OSC を用いて、iCLIP 法による Vasa 結合 RNA の同定を試みた。iCLIP 法は結合する RNA の配列だけでなく、タンパク質の RNA 結合位置を明らかにすることが可能な方法である。次世代シーケンサーを用いた解析の結果、iCLIP 法で得られた Vasa 結合位置と PIWI タンパク質に結合する piRNA の 5'末端の位置は、定まった距離にあることが判明した。この結果は、Vasa が piRNA と PIWI タンパク質の複合体から標的 RNA を乖離するときには決まった位置で行う可能性を示した。

3) ゲノム編集による Zuc 検出可能細胞株の樹立

Zucchini(Zuc)は、piRNA 生合成に必須のエンドヌクレアーゼである。Zuc は N 末領域のトランスメンブレン領域によりミトコンドリアに局在し、ミトコンドリア上で piRNA 前駆体を切断することで piRNA の成熟に寄与する。近年、Zuc の結晶構造解析など様々な研究が進められてきたが、これまで Zuc に対する良質なモノクローナル抗体が作製できず、強制発現を用いた系により解析が進められてきた。そのため、未だ Zuc が piRNA 成熟化に関わる詳細な分子メカニズムの解明には至っていない。そこで、Δmbt-OSC 樹立時の条件を活用し、ゲノム上の Zuc 領域に、アフィニティータグとして頻りに用いられる FLAG タグ配列を挿入することで、既存の抗体による内在 Zuc の検出を目指すという着想に至った。FLAG タグ配列の挿入にあたり、ゲノムの欠損を誘導する際に働く Ku70 を発現抑制し、Cas9 の導入時に相同配列をもつ FLAG タグ配列を導入した。その結果、Zuc 遺伝子へ FLAG タグ配列の挿入した細胞株、Zuc-FLAG OSC の樹立に成功した。Zuc-FLAG OSC では、FLAG 抗体を用いた内在 Zuc の検出が可能である(図 3)。Zuc に FLAG 配列が挿入されたことに起因する未成熟 piRNA の増加や、ターゲット遺伝子の脱抑制は見られなかった。強制発現を用いた系では、発現量の調整が難しく免疫染色による局在の確認が困難であったが、Zuc-FLAG OSC を用いた FLAG 抗体による免疫染色により局在の観察がより容易になった。今後、Zuc-FLAG OSC を用いた Zuc の piRNA 生合成における詳細な作用機序の解析が期待できる。

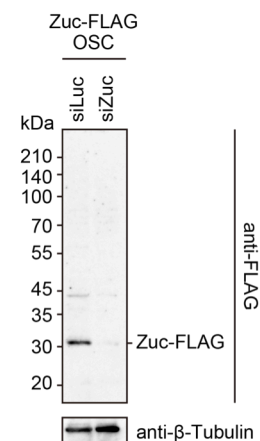


図 3 Zuc-FLAG OSC を用いたウェスタンブロットング。siZuc による Zuc のノックダウンにより anti-FLAG 抗体で検出されるシグナルが消失することから見られるバンドが内在 Zuc に起因するものとわかる。

Abstract

In *Drosophila* germ cells, piRNAs are amplified through a PIWI-slicer-dependent, feed-forward loop termed the ping-pong pathway, yielding secondary piRNAs. However, the detailed mechanism remains poorly understood, largely because an *ex vivo* model system amenable to biochemical analyses has not been available. Here, I show that CRISPR-mediated loss-of-function of *lethal (3) malignant brain tumor* [*l(3)mbt*] leads to ectopic activation of the germ-specific ping-pong pathway in ovarian somatic cells. Perinuclear granules resembling nuage, the ping-pong center, appeared following *l(3)mbt* mutation. I refer to the *l(3)mbt* depleted cell line as Δ mbt-OSC. Using Δ mbt-OSC, I further investigated Vasa functions in the nuage formation and also in the ping-pong pathway and found that the RNA-binding activity of Vasa is required for nuage formation, although other unknown factor(s) might also be required. I also found by performing Vasa iCLIP that Vasa bound to AGO3-bound piRNA intermediates in the ping-pong pathway. The activation of the ping-pong machinery in cultured cells is (and will be) very helpful to facilitate the elucidation of the mechanism underlying secondary piRNA biogenesis in *Drosophila*. It is known that the CRISPR-mediated genome editing can also be used to insert sequences in the genome. Using the method, I established another OSC line that endogenously expresses Zucchini (Zuc)-FLAG. The cells line will be useful to elucidate the precise function of Zuc the piRNA biogenesis. Thus, both cell lines established by the CRISPR-mediated genome editing will be useful to elucidate the molecular mechanisms of the piRNA pathways.

Abbreviations

Abbreviations

Abbreviation	Full name
Ago	Argonaute
APS	Ammonium Peroxodisulfate
Armi	Armitage
Aub	Aubergine
BSA	Bovine Serum Albumin
CLIP	Cross-linking immunoprecipitation
Cuff	Cutoff
Del	Deadlock
DNA	Deoxyribonucleic acid
DSB	double-stranded breaks
DTT	Dithiothreitol
EGFP	Enhanced Green Fluorescent Protein
endo-siRNA	Endogenous siRNA
FBS	Fetal Bovine Serum
flam	flamenco
GST	Glutathione S-transferase
HDR	Homology-directed repair
HRP	Horseradish peroxidase
iCLIP	Individual-nucleotide resolution CLIP
IgG	Immunoglobulin G
indel	insertion or deletion
IP	Immunoprecipitation
kb	Kilobase
kDa	Kilodalton
Krimp	Krimper
I(3)mbt	lethal (3) malignant brain tumor
Luc	Luciferase
Mael	Maelstrom
MBTS	I(3)mbt-signature
miRNA	Micro RNA
mRNA	Messenger RNA

n.i.	Non immune
ncRNA	Non-coding RNA
NHEJ	non-homologous end joining
NLS	Nuclear Localization Signal
NP40	Nonidet P-40
nt	Nucleotide
OSC	Ovarian Somatic Cell
PAGE	Polyacrylamide gel electrophoresis
Panx	Panoramix
piRNA	PIWI-interacting RNA
Piwi	P-element induced wimpy testis
RDC	Rhino-Deadlock-Cutoff
Rhi	Rhino
RISC	RNA-induced silencing complex
RNA	Ribonucleic acid
RNAi	RNA interference
S2	Schneider 2
sDMA	symmetrical dimethyl arginine
SDS	Sodium lauryl sulfate
SDS-PAGE	(refer to each abbreviation)
sgRNA	single-guide RNA
Shu	Shutdown
siRNA	Small-interference RNA
SoYb	Sister of Yb
Spn-E	Spindle-E
T-PBS	Phosphate buffered saline with Tween20
Tris	Tris (hydroxymethyl) aminomethane
TEMED	Tetramethylethylenediamine
tj	traffic jam
Vret	Vreteno
Yb	Female sterile (1) Yb
Zuc	Zucchini

Introduction

Introduction

RNA silencing

RNA silencing is gene repression mechanisms mediated by small RNAs of ~20-30 nucleotides and Argonaute proteins. The small RNAs and Argonaute proteins associate with each other in a stoichiometric manner and form the RNA-induced silencing complexes (RISCs), the engine of RNA silencing (Figure 1) (Yamashiro and Siomi 2018).

The RISCs recognize targets to silence depending on the complementarities between RNA transcripts transcribed from the target genes and small RNAs which are contained in the RISCs. Although the RISC assembly occurs in the cytoplasm, some RISCs are translocated to the nucleus where they repress the target genes by recruiting DNA- and/or histone-modifying enzymes to the gene loci for inducing local heterochromatinization, resulting in inhibition of the transcription (Siomi et al. 2011). This is categorized as transcriptional gene silencing (Figure 1). Other RISCs stay in the cytoplasm even after the complex assembly and repress target genes by cleaving the RNA transcripts. This is categorized as post-transcriptional gene silencing (Figure 1).

The subcellular localization of RISCs is determined by the nuclear localization signal (NLS) of Argonaute proteins: if the Argonaute protein has an NLS, the RISC is localized to the nucleus. If the Argonaute protein has no NLS, the RISC is localized to the cytoplasm. The RISCs are found in a variety of

species, starting from yeasts to humans. Thus, RNA silencing is highly conserved, very important mechanisms in living organisms.

Argonaute family of proteins and small RNAs

The numbers of members of the Argonaute family of proteins are different among species. For example, humans have eight members while *Drosophila* has five members (Figure 2). The Argonaute proteins are divided into two subfamilies; AGO subfamily and PIWI subfamily. In *Drosophila* AGO1 and AGO2 belong to the AGO subfamily, and Piwi, Aub and AGO3 belong to the PIWI subfamily.

AGO subfamily proteins are ubiquitously expressed and bind one of two types of small RNAs, microRNAs (miRNA) and small interference RNAs (siRNAs). In contrast, PIWI subfamily proteins are germline-specific and bind only PIWI-interacting RNAs (piRNAs). The target genes of AGO and PIWI subfamily proteins are different from each other: in general, AGO proteins silence protein-coding genes while Piwi proteins silence transposons (Siomi et al. 2011). In *Drosophila*, miRNAs and siRNAs are normally ~21-22 nucleotide-long whereas piRNAs are slightly longer; ~24-30 nucleotide-long.

Endogenous siRNAs (endo-siRNAs) in *Drosophila* are known to repress transposons upon binding with AGO2 (Kawamura et al. 2008). The endo-siRNAs are ubiquitously expressed. However, because of PIWI subfamily proteins are expressed in the germlines, lack of endo-siRNAs does not leads to

the derepression of transposons in the germlines (Vagin et al. 2006).

piRNAs: functions and biogenesis

Like PIWI proteins, piRNAs are mainly expressed in the germline. The germlines gonads (ovaries and testes) in *Drosophila* are composed of two types of cells, germ cells and somatic cells surrounding the germ cells (Figure 3A). The piRNA-mediated transposon silencing occurs in both cell types. In somatic cells, only Piwi is expressed, and Piwi is imported to the nucleus after piRNA loading where it represses transposon at the transcription level. On the other hand, in germ cells not only Piwi but also Aub and AGO3 are expressed (Figure 3B). Piwi in germ cells represses transposons similarly to Piwi in somatic cells. In contrast, germ cell-specific PIWI proteins, Aub and AGO3, remain to be in the cytoplasm even after piRISC formation (Iwasaki et al. 2015). Aub and AGO3 are localized at the perinuclear granules known as nuage and repress transposons by cleaving their mRNAs there (Brennecke et al. 2007; Gunawardane et al. 2007; Lim et al. 2007; Nishida et al. 2007; Huang et al. 2014).

piRNAs arise mainly from RNA transcripts transcribed from the piRNA clusters, intergenic regions rich in fragmented transposons. The piRNA clusters are often located in pericentromeric and telomeric heterochromatin regions and are transcribed by RNA Polymerase II (Sienski et al. 2012). The piRNA clusters in *Drosophila* are divided into two types: uni-strand and dual-strand piRNA clusters (Figure 4A). Uni-strand clusters are transcribed in one fixed direction.

flamenco (*flam*) is a representative uni-strand cluster, containing various transposons fragments, such as *mdg1*, *gypsy*, *idefix*, and *ZAM*. The uni-strand clusters are used mainly in the ovarian somatic cells, while the dual-strand clusters are transcribed in both directions and are mainly used in germ cells (Brennecke et al. 2007; Malone et al. 2009). *42AB* is a representative dual-strand cluster. The dual-strand clusters regions are accumulated by H3K9me3. Rhino, a HP1 homlog, interacts with H3K9me3 on the loci, and then Deadlock, and Cutoff interact with Rhino (Figure 4B; Mohn et al. 2014; Klattenhoff et al. 2009; Pane et al. 2011; Le Thomas et al. 2014; Yu et al. 2015a). These factors are necessary for initiating the transcription of the dual-strand clusters. piRNAs arise from not only piRNA clusters but also 3' UTR of some protein-coding genes, a representative of which is *traffic jam* (*tj*) (Figure 4A). These piRNAs derived from protein-coding genes are called genic piRNAs. The functions of genic piRNAs remain unclear.

Cultured cells for piRNA biogenesis study

To elucidate the molecular mechanisms of the piRNA pathway biochemically, cultured cell lines that consist of cells isolated from the gonad are useful. Such cell line, fGS/OSS, was previously established from *Drosophila* ovary (Niki et al. 2006). The cell line contained Vasa-positive germ cells and Vasa-negative somatic cells. Later, another cell line, OSC (ovarian somatic cell) was established from fGS/OSS (Saito et al. 2009). In OSC, Vasa is not

expressed, because it does not contain germ cells. Around the same time, a piRNA study using BmN4 cell was reported (Kawaoka et al. 2009). BmN4 cells were derived from the ovaries of *Bombyx mori* and accommodate the ping-pong pathway. However, BmN4 cells are lepidopteran-origin and express only two PIWI members, Siwi (*Bombyx mori* homolog of Aub) and AGO3, but lack a homolog of *Drosophila* Piwi. Nowadays these cell lines OSC and BmN4 cell are extensively used in the investigation to understand the molecular mechanisms underlying the piRNA pathways, particularly piRNA biogenesis (Figure 5). To reveal the precise mechanism of the *Drosophila* ping-pong pathway, an *ex vivo* *Drosophila* model system amenable to biochemical analyses is required but such cell lines have not been available.

Biogenesis of piRNAs in Drosophila ovarian somatic cells

In ovarian somatic cells, piRNA precursors arising from the piRNA clusters accumulate at specific granules termed Flam bodies and/or Dot COM and are then processed at Yb bodies (Saito et al. 2010; Dennis et al. 2013; Murota et al. 2014). In parallel, Yb centralizes multiple primary piRNA factors to Yb bodies, including Armitage (Armi), Vreteno (Vret), Sister of Yb (SoYb), and Shutdown (Shu) (Figure 3B, 6; Iwasaki et al. 2015). Yb and Armi containing a DEAD-box RNA helicase domain bind to RNAs. These binding RNAs studies revealed that Yb binds to piRNA precursors and Armi binds to piRNA intermediates (Saito et al. 2010; Murota et al. 2014). Yb and Armi perform

important role in piRNA processing at Yb bodies, however their detailed functions are studying. Also, detailed functions of other Yb bodies' components, Vret, SoYb, and Shu, at Yb bodies remain unknown. The piRNA intermediates are processed by not only Yb bodies' factors but also mitochondrial factors such as Zucchini (Zuc) (see ***Biogenesis of phased piRNAs and Zucchini***). The matured piRNAs and Piwi are imported to the nucleus, and repress transposon working with nuclear factors such as Maelstrom (Mael) and GTSF1. Mael localizes to cytoplasm and is required for piRNA biogenesis in germ cells, however in somatic cells, Mael localizes to nucleus and is little effect to piRNA biogenesis, while lack of Mael lead to transposon activation (Lim AK et al. 2007; Saito et al. 2010; Sienski et al. 2012; Ohtani et al. 2013). The detailed functions of Mael in both cells remain unclear. GTSF1 interacts with Piwi and Panoramix (Panx) in nucleus (Dönertas D et al. 2013; Ohtani et al. 2013; Sienski et al. 2015; Yu et al. 2015b). The complex is required for Piwi-dependent histone methylation and repression of transposon transcription.

Biogenesis of piRNAs in Drosophila ovarian germ cells

Drosophila germ cells express Aub, AGO3 and Piwi (Saito et al. 2006; Nishida et al. 2007; Gunawardane et al. 2007; Brennecke et al. 2007). Using *Drosophila* germ tissues and BmN4, the mechanisms of ping-pong pathway are revealing. Of those, Aub and Piwi, but not AGO3, are loaded with primary piRNAs derived from the piRNA clusters (Figure 7; Malone et al. 2009; Li et al.

2009). Piwi-piRISCs are then transported to the nucleus, where they repress transposons transcriptionally. In contrast, Aub-piRISCs remain to be in the cytoplasm, and repress transposons by cleaving their mRNAs in a slicer-dependent manner. The Aub cleavage on the targets occurs at the position across from nucleotides 10 and 11 of the piRNAs. This reaction gives rise to two RNA pieces, namely 5' and 3' cleavage products. The 3' product that was released from the Aub complex by RNA helicase Vasa, a piRNA biogenesis factor, is loaded onto AGO3 (Xiol et al. 2014; Nishida et al. 2015). Then, this RNA is further processed at the 3' end by endonuclease Zuc and becomes mature piRNA (see ***Biogenesis of phased piRNAs and Zucchini***). AGO3-piRISC then cleaves its target RNAs and the 3' products are processed into Aub-bound piRNAs after being loaded onto nascent Aub. Because of these unique reactions, Aub-piRNAs and AGO3-piRNAs overlap through ten nucleotides from their 5' ends, and Aub-piRNAs have 1st U bias while AGO3-piRNAs have 10th A bias. Also, Aub-piRNAs are mostly antisense to transposon mRNAs, while Ago3-piRNAs are rich in sense piRNAs. These traits of Aub and AGO3-bound piRNAs are collectively called the ping-pong signatures. The slicer-dependent feed-forward loop mechanism is termed the ping-pong pathway, yielding a substantial amount of secondary piRNAs (Gunawardane et al. 2007; Brennecke et al. 2007). The ping-pong pathway is occurred at nuage, because secondary piRNA biogenesis factors are localized to nuage (Figure 3B).

Biogenesis of phased piRNAs and Zucchini

Yb bodies and nuage are surrounded by mitochondria (Murota et al. 2014). This unique spatial arrangement in the cytoplasm enables mitochondrial factors such as Zuc to process the piRNA intermediates into mature piRNAs (Nishimasu et al. 2012; Ipsaro et al. 2012). Zuc containing mitochondrial transmembrane region at the N-terminal region locates on the surface of mitochondria (Nishimasu et al. 2012; Ipsaro et al. 2012). In the primary and the ping-pong pathway, the 3' ends of Piwi- and Aub-piRNAs are decided mainly by Zuc cleavage. Recently, the Zuc dependent piRNA biogenesis was reported (Figure 8; Mohn et al. 2015; Han et al. 2015). Newly produced 5' ends by the Zuc cleavage are bound with Piwi/Aub and cleaved once again at the 3' ends by Zuc, producing Piwi bound piRNA termed phased piRNA. However, the detailed mechanism of this pathway remains elusive.

Piwi- and Aub- piRNAs *in vivo* have a strong 1st U bias. The phased piRNA biogenesis suggests that 5' end of piRNAs are decided by Zuc cleavage, which suggests that 1st U bias of Piwi- and Aub- piRNAs depend on Zuc cleavage. However Zuc have little nucleotide bias for RNA cleavage (Nishimasu et al. 2012). The mechanism of determination of 1st U bias of piRNAs remains unclear. These previous Zuc study were mainly confirmed by Zuc over-expression in *Drosophila* cells *in vivo* or *E.coli in vitro*, because anti-Zuc antibodies are not available. Thus the endogenous Zuc detectable system has the potential to reveal these questions.

TUDOR domain-containing piRNA factors

Many piRNA biogenesis factors, such as Yb, Armi, Vret, Tud, Krimper (Krimp), Qin and Spindle-E (Spn-E) contain TUDOR domain. They play important role in processing piRNAs. PIWI proteins contain arginine-glycine-rich regions at N-terminal regions, which are symmetrically dimethylated by PRMT5 (Kirino et al. 2009; Nishida et al. 2009). The symmetrical dimethyl arginine (sDMA) modification in PIWI proteins is required for interaction with Tudor, a TUDOR domain containing protein. Tudor is required for development and piRNA factors localization (Boswell and Mahowald 1985; Arkov et al. 2006). On the other hand, Krimp interacts with non-sDMA AGO3 (Olivieri et al. 2012; Sato et al. 2015). Krimp promotes its binding AGO3's sDMA modification and AGO3 localization to nuage (Figure 9; Olivieri et al. 2012; Sato et al. 2015). These activities are required for Aub-dependent piRNA loading to AGO3 (Olivieri et al. 2012; Sato et al. 2015). In germ cells Krimp localizes to nuage, although in somatic cells Krimp forms granules termed Krimp bodies. The role of Krimp bodies remains elusive. Qin represses Aub-Aub heterotypic ping-pong and prevents the cleavage products of Aub from becoming Piwi-bound piRNAs (Wang et al. 2015). Spn-E interacts with Qin, Aub and Ago3, and localizes to nuage (Gunawardane et al. 2007; Lim et al. 2007; Andress et al. 2016). The molecular function of Spn-E in piRNA biogenesis remains unclear.

Vasa, a principal nuage component

Vasa, a DEAD-box RNA helicase, is essential for development (Hay et al. 1988; Lasko and Ashburner, 1988). In the ping-pong pathway, Vasa is required for moving piRNA intermediate from Aub to AGO3 (Xiol et al. 2014; Nishida et al. 2015), however the detailed mechanisms of releasing RNA such as the position where Vasa starts to unwind RNA remain unclear. Also, Vasa has activity to receive the dual-strand cluster transcript RNAs exported by UAP56 to use the ping-pong pathway in cytoplasm (Zhang et al. 2012). Furthermore, Vasa is required for nuage formation where the ping-pong pathway activated. In ovarian germ cells, loss of Vasa leads to nuage collapse (Nagao et al. 2011), thus Vasa is the first to localize to the nuage (Findley et al. 2003). Vasa localization is followed by piRNA factors: Spn-E, Aub, Ago3, and Mael (Nagao et al. 2011).

Vasa contains a disorder region at the N-terminal region and RNA helicase domain DEAD box at the C-terminal region. The previous report in mice showed that the N-terminal disorder region plays a key role in the formation of granules *in vitro* (Figure 10; Nott et al. 2015). Also, the crystal structure of Vasa was solved, which showed the responsible amino acids for exhibiting the Vasa activities (Figure 10; Sengoku et al. 2006). Vasa have dual-strand RNA helicase activity hydrolyzing ATP. A single mutation in DEAD-box (E400Q mutant in *Drosophila*) leads to lose Vasa ATP-hydrolyzing activity (Sengoku et al. 2006; Xiol et al. 2014; Nishida et al. 2015). E400Q mutant Vasa has RNA-binding

activity, however because of losing ATP-hydrolyzing activity, the Vasa fail to release RNAs (Sengoku et al. 2006; Xiol et al. 2014; Nishida et al. 2015). The ATPase mutant Vasa in BmN4 cells forms large nuage and the Vasa in ovarian germ cells forms granules that are removed from the perinuclear location (Xiol et al. 2014). Also, Arg528 in Vasa is widely conserved within the DEAD-box family and interact with the RNAs. Indeed, R528A mutant Vasa fail to bind RNAs (Sengoku et al. 2006).

These previous Vasa study were mainly confirmed by BmN4 cell or germ tissues *in vivo* or *E.coli in vitro*, because *Drosophila* stable Vasa-positive cell lines such as germ cells are not available.

The CRISPR-Cas9 system

The CRISPR-Cas9 system was originated from a bacterial defense system against invading viral pathogens, based on the principles of Watson–Crick base pairing, and provides a platform for high-efficiency genome engineering in many organisms (Jinek et al. 2012; Cong et al. 2013; Mali et al. 2013; Jinek et al. 2013; Ran et al. 2013). The Cas9 nuclease from the type II CRISPR system of *Streptococcus pyogenes* has recently been used successfully for genome editing in a variety of experimental models (Hsu et al. 2014; Sander et al. 2014). Cas9 nuclease can be guided to its DNA target by a single-guide RNA (sgRNA), which is a synthetic fusion between trans-activating crRNA and the CRISPR RNA (Jinek et al. 2012; Cong et al. 2013; Mali et al.

2013). Cas9 and its associated sgRNA introduce double-stranded break (DSB) at specific locations in the genome, which are repaired via non-homologous end joining (NHEJ) or homologous recombination (Figure 11, Bibikova et al. 2002). NHEJ repair results in insertion or deletion (indel) mutations at the cleavage site, which can cause loss of function if the DSB occurs in a coding gene. Homology-directed repair (HDR) is an alternative DNA repair pathway with a typically lower frequency than NHEJ, which can generate precise genetic modification at a target site in the presence of the corresponding homologous template (Figure 11, Capecchi et al. 1989). HDR can also be used to generate cell lines expressing an endogenous protein tagged with a small peptide, such as enhanced green fluorescent protein (EGFP) or FLAG.

l(3)mbt, a repressor of piRNA biogenesis factors

In *Drosophila*, mutations in *lethal (3) malignant brain tumor* [*l(3)mbt*] generate malignant brain tumors with metastatic potential (Gateff et al. 1993; Janic et al. 2010) due to derepression of *l(3)mbt*-signature (MBTS) genes (Figure 12; Janic et al. 2010). Multiple MBTS genes encode proteins with germline functions, and mutations in these genes, for instance, *piwi*, rescue the brain tumor phenotype (Janic et al. 2010). MBTS genes with germline functions include ping-pong factors, such as *aub* and *vasa* (Janic et al. 2010). A few small RNAs in *l(3)mbt* mutant brain tumors were annotated as piRNAs (Janic et al. 2010). These findings of *l(3)mbt* mutations resulting in ectopic acquisition of

germline traits in the brain prompted us to examine if depletion of *l(3)mbt* in OSC initiates the ping-pong pathway and causes the accumulation of secondary piRNAs in cell.

L(3)mbt is a member of LINT complex containing Lint-1, CoREST and L(3)mbt, and the complex represses various gene expression (Figure 12, Meier et al. 2012). Also, L(3)mbt is included in dREAM complex, the complex is related to amplify DNA (Lewis et al. 2004). Previous reports showed L(3)mbt functions, however detailed expression regulate manner remains poorly understood.

The aim of this study

Previously an ex vivo *Drosophila* model system amenable to biochemical analyses of the ping-pong pathway has not been available, so previous ping-pong pathway analyses were performed using *Drosophila* germ tissues and cultured BmN4 cells. However, *Drosophila* germ tissues take a lot of time because flies are grown. Also BmN4 cells lack a homolog of *Drosophila* Piwi, and *Bombyx mori* genome data is deficient. These problems make difficult to analyze the ping-pong pathway. For instance, in the ping-pong pathway, that AGO3 cleavage products are unwound by unknown factor(s) is expected, however the problems make the analysis of the factor difficult. For further ping-pong pathway analysis, helpful cell line was desired. Fortunately, recent study showed loss of *l(3)mbt* led to ectopic expression of ping-pong factors in *Drosophila* brain cells (Janic et al. 2010). Moreover genome editing using the

CRISPR/Cas9 system was developed (Jinek et al. 2012; Cong et al. 2013; Mali et al. 2013; Jinek et al. 2013; Ran et al. 2013). I will perform *I(3)mbt* genome editing using the CRISPR/Cas9 system to produce new system to analyze the ping-pong pathway.

Vasa, a DEAD-box RNA helicase, is essential for germline development and also for piRNA biogenesis (Hay et al. 1988; Lasko and Ashburner, 1988), particularly in the ping-pong pathway (Xiol et al. 2014; Nishida et al. 2015). Genetic and biochemical analysis to reveal the molecular functions in the pathways have extensively been performed. However, molecular mechanisms underlying Vasa-driven nuage formation and how Vasa releases cleaved RNAs from the Aub-piRISC remain poorly understood.

Vasa has been shown to be the top in hierarchy in the formation of nuage where the ping-pong pathway amplifies piRNAs (Findley et al. 2003). Vasa contains a disorder region and DEAD-box helicase domain (Sengoku et al. 2006). A previous report in mice showed that the disorder region of Vasa plays a key role in the granules formation (Nott et al. 2015). Other reports showed that Vasa has the activity to receive the transcript RNAs exported by UAP56 and suggested that this action might be important in the nuage assembly (Zhang et al. 2012). However, the tight link between the RNA-binding activity of Vasa and nuage formation has not been investigated. Also, the crystal structure of Vasa was solved (Sengoku et al. 2006), which revealed the responsible amino acids for exhibiting the Vasa's RNA-binding and ATP-hydrolyzing activities. To

understand how Vasa triggers nuage formation, I will produce various deletion and point mutants of Vasa that are defective in ATP hydrolysis and RNA binding and perform various biochemical experiments by expressing them in OSCs. Furthermore, I will perform co-immunoprecipitation experiments to find new factors that possibly play roles along with Vasa in the nuage formation. To understand how molecularly Vasa releases cleaved RNAs from Aub-piRISC, I will perform UV crosslinking and immunoprecipitation (iCLIP) and bioinformatic analyses.

Zuc is an endonuclease necessary for piRNA phasing (Mohn et al. 2015; Han et al. 2015). However, the precise mechanism of how Zuc produces phase piRNAs remains elusive. Production of anti-Zuc antibodies has been extensively attempted in the laboratory; however, such antibodies are still unavailable. I thought that it would be very helpful if I produce cell line(s) that express FLAG-tagged Zuc endogenously. I will use the CRISPR/Cas 9 system to produce such cell lines and perform biochemical analyses using the cells to analyze the Zuc function in phased piRNA biogenesis.

Summary of this study

In this study I showed as follows:

- 1) Δ mbt-OSC, *I(3)mbt* depleted cell line, was established using the CRISPR/Cas9 genome editing.

- 2) In Δ mbt-OSC, ping-pong piRNA factors were upregulated and ping-pong factors are activated.
- 3) Vasa, one of ping-pong factors, RNA binding activity was required for forming the nuage-like granules, although other unknown factor(s) also might be required.
- 4) Vasa binds to AGO3-bound piRNA intermediates in the ping-pong pathway, and the binding position is around 5' end of AGO3-piRNAs.
- 5) Zuc-FLAG OSC, endogenous Zuc detectable OSC, was established inserting FLAG-tag sequence in Zuc genome region.
- 6) The knock-in/out method for OSC is available.

Δ mbt-OSC is a unique ping-pong pathway activated cell line derived from *Drosophila*. Also Zuc-FLAG OSC is unique cell line to be able to detect endogenous Zuc by common antibody, anti-FLAG antibody. These cell lines are contributing to detailed piRNA biogenesis mechanism studies. Vasa detailed activity in the ping-pong pathway actually is gradually revealing.

Materials and Methods

Materials and Methods

Fly stock, cell culture and RNAi

Oregon-R was maintained at 25°C. Δ mbt-OSCs and OSCs were grown at 26°C in culture medium prepared from Shields and Sang M3 Insect Medium (Sigma) supplemented with 0.6 mg/mL glutathione, 10% FBS, 10 mU/mL insulin, and 10% fly extract (Saito et al. 2009). Cell proliferation was monitored with the xCELLigence RTCA SP system (ACEA). For the RNAi of OSCs trypsinized cells (3×10^6 cells) were suspended in 100 μ L of Solution V of the Cell Line Nucleofector Kit V (Amaxa Biosystems) together with 200 pmol of siRNA duplex. Transfection was conducted in electroporation cuvettes using a Nucleofector device 2b (Amaxa Biosystems). For the RNAi of Δ mbt-OSCs and OSCs trypsinized cells (3×10^6 cells) were suspended in 20 μ L of Solution SF of the Cell Line Nucleofector Kit SF (Amaxa Biosystems) together with 200–400 pmol of siRNA duplex. Transfection was conducted in a 96-well electroporation plate using a Nucleofector device 96-well Shuttle (Amaxa Biosystems). The transfected cells were transferred to fresh OSC medium and incubated at 26°C for 2–4 days for further experiments. S2 cells were grown at 26°C in Schneider's Insect medium (Sigma) supplemented with 10% fetal calf serum (Gibco), 50 μ g/mL streptomycin, and 50 μ g/mL penicillin (Sato et al. 2010). For RNAi in S2 cells, *l(3)mbt* cDNA was amplified by RT-PCR from OSCs total RNA using gene-specific primers. It should be noted that the 5' end of each primer

contained the T7 RNA polymerase promoter sequence. PCR products were purified using the FastGene Gel/PCR Extraction Kit (NIPPON Genetics) according to the manufacturer's instructions. Purified PCR products were used to produce dsRNAs using a T7-Scribe Standard RNA IVT Kit (CELLSCRIPT). The resultant RNAs were purified according to the manufacturer's instructions, heated for 5 min at 95°C, and then left to cool to room temperature. Then, 5×10^6 cells were suspended with 5 µg of dsRNA and incubated for 4 days at 26°C. The siRNAs and PCR primers used in this study are summarized in Table 1.

Plasmid constructs and OSCs transfection

Myc-Aub, Myc-AGO3, Myc-Vasa and Myc-EGFP vectors were kindly gifted by Dr Kaoru Sato (Sato et al. 2015, Sumiyoshi et al 2016). To construct Myc-EGFP-Vasa containing a full-length *vasa*, a disorder *vasa* or a helicase *vasa* expressing plasmid, each Vasa were amplified from Myc-Vasa by RT-PCR and a vector containing the actin 5C promoter, myc and EGFP was amplified from the Myc-EGFP vector, and then each Vasa was assembled into amplified EGFP containing vector using NEBuilder HiFi DNA Assembly Master Mix (NEB). To construct Myc-EGFP-Vasa containing mutant *vasa*, D400Q Vasa and R528A Vasa, expressing plasmid were constructed from the Myc-EGFP-full-length-Vasa vector by inverted PCR using PrimeSTAR Max (Clontech). To construct FLAG-Nup358 plasmid first inverted PCR were performed to produce pAc-FLAG construct from pAcM. Then, full-length *nup358*, was amplified by

RT-PCR. RT-PCR products and pAc-FLAG construct were assembled using NEBuilder HiFi DNA Assembly Master Mix (NEB). To construct Myc-EGFP-CG7194 a *cg7194a* cDNA was amplified from RT-PCR, then cDNA was assembled into amplified EGFP containing vector using NEBuilder HiFi DNA Assembly Master Mix (NEB). The primers I used are shown Table 1.

SgRNA-expressing for *I(3)mbt* knockout vectors were produced by inverse PCR using pU6-BbsI-chiRNA (Addgene, 45946). Primers are summarized in Table 1. For constructing sgRNA expression vector for *zuc* genome editing, a single-stranded DNA oligo encoding the sgRNA is annealed with its complementary oligo, and then resultant double-stranded DNA oligo is phosphorylated and ligated with BbsI-digested pU6-BbsI-chiRNA (Addgene 45946). To construct the linearized donor vector containing *zuc* genome homology right/left arms sequence and FLAG-tag sequence, *zuc* genome homology arms were amplified by genome PCR using Q5 High-Fidelity DNA Polymerase (NEB) from OSCs, and then the arms and 3×FLAG:T2A:EGFP fragment were assembled into a linearized pUC19 vector using NEBuilder HiFi DNA Assembly Master Mix (NEB).

OSCs and Δ mbt-OSCs transfection were performed using Xfect Transfection Reagent (Clontech) or ScreenFect A (Wako) following the manufacturer's protocol. When Xfect Transfection Reagent were used, 200 μ L of Xfect Transfection Reagent Buffer (Clontech) containing 4 μ g of plasmid(s) and 1.2 μ L of Xfect Polymer (Clontech) were added to 3×10^6 OSCs in 3.5 cm dish. 2

days later the cells were used each experiments. When ScreenFect A were used, 240 μL of kit attached Dilution Buffer (Wako) containing 1 μg of plasmid(s) and 6 μL of kit attached Transfection Reagent (Wako) were added to 3×10^6 OSCs in 3.5 cm dish. 2 days later the cells were used each experiments.

Establishment of cultured Δmbt -OSC and Zuc-FLAG OSC

Gene knockout in OSC used the CRIPSR/Cas9 system and isolation of knockout OSC. 3×10^6 OSCs were transfected with 0.2 μg of a plasmid expressing both pBS-Hsp70-Cas9 (Addgene, 46294) and the blasticidin resistance gene, and 4 μg of two sgRNA-expressing plasmids (GM76 and E2) using Xfect Transfection Reagent (TaKaRa Clontech). After incubation for 24 h, blasticidin (Thermo Fisher Scientific Inc., R210-01) was added to the culture medium at 50 $\mu\text{g}/\text{mL}$. Next day, 5.0×10^3 cells were passaged in 3.5-cm dishes and allowed to grow in blasticidin-containing medium. During culturing, cells were washed with the medium to remove non-adherent dead cells. After 6–7 days of culture, 5.0×10^3 cells were passaged in 6-cm dishes and allowed to grow in blasticidin-containing medium. After further incubation for a few days, colonies were picked and passaged in single wells of 24-well plates. The next day, these colonies were suspended with a Tip Strainer (BEL-ART) and allowed to grow to confluence. To detect the genomic deletion, genomic DNA was extracted using QuickExtract DNA Extraction Solution (Epicenter) following the

manufacturer's protocol, and the genomic region flanking the CRISPR target site was amplified by PCR and then analyzed using MultiNa (Shimadzu).

Gene knockin in OSC used the CRISPR/Cas9 system and isolation of knockin OSC. 3×10^6 OSCs were transfected with 40 pmol ku70 siRNA using Nucleofector device 96-well Shuttle. After incubation for 24 h, the OSCs were transfected with 0.3 μg of a linearized donor vector which contains *zuc* genome homology arm sequence and FLAG-tag sequence, 0.3 μg of a plasmid expressing both pBS-Hsp70-Cas9 (Addgene, 46294) and the blasticidin resistance gene, and 4 μg of sgRNA-expressing plasmids using ScreenFect A (Wako). After incubation for 24 h, blasticidin (Thermo Fisher Scientific Inc., R210-01) was added to the culture medium at 50 $\mu\text{g}/\text{mL}$. Next day, 5.0×10^3 cells were passaged in 3.5-cm dishes and allowed to grow in blasticidin-containing medium. During culturing, cells were washed with the medium to remove non-adherent dead cells. After 6–7 days of culture, 5.0×10^3 cells were passaged in 6-cm dishes and allowed to grow in blasticidin-containing medium. After further incubation for a few days, colonies were picked and passaged in single wells of 24-well plates. The next day, these colonies were suspended with a Tip Strainer (BEL-ART) and allowed to grow to confluence. To detect the genomic deletion, genomic DNA was extracted using QuickExtract DNA Extraction Solution (Epicenter) following the manufacturer's protocol, and the genomic region flanking the CRISPR target site was amplified by PCR and

then analyzed using MultiNa (Shimadzu). Detailed protocols for knockout/in were described (Sumiyoshi et al. 2016; Ishizu et al. 2017).

Immunoprecipitation

The immunoprecipitation of Piwi and Aub complexes from Δ mbt-OSCs or OSCs were performed using anti-Piwi and anti-Aub antibodies in NP40 buffer (30mM Hepes-KOH (pH 7.3), 5mM DTT, 2mM Mg(OAc)₂, 0.1% NP-40, 150mM KOAc and protease inhibitor). Immunoprecipitation of AGO3 complexes were performed using an anti-AGO3 antibody (a kind gift from Dr. Dahua Chen, Chinese Academy of Sciences, China) in RIPA buffer (50mM Tris-HCl (pH8.0), 1mM DTT, 150 mM NaCl, 0.1% SDS, 1% Triton-X 100, 0.5% Na-deoxycolate, and protease inhibitor). The Co-immunoprecipitation of Vasa complexes from Δ mbt-OSC was performed using an anti-Vasa antibody in IP buffer (Figure 39: 30mM Hepes-KOH (pH 7.3), 5mM DTT, 2mM Mg(OAc)₂, 0.1% NP-40, 150mM KOAc, protease inhibitor, and 1 μ g RNase A (Roche) or 40units of RNasin Plus Ribonuclease Inhibitor (PROMEG, N2611)) (Figure 42: 30mM Hepes-KOH (pH 7.3), 5mM DTT, 1mM EDTA, 0.1% NP-40, 150mM KOAc and protease inhibitor).

OSCs, Δ mbt-OSCs or S2 cells were collected and washed once by PBS (Wako). Then discard PBS (Wako) and added IP buffer. The cells incubated on ice at 5 minutes, and then they were mixed by 25G FLOW MAX (NIPRO) five times and 30G Disposable needle (Dentronics) twice with syringe (TERUMO). The cells were centrifuged for 20 minutes at 15,000rpm, 4°C. The

supernatant was collected as lysate. Next, 50 μ L of DynabeadsTM protein G (Invitrogen) was washed by IP buffer twice. And then antibodies were added to IP buffer containing the beads and incubated for 20 minutes at room temperature. 20 minutes later, the beads were washed twice and mixed lysate, and then rotate 2 hours at 4 $^{\circ}$ C. 2 hours later, the lysate were discarded and the beads washed four times by IP buffer. When IP samples were used for western blotting analysis, 20 μ L of 2 \times Sample buffer (19% glycerol, 100mM Tris-HCl pH 6.8, 4% SDS, 2 \times 10⁻⁴ % Bromophenol Blue, 200mM DTT) were added to the beads and incubated for 5 minutes at 95 $^{\circ}$ C. When IP samples were used for Visualization of small RNAs, 200 μ L of NFW were added to the beads. When IP samples were used for iCLIP, 50 μ L of IP buffer were added to the beads. In each experiment, n.i. (mouse IgG) were used as a negative control.

Western blotting

Anti-Piwi, anti-Aub, anti-AGO3, anti-Krimp, anti-Spn-E, anti-Tud, anti-Vret, anti-Mael, anti-Armi, anti-GTSE1, anti-Yb, and anti-sDMA-AGO3 antibodies were kindly gifted by Dr Kaoru Sato and Kazumichi M. Nishida (Saito et al. 2006; Nishida et al. 2007; Gunawardane et al. 2007; Nishida et al. 2009; Saito et al. 2010; Sato et al. 2011; Nagao et al. 2011; Ohtani et al. 2014; Sato et al. 2015). The anti-Qin antibody was kindly gifted by Dr. Toshie Kai. The mouse monoclonal anti-Vasa antibody was raised specifically against the full-length protein and was purified from the culture supernatant of hybridoma cells under

standard procedures using Thiophilic-Superflow Resin (BD Biosciences). The anti- β Tub antibody was obtained from the Developmental Studies Hybridoma Bank. These antibodies were used at a dilution of 1:1,000. Anti-mouse IgG, HRP-linked antibody (MP Biomedicals, 55558), and anti-rabbit IgG, HRP-linked antibody (CST) were used at dilutions of 1:5,000 and 1:1,000, respectively.

The samples for Western blotting were produced from immunoprecipitation (see ***Immunoprecipitation***) samples or collected cells. The cells were collected by centrifuged at 1500rpm, room temperature for 5 minutes. The supernatant was discarded and cells were mixed with 2 \times Sample buffer and the cells were incubated at 95 $^{\circ}$ C for 5 minutes. 5 minutes later SDS-PAGE was performed. The SDS-PAGE gel contained running gel (30w/v % Acrylamide / Bis Mixed Solution (Wako), N, N, N', N'-Tetramethylenediamine (TEMED) (Wako), 10% Ammonium peroxodisulfate (APS) (Wako) and 1.5M Tris-HCl pH 8.8) and stacking gel (30w/v % Acrylamide / Bis Mixed Solution (Wako), N, N, N', N'-Tetramethylenediamine (TEMED) (Wako), 10% Ammonium peroxodisulfate (APS) (Wako) and 0.5M Tris-HCl pH 6.8). The electrophoresis was performed at 200V for 1 hour, and then the gel was transferred to the PVDF membrane (Merck Millipore) at 1 hour. 1 hour later, the membrane was soaked to 5% skim milk (Morinaga Milk Industry) in PBS-T (0.1% tween 20, 1L of PBS, 9L of distilled water in 10L scale) for 30 minutes. Next the primary antibody reaction was performed for 1 hour. 1 hour later, the membrane was washed three times by PBS-T, and then secondary antibody reaction was performed for

30 minutes. Then, the membrane was washed three times, and treated with Clarity™ Western ECL Substrate (BIORAD) and the signals were detected with ImageQuant LAS 4000 (GE Healthcare Life Sciences).

Immunofluorescence

To perform immunostaining of Δ mbt-OSCs, OSCs and S2 cells, the cells were spread onto MICRO COVER GLASS (MATSUNAMI). First, the cells were fixed using PBS (Wako) containing 4% formaldehyde (Wako) for 15 minutes. Then, the cells were permeabilized by PBS (Wako) containing 0.1% Triton™ X-100 (Sigma Aldrich) for 15 minutes. Next, the primary antibody reaction was performed using PBS containing antibodies for 1 hour. The anti-Myc (Sigma C3956), Anti-FLAG (Sigma F3165), Anti-Piwi, anti-Aub, and anti-Krimp, anti-AGO3, and anti-Yb antibodies were used at 1:500 as primary antibodies. The anti-Vasa antibody was used at 1:250 as primary antibodies. After primary antibody reaction, the cells were washed using PBS three times for 10 minutes each. Then, the secondary antibody reaction was performed using PBS containing antibodies for 30 minutes. Alexa Fluor488-conjugated anti-mouse IgG, Alexa Fluor546 conjugated anti-mouse IgG1, and Alexa Fluor488-conjugated anti-mouse IgG2a (Molecular Probes) were used as secondary antibodies. The cells were washed by PBS three times for 10 minutes each, and the cells were mounted in VECTASHIELD with DAPI (4',6-diamidino-2-phenylindole dihydrochloride) (Vector). All images were

collected using a Zeiss LSM510 laser scanning microscope (Carl Zeiss). Image processing and annotation were performed using Adobe Photoshop (Adobe), ZEN (Carl Zeiss), and ImageJ software (National Institute of Health).

qRT-PCR

Total RNAs were isolated using ISOGEN (Nippon Gene) according to the manufacturer's instructions. Total RNAs were treated with DNase to eliminate DNA contamination. Total RNA (1 µg) was annealed with an oligo-dT primer and reverse transcribed using a Transcriptor First strand cDNA Synthesis Kit (Roche) according to the manufacturer's instructions. The resulting cDNAs were amplified with StepOnePlus (Applied Biosystems) using SYBR Premix Ex Taq (TaKaRa). The primer sets used are shown in Table 1. The amplification efficiency of a qPCR reaction was calculated based on the slope of the standard curve. After confirming the amplification efficiency values (between 95% and 105%), relative steady-state RNA levels were determined from the threshold pathway for amplification.

Visualization of small RNAs

The 100 µL of immunoprecipitation (see ***Immunoprecipitation***) samples were purified by phenol-chloroform extraction and precipitated with ethanol. The RNA pellet diluted with 26 µL of NFW, and then 3µL of 10× Antarctic Phosphatase Buffer (NEB) and 1µL of Antarctic Phosphatase (NEB)

were added. The solution were incubated at 37°C for 30 minutes and then 65°C for 5 minutes. The dephosphorylated sample were purified by phenol-chloroform extraction and precipitated with ethanol. Then, The RNA pellet diluted with 25 μ L of NFW, and then 3 μ L of 10 \times T4 Polynucleotide Kinase Buffer (NEB), 1 μ L of T4 Polynucleotide Kinase (NEB) and 1 μ L of γ -³²P-ATP were added. The solution were incubated at 37°C for 1 hour. The radiolabeled RNAs were separated on a denaturing polyacrylamide gel (40(w/V)%-Acrylamide/Bis Mixed Solution (Nacalai), N, N, N', N'-Tetramethylethylenediamine (TEMED) (Wako), 10% Ammonium peroxodisulfate (APS) (Wako) 7M Urea and 1 \times TBE (50mM Tris, 50mM Boric acid, 2mM 2Na)). The signal was detected using a Typhoon FLA 9500 (GE Healthcare).

Preparation of total RNA libraries and bioinformatic analysis

rRNAs were removed from isolated total RNAs using a Ribo-Zero rRNA Removal Kit (Human/Mouse/Rat) (Illumina). Total mRNA libraries were prepared using a TruSeq Stranded mRNA HT Sample Prep Kit (Illumina) according to the manufacturer's instructions and sequenced using a HiSeq 2500 (Illumina). Paired-end sequence reads were split into forward and reverse reads and mapped separately on the *Drosophila* genome (Dm3, BDGP Release 5), and then annotated to *Drosophila* genes defined in the UCSC Genome Browser (FlyBase) using Cuffcompare. Differential expression analysis of mRNA-seq expression profile was performed using edgeR package in R. The lists of

differentially expressed genes ($p < 0.05$) were applied for functional annotation (gene ontology) analysis using DAVID. Paired-end sequence reads were also mapped to the transposon consensus sequences (Senti et al. 2015). To compare mRNA abundance between two libraries, FPKM (fragments per kilobases of exons per million mapped reads) normalization was performed.

Preparation of small RNA libraries and bioinformatic analysis

The 20–30 nt small RNA libraries were prepared manually based on the manufacturer's instructions of a TruSeq Small RNA Sample Prep Kit (Illumina), and then sequenced using MiSeq (Illumina). Reads perfectly mapped on the *Drosophila* genome (Dm3, BDGP Release 5) were used. Alignments overlapping with rRNAs, tRNAs and snoRNAs were removed, and then small RNAs in the range of 24–30 nt were selected. The mapped reads for immunoprecipitation libraries do not reflect actual cellular abundance and, therefore, a relative comparison of how piRNA sequences are loaded on to each PIWI protein were performed. For transposon analysis, all 24–30 nt small RNAs were mapped to *Drosophila* transposable element sequences obtained from the UCSC Genome Browser (RepeatMasker). Sense/antisense strand bias, sequence logo, and ping-pong signature on each transposon or all transposons were calculated from the mapping data. To calculate ping-pong Z_{10} scores, overlaps at position 1–9 and 11–25 nt were used as background. Phasing analysis was performed. The score for a 3'-to-5' distance was calculated by

Σ minimal (M_i , N_{i+x}); M_i is the number of upstream reads whose 3' ends are located at position i , and N_{i+x} is the number of downstream reads whose 5' ends are located at position $i+x$. To calculate the ping-pong Z_1 score, overlaps at position 0 and 2–50 nt were used as background.

Co-Immunoprecipitation and Silver Stain

The samples for Silver Stain were produced from co-immunoprecipitation (see ***Immunoprecipitation***). Then, the electrophoresis was performed at 250V for 2 hour using the SDS-PAGE gel. The gel was stained using SilverQuest™ Silver Staining Kit following the manufacturer' s protocol. (Life technologies, LC6070).

RNA UV-crosslink for iCLIP and bioinformatic analysis

100% confluent 10cm dish cells were prepared. Discard medium and the cells were washed using PBS (Wako). Then, performed 100 mJ/cm² of UV-crosslink(254 nm) to the cells for 2 times. Add 500 μ L of PBS (Wako) and collect the cells. The cells were centrifuged at 10,000 rpm 4°C for 2 minutes. Then, Immunoprecipitation was performed (see ***Immunoprecipitation***). Next 1 μ L of RNase T1 (Thermo Fisher Scientific, EN0541) added to IP samples and the samples were incubated for 15 minutes at room tempature. Then the samples washed by High salt wash buffer (20mM Hepes-KOH (pH 7.3), 1mM DTT, 500mM NaCl, 0.05% NP-40, and protease inhibitor) three times. The High

salt wash buffer was discarded and the samples were dephosphorylated using T4 PNK (NEB) following the manufacturer' s protocol. 30 minutes later of incubation, the samples were washed using T4 PNK buffer (NEB). Then, collected RNAs with protein were ligated with RI labeled 3' adapter using T4 RNA Ligase 2 (NEB) following the manufacturer' s protocol. SDS-PAGE was performed using NuPAGE® Novex Bis-Tris Gel (Thermo Fisher Scientific) following the manufacturer' s protocol. After SDS-PAGE, blotting was performed using XCell II™ Blot Module (Thermo Fisher Scientific) following the manufacturer' s protocol. RNA signal was observed by RI signal, so RNA signal observed area was taken from the blotted membrane. The taken membrane was put in new tube, and 90 µL of Nuclease-Free Water, 100 µL of 2×ProK buffer and 10 µL of ProK solution (Sigma-Aldrich) were added. The tube was incubated at 55°C for 30 minutes. Then, the RNAs were purified by phenol-chloroform extraction and precipitated with ethanol. Reverse transcription was performed to the RNAs using SuperScript III (Thermo Fisher Scientific). The cDNAs were cyclized using CirLigase II (Epicentre). At last the cyclized cDNAs were amplified by PCR using Q5 (NEB), then the products were read using MiSeq (Illumina). Reads mapped on the *Drosophila* genome (Dm6) were used. For analysis, I mapped all RNAs to *Drosophila* transposable element sequences obtained from the UCSC Genome Browser (RepeatMasker). Sense/antisense strand bias and annotation were analyzed from the mapping data. To show the distances each piRNAs I wrote new computing scripts, pipong and pipphase,

using Shell script. The pipong computes distances between two given nucleotide positions on opposite strands. The piphase computes distances between two given nucleotide positions on same strands. Using the iCLIP data and Aub and AGO3-piRNAs data piRNA's distances were calculated by pipong and piphase.

Results

Results

1.1 Loss of *l(3)mbt* leads to ectopic expression of ping-pong factors in OSCs

l(3)mbt is expressed in ovarian somatic cells (Gelbart and Emmert 2013). I therefore treated OSCs with *l(3)mbt* siRNA (Figure 13A). The mRNA expression of *l(3)mbt* was significantly decreased upon RNAi treatment (Figure 13B). In contrast, the expression of *ago3* and *vasa* were significantly up-regulated after *l(3)mbt* siRNA treatment, while changes in the expression of *piwi* mRNA were negligible (Figure 13B). Western blotting detected AGO3, Vasa and Aub in the *l(3)mbt*-depleted cell, while the levels of Piwi, Yb, Armi, and Krimp (Saito et al. 2009; Sato et al. 2015; Iwasaki et al. 2015) remained unchanged (Figure 13C).

I then set out to ablate *l(3)mbt* function by editing the *l(3)mbt* locus in OSCs using the CRISPR/Cas9 system. With reference to two mutant alleles, *l(3)mbt*^{GM76} and *l(3)mbt*^{E2} (Janic et al. 2010; Wismar et al. 1995; Yohn et al. 2003), sgRNAs were designed to target MBT domains (Figure 14A). The each two mutant has an effect on tumorigenesis in the fly brain (Janic et al. 2010; Wismar et al. 1995). A genomic PCR fragment amplified using a primer set flanking the sgRNA targeting sites was shortened after CRISPR/Cas9 treatment (Figure 14B). The fragment of sequencing revealed that a 558 nucleotide (nt) deletion occurred at the *l(3)mbt* locus (Figure 14A). Hereafter, I refer to the cell

line as Δmbt -OSC.

Deep-sequencing and comparison of mRNAs expression in Δmbt -OSCs and OSCs revealed that, in addition to *ago3* and *vasa*, other ping-pong factors such as *aub*, *qin*, *tapas*, and *tejas* (Specchia et al. 2010; Gangaraju et al. 2011; Handler et al. 2013; Czech et al. 2013; Patil et al. 2014; Iwasaki et al. 2015), were markedly up-regulated in Δmbt -OSCs (Figure 15). I with help from Hitomi Yamamoto, confirmed increased expression of Aub, AGO3, and Vasa in Δmbt -OSCs by western blotting (Figure 16). The expression of Piwi and other piRNA factors examined, such as Yb and Armi (Iwasaki et al. 2015), were nearly identical between the two cell lines (Figure 16), although a few factors showed slight changes in their mRNA levels (Figure 15). Germ-specific genes tended to be more sensitive to lack of *l(3)mbt* than germ + soma and soma-specific genes (Figure 15). The expression of Yb in Δmbt -OSCs suggests that CRISPR-mediated lack of *l(3)mbt* had little effect on the elimination of somatic traits from the mutant cells. Focusing on the expression of MBTS genes revealed that many, if not all, were up-regulated in Δmbt -OSCs (Figure 17). The highest up-regulation was observed for *ago3* (21.5-fold in Δmbt -OSC) among non-MBTS genes that are up-regulated by mutations in *mbt* genes other than MBTS (Janic et al. 2010). Results of transcriptome-wide analysis were summarized in Tables 2. I confirmed that loss of *l(3)mbt* had very little effect on the proliferation speed of OSC (Figure 18).

1.2 Loss of *l(3)mbt* activates the ping-pong pathway in OSCs

To compare Piwi-piRNA profile between Δmbt -OSCs and OSCs, Piwi was immunoprecipitated from both cell lines, and extracted RNAs were ^{32}P -labeled. piRNAs purified with similarly from both cell lines (Figure 19A). I then deep-sequenced Piwi-bound piRNAs in Δmbt -OSCs and compared the reads with those from OSCs (Figure 20-25; Saito et al. 2009). This revealed that both sets of piRNAs show strong 1st U bias and antisense orientation in transposon. The levels piRNAs from Δmbt -OSCs and OSCs mapped to each transposon were highly similar ($R^2 = 0.872$). piRNAs were mapped similarly to *flam*, a soma-specific single-strand piRNA cluster, *tj*, a genic piRNA source, and *mdg1*, a transposon (Brennecke et al. 2007; Saito et al. 2009; Malone et al. 2009; Robine et al. 2009). piRNAs mapped to *42AB*, a germ-specific dual-strand piRNA cluster (Brennecke et al. 2007; Malone et al. 2009), were not contained in Piwi-bound piRNAs. This was expected because a component of the Rhino-Deadlock-Cutoff (RDC) complex, *cutoff*, necessary for producing piRNAs from dual-strand piRNA clusters including *42AB* (Mohn et al. 2014; Zhang et al. 2014) was undetected in both OSC lines (Figure 15). Another component, *rhino*, whose expression was low in OSCs, was even lower in Δmbt -OSCs, while *deadlock* was expressed moderately in both OSCs and Δmbt -OSCs (Figure 15).

In Δmbt -OSCs, both Aub and AGO3 purified with piRNAs (Figure 19B). Deep-sequencing these small RNA populations clarified that Aub- and AGO3-bound piRNAs show distinct features (Figure 20-25). While Aub-piRNAs

showed significant 1st U bias and were mostly antisense in transposon, AGO3-piRNAs had strong 10th A bias and sense biases in transposon. The correlation was low between levels of Piwi- and AGO3-bound piRNAs mapped to each transposon ($R^2 = 0.149$), while the correlation was significantly high between levels of Piwi- and Aub-bound piRNAs ($R^2 = 0.874$). Both *flam*-piRNAs and *tj*-piRNAs were found with Aub-bound piRNAs, but not with AGO3-bound piRNAs. *42AB*-piRNAs were detected with neither Aub-bound piRNAs nor AGO3-bound piRNAs. Additionally, plotting the distribution of Aub- and AGO3-bound piRNAs to transposons, *DM412*, *DM297*, and *mdg1*, indicated the production of piRNAs from the same coordinate but in the opposite strand.

Previously reports showed that both Myc-Aub and Myc-AGO3 expressed in OSCs by transfection are loaded with primary piRNAs, including *flam*- and *tj*-piRNAs, which are normally loaded onto endogenous Piwi (Olivieri et al. 2012; Sato et al. 2015). The finding emphasized the compatibility of AGO3 with primary piRNA loading. However, AGO3 in Δ mbt-OSC avoided binding primary piRNAs; this was especially apparent when *tj*-piRNAs were compared (Figure 24; Sato et al. 2015). Krimp sequesters unloaded AGO3 to Krimp bodies and blocks AGO3-primary piRNA loading in OSC (Olivieri et al. 2012; Sato et al. 2015). Krimp is required for AGO3 function in ovary germ cells, *i.e.*, sDMA modification and secondary piRNA association (Sato et al. 2015; Webster et al. 2015); therefore, it would be expected that in Δ mbt-OSCs, AGO3 loading with secondary piRNAs might be under the control of Krimp. Indeed, I with help from

Dr. Kaoru Sato and Hitomi Yamamoto confirmed that AGO3 was sDMA-modified in Δ mbt-OSCs, as in ovaries, while Myc-AGO3 in OSCs was sDMA free (Figure 26). Yet, this does not exclude the possibility that unknown factors other than Krimp may also be involved in regulation of AGO3 sDMA-modification, along with Krimp.

If AGO3-bound piRNAs were produced via the ping-pong pathway in an Aub-slicer dependent manner, a ping-pong signal, *i.e.*, complementary overlap of 10 nt from the 5' ends, should be observed between Aub- and AGO3-bound piRNAs. piRNA production by such a ping-pong pathway was evaluated, and a significant ping-pong signature was observed between Aub- and AGO3-bound piRNAs (Figure 27). These results, along with mapping data shown in Figure 25, further support the idea that AGO3-bound piRNAs are Aub-slicer products via the ping-pong pathway.

Piwi-bound primary piRNAs in OSCs include a unique subset of piRNAs called phased piRNAs (Mohn et al. 2015; Han et al. 2015). Examination of piRNAs in Δ mbt-OSCs by focusing on this trait indicated that phased piRNAs with $d = 1$ (this means that two piRNAs can be mapped right next to each other on the same genomic strand without a nucleotide gap between them) are particularly abundant in Piwi-bound piRNAs ($Z_1 = 22.3$). The result was comparable to Piwi-bound piRNAs ($Z_1 = 16.8$) in OSCs (Figure 28A,B). Z_1 scores of Aub- and AGO3-bound piRNAs in OSCs were 11.5 and 2.9, respectively (Figure 28A), suggesting that AGO3-bound piRNAs mainly exclude

phased piRNAs (Mohn et al. 2015; Han et al. 2015). In contrast, piRNAs loaded onto Myc-AGO3 in OSCs (Sato et al. 2015) indicated a significant phasing pattern ($Z_1 = 12.9$) (Figure 28C). These results further support the idea that AGO3 in Δmbt -OSCs avoids binding of primary piRNAs, in contrast to Myc-AGO3 in OSCs.

1.3 Appearance of perinuclear granules resembling nuage in Δmbt -OSCs

Vasa, a germ-specific DEAD-box RNA helicase, plays an essential role in the ping-pong pathway by displacing cleaved RNAs from Aub-piRISCs (or its counterpart Siwi-piRISCs in silkworm) in an ATP hydrolysis-dependent manner (Xiol et al. 2014; Nishida et al. 2015). Aub, AGO3, and Vasa co-localize to nuage in *Drosophila* ovaries (Lim and Kai 2007; Malone et al. 2009; Iwasaki et al. 2015). Immunostaining in Δmbt -OSCs revealed that Aub and Vasa mostly coincide at perinuclear granules that look similar to nuage (Figure 29A). Myc-Aub exogenously expressed in OSCs was uniformly distributed in the cytosol and failed to form granules (Sato et al. 2015). Signals of Myc-Vasa in OSCs were slightly stronger at the perinuclear region in the cytoplasm (Figure 29B). Myc-Aub co-expressed with Vasa in OSCs was distributed almost evenly in the cytoplasm (Figure 29B). These results suggest that some factor(s) whose expression is up-regulated by loss of *l(3)mbt* function promotes Aub to form nuage-like granules with Vasa in Δmbt -OSCs.

I with help from Dr. Kaoru Sato and Hitomi Yamamoto confirmed

various piRNA factors localization using immunostaining. Aub and AGO3 also colocalized to nuage-like granules (Figure 29C). In OSCs Krimp sequesters unloaded AGO3 to Krimp bodies, which are generally present at a frequency of one per cell (Figure 30A; Olivieri et al. 2012; Sato et al. 2015). However, in Δmbt -OSCs, AGO3-positive granules were more numerous than one per cell and some could be superimposed with Aub-positive granules. This led us to examine the cellular localization of Krimp in Δmbt -OSCs and we found that co-localization of Krimp with AGO3 was apparent (Figure 30A), as occurs in ovaries where Krimp normally accumulates at nuage. Krimp bodies are present only when piRNA biogenesis is defective because of loss of piRNA factors such as *aub*. These results support the intriguing idea that Δmbt -OSCs likely recapitulate formation of the ping-pong center, nuage. We then examined the spatial relationship between Yb and Aub-positive granules in Δmbt -OSCs. Yb and Aub signals only occasionally coincide (Figure 30B), although the number of Yb bodies may be higher in Δmbt -OSCs compared with that in OSCs. These results suggest that primary and secondary piRNA biogenesis pathways may occur separately at Yb bodies and Aub-positive nuage-like granules, respectively, in Δmbt -OSCs.

1.4 The ping-pong pathway in Δmbt -OSCs

In *vasa* mutant ovaries, Aub does not accumulate in the nuage and is evenly distributed in the cytoplasm of nurse cells (Lim and Kai 2007; Malone et

al. 2009; Iwasaki et al. 2015). I with help from Dr. Kaoru Sato and Hitomi Yamamoto, therefore asked how lack of Vasa affects Aub localization in Δmbt -OSCs. Treatment of Δmbt -OSCs with *vasa* siRNA duplexes caused Aub to be largely dispersed in the cytoplasm (Figure 31A,B). I confirmed that under such conditions, AGO3 was loaded with far fewer piRNAs, although Aub-piRNA association remained largely unchanged (Figure 32). Thus, lack of Vasa disrupted the ping-pong pathway in Δmbt -OSCs, as expected. These results strongly suggest that ping-pong pathway was activated in Δmbt -OSCs.

1.5 Loss of *I(3)mbt* fails to activate the ping-pong pathway in S2 cells

The *Drosophila* cell line, S2, is of embryonic and somatic origin; therefore, piRNAs and PIWI proteins are under detection levels (Saito et al. 2006; Saito et al. 2009). I examined whether *I(3)mbt* knockdown has an effect on piRNA production in S2 cells. Upon RNAi, Aub was slightly up-regulated (Figure 33). However, very low levels of other piRNA factors, including Piwi, AGO3, and Vasa, were detected (Figure 33). Although *Drosophila* brains and S2 cell are both non-gonadal and somatic, the mechanism by which *I(3)mbt* controls downstream genes in these cells seems to be distinct.

1.6 Piwi-piRNAs in Δmbt -OSCs

Piwi was expressed in Δmbt -OSCs to a similar extent to that in OSCs (Figure 19A). In the two cell lines, Piwi-bound piRNAs were highly comparable in

all aspects including piRNA origins, and nucleotide and strand biases (Figure 19-27). Thus, Piwi in Δmbt -OSCs should be similarly functional in repressing transposon activities compared with Piwi in OSCs. Indeed, Piwi was localized to the nucleus in both Δmbt -OSCs and OSCs (Figure 34A). The levels of transposon mRNAs were not drastically changed by lack of *l(3)mbt* ($R^2 = 0.988$, Figure 34B), suggesting that *l(3)mbt* is dispensable in transposon silencing in ovarian somas.

第2章

本章については5年以内に雑誌等で刊行予定のため
非公開

3.1 Establishment of Zuc-FLAG OSCs using the CRISPR/Cas9 system

Zuc is an endonuclease necessary for piRNA phasing (Mohn et al. 2015; Han et al. 2015). However, the precise mechanism of how Zuc produces phase piRNAs remains elusive. Production of anti-Zuc antibodies has been extensively attempted in the laboratory; however, such antibodies are still unavailable. I thought that it would be very helpful if I produce cell line(s) that express FLAG-tagged Zuc endogenously. I therefore with help from Dr. Hirotugu Ishizu attempted to establish new endogenous Zuc detectable OSCs line by knocking in FLAG-tag sequence into *zuc* locus using the same method I used for the establishment of Δ mbt-OSCs. Previous reports have shown that knocking down of Ku70 led to increase of knock-in efficiency (Ma et al. 2014; Chu et al. 2015), so we knocked down Ku70 in OSCs and transfected donor DNA including FLAG-tag together with Cas9 and guide RNA. We succeeded in obtaining a few FLAG knock in cell lines. Hereafter, I refer to these cells as Zuc-FLAG OSCs (Figure 43A). Western blotting of Zuc-FLAG OSCs detected Zuc by anti-FLAG antibody (Figure 43B), and Immunofluorescence in Zuc-FLAG OSCs showed Zuc on the mitochondrion (Figure 43C). Insertion of FLAG-tag sequence into Zuc gene does not affect expression of *zuc*, transposon repression and piRNA maturation (Figure 44A,B). These results suggest that endogenous Zuc detectable OSCs, Zuc-FLAG OSCs, is very helpful for piRNA analysis.

Discussion

Discussion

1.1 Δmbt -OSC accommodates the ping-pong pathway

I established a new ping-pong pathway activated cell line by *l(3)mbt* depletion (Figure 45A). Previously an ex vivo *Drosophila* model system amenable to biochemical analysis of the ping-pong pathway has not been available, however the cell, Δmbt -OSC, is a unique ping-pong pathway activated cell line derived from *Drosophila* cell. Moreover gene expression and repression in Δmbt -OSC is easier than that in ovarian tissues. The cell is (and will be) very helpful to facilitate the elucidation of the mechanism underlying secondary piRNA biogenesis.

1.2 Transcription of the piRNA factors driven by *l(3)mbt*

Previous reports suggested that L(3)mbt is contained in LINT complex and dREAM complex, and L(3)mbt manage piRNA factors transcription in somatic cells (Meier et al. 2012; Lewis et al. 2004; Janic et al. 2010). Indeed, many ping-pong pathway factors are expressed by *l(3)mbt* depletion in OSCs (Figure 15,16). However effect of loss of *l(3)mbt* in S2 cells is partially (Figure 33). Why the difference is occurred? L(3)mbt plays key role in expression of piRNA factors, however detailed mechanisms of regulation such as how to recognize targets by L(3)mbt remains poorly understood. To solve these questions, I started to produce L(3)mbt antibody. I produced L(3)mbt antigen

containing Glutathione S-transferase (GST). The purified antigen was injected to mice. In that time Hitomi Yamamoto was also interested in L(3)mbt function. She took over my L(3)mbt study and produced the anti-L(3)mbt antibody. She has already performed analysis such as co-IP and ChIP-seq (data will be shown someday by her). I hope that she will reveal detailed mechanisms of regulation of piRNA factors by L(3)mbt.

1.3 Dual-strand clusters expression in Δ mbt-OSCs

In Δ mbt-OSC, Aub-piRNAs and AGO3-piRNAs have ping-pong signatures, and loss of Vasa, a ping-pong essential factor, leads to lack of ping-pong-dependent piRNAs, however dual-strand clusters are not expressed (Figure 19-21,24-27). One reason might be that RDC complex, an essential complex for expression of dual strand clusters, is defected. In Δ mbt-OSC Deadlock is expressed, however Rhino is slightly expressed and Cutoff is not detected (Figure 15). Forced expression of Deadlock and Cutoff might make dual strand clusters be expressed.

1.4 AGO3 piRNA derivation in Δ mbt-OSCs

My result showed that AGO3-bound piRNA originated from sense strand transposon (Figure 21A). Where do transposon mRNAs that give rise to AGO3-bound piRNAs come from in Δ mbt-OSCs? Previous study showed that overexpression of Myc-Aub in OSCs caused a slight but significant increase in

the levels of *mdg1* and *DM297*, which are targets of Piwi in OSCs (Sato et al. 2015). This de-repression of transposons could be because Myc-Aub competes with endogenous Piwi for primary piRNAs, impairing the Piwi-mediated transcriptional silencing activity. Indeed, AGO3-bound piRNAs included piRNAs originating from *mdg1* and *DM297* mRNAs (Figure 21A). These results raise the intriguing idea that both transcriptional and post-transcriptional transposon silencing (*i.e.*, the ping-pong pathway) occur in Δ mbt-OSCs, mediated by nuclear Piwi-piRNA and cytoplasmic Aub-piRNA complexes, respectively, as in germ cells in fly ovaries.

1.5 sDMA modification regulator of AGO3

I showed that AGO3 was sDMA-modified in Δ mbt-OSCs, as in ovaries, while Myc-AGO3 in OSCs was sDMA free (Figure 26). Krimp is crucial for sDMA modification and secondary piRNA association in AGO3 (Olivieri et al. 2012; Sato et al. 2015). The result indicated that in Δ mbt-OSCs, AGO3 loading with secondary piRNAs might be under the control of Krimp. However, I wonder how the beginning of secondary piRNA biogenesis is recognized and Krimp starts to promote AGO3 sDMA modification. In OSCs Krimp bodies are generally present at a frequency of one per cell and expressed AGO3 is localized to the bodies (Figure 30A; Olivieri et al. 2012; Sato et al. 2015). However, in Δ mbt-OSCs, AGO3-positive granules were more numerous than one per cell and some could be superimposed with Aub-positive or Krimp-positive granules (Figure 29C,30A).

These results make me imagine that the beginning of secondary piRNA biogenesis affect localization of AGO3 and Krimp. The factor(s) affected their localization directly need to be examined in detail.

1.6 piRNA factors localization

In Δ mbt-OSCs, nuage is formed, and piRNA factor(s) are localized there as previous reports showed in germ cell (Figure 29-31; Findley et al. 2003; Nagao et al 2011). This means that the cell is help for studying piRNA factors localization. The nuage localization hierarchy was previously shown, however the relation between protein function and localization is mainly unknown. Δ mbt-OSCs might clarify meaning of nuage localization of these factors.

第2章

本章については5年以内に雑誌等で刊行予定のため
非公開

第2章

本章については5年以内に雑誌等で刊行予定のため
非公開

第2章

本章については5年以内に雑誌等で刊行予定のため
非公開

3.1 Zuc-FLAG OSC, a helpful for Zuc study cell line

I established Zuc-FLAG OSCs, a Zuc detectable OSC line (Figure 45C). In the cell, FLAG Immunostaining showed more correct and clear Zuc localizations (Figure 43A). Previously anti-Zuc antibody was not available, so functional studies of Zuc have been confirmed by over-expression of Zuc in OSCs or *E.coli*. Although Zuc is largely essential for phased piRNA biogenesis, a recently found piRNA biogenesis pathway, studies for the pathway were difficult using previous systems. The cell line must be so helpful for studying phased piRNA biogenesis. I have already obtained various co-factor of Zuc and I am analyzing these co-factors. This cell will reveal detailed endogenous Zuc activity.

3.2 The method of genome editing using the CRISPR/Cas9 system

I with help from Dr. Hirotsugu Ishizu, established Zuc-FLAG OSC using the CRISPR/Cas9 system, also I established Δ mbt-OSC. These results showed

that knock-in/out method for OSC is available. The method of knock-in/out for OSC is surely helpful for piRNA biogenesis analysis.

References

References

Andress A, Bei Y, Fonslow BR, Giri R, Wu Y, Yates JR 3rd, Carthew RW. 2016 Spindle-E cycling between nuage and cytoplasm is controlled by Qin and PIWI proteins. *J Cell Biol.* **213**: 201-211.

Arkov AL, Wang JY, Ramos A, Lehmann R. 2006 The role of Tudor domains in germline development and polar granule architecture. *Development* **133**: 4053-4062.

Bibikova M, Golic M, Golic KG, Carroll D. 2002. Targeted chromosomal cleavage and mutagenesis in *Drosophila* using zinc-finger nucleases. *Genetics* **161**: 1169–1175.

Boswell RE, Mahowald AP. 1985 tudor, a gene required for assembly of the germ plasm in *Drosophila melanogaster*. *Cell* **43**: 97-104.

Brennecke J, Aravin AA, Stark A, Dus M, Kellis M, Sachidanandam R, Hannon GJ. 2007. Discrete small RNA-generating loci as master regulators of transposon activity in *Drosophila*. *Cell* **128**: 1089–1103.

Capecchi MR. 1989. Altering the genome by homologous recombination. *Science* **244**: 1288–1292.

Cong L, Ran FA, Cox D, Lin S, Barretto R, Habib N, Hsu PD, Wu X, Jiang W, Marraffini LA, Zhang F. 2013. Multiplex genome engineering using CRISPR/Cas systems. *Science* **339**: 819–823.

Chu VT, Weber T, Wefers B, Wurst W, Sander S, Rajewsky K, Kühn R. 2015. Increasing the efficiency of homology-directed repair for CRISPR-Cas9-induced precise gene editing in mammalian cells. *Nat. Biotechnol.* **33**:543–548

Czech B, Preall JB, McGinn J, Hannon GJ. 2013. A transcriptome-wide RNAi screen in the *Drosophila* ovary reveals factors of the germline piRNA pathway. *Mol Cell* **50**: 749–761.

Dennis C, Zanni V, Brassat E, Eymery A, Zhang L, Mteirek R, Jensen S, Rong YS, Vaury C. 2013. "Dot COM", a nuclear transit center for the primary piRNA pathway in *Drosophila*. *PLoS One* **8**: e72752.

Dönertas D, Sienski G, Brennecke J. 2013 *Drosophila* Gtsf1 is an essential component of the Piwi-mediated transcriptional silencing complex. *Genes Dev.* **27**: 1693-1705.

Findley SD, Tamanaha M, Clegg NJ, Ruohola-Baker H. 2003. Maelstrom, a *Drosophila* spindle-class gene, encodes a protein that colocalizes with Vasa and RDE1/AGO1 homolog, Aubergine, in nuage. *Development* **130**: 859-871.

Gangaraju VK, Yin H, Weiner MM, Wang J, Huang XA, Lin H. 2011. *Drosophila* Piwi functions in Hsp90-mediated suppression of phenotypic variation. *Nat Genet* **43**: 153–158.

Gateff E, Löffler T, Wismar J. 1993. A temperature-sensitive brain tumor suppressor mutation of *Drosophila melanogaster*: developmental studies and molecular localization of the gene. *Mech Dev* **41**: 15–31.

Gelbart WM, Emmert DB. 2013. FlyBase high throughput expression pattern data.

Gunawardane LS, Saito K, Nishida KM, Miyoshi K, Kawamura Y, Nagami T, Siomi H, Siomi MC. 2007. A slicer-mediated mechanism for repeat-associated siRNA 5' end formation in *Drosophila*. *Science* **315**: 1587–1590.

Han BW, Wang W, Li C, Weng Z, Zamore PD. 2015. piRNA-guided transposon cleavage initiates Zucchini-dependent, phased piRNA production. *Science* **348**: 817–821.

Handler D, Meixner K, Pizka M, Lauss K, Schmied C, Gruber FS, Brennecke J. 2013. The genetic makeup of the *Drosophila* piRNA pathway. *Mol Cell* **50**: 762–777.

Hay B, Jan LY, Jan YN. 1988 A protein component of *Drosophila* polar granules is encoded by *vasa* and has extensive sequence similarity to ATP-dependent helicases. *Cell* **55**: 577-87.

Hsu PD, Lander ES, Zhang F. 2014. Development and applications of CRISPR-Cas9 for genome engineering. *Cell* **157**: 1262–1278.

Huang H, Li Y, Szulwach KE, Zhang G, Jin P, Chen D. 2014 AGO3 Slicer activity regulates mitochondria-nuage localization of Armitage and piRNA amplification. *J Cell Biol.* **206**: 217-230.

Ipsaro JJ, Haase AD, Knott SR, Joshua-Tor L, Hannon GJ. The structural biochemistry of Zucchini implicates it as a nuclease in piRNA biogenesis. 2012. *Nature* **491**: 279–283.

Ishizu H, Iwasaki YW, Hirakata S, Ozaki H, Iwasaki W, Siomi H, Siomi MC. 2015. Somatic primary piRNA biogenesis driven by *cis*-acting RNA elements and *trans*-acting Yb. *Cell Rep* **12**: 429–440.

Ishizu H, Sumiyoshi T, Siomi MC. 2017 Use of the CRISPR-Cas9 system for genome editing in cultured *Drosophila* ovarian somatic cells. *Methods*. **126**:186-192.

Iwasaki YW, Siomi MC, Siomi H. 2015. PIWI-interacting RNA: its biogenesis and functions. *Annu. Rev. Biochem.* **84**: 405–433.

Janic A, Mendizabal L, Llamazares S, Rossell D, Gonzalez C. 2010. Ectopic expression of germline genes drives malignant brain tumor growth in *Drosophila*. *Science* **330**: 1824–1827.

Jinek M, Chylinski K, Fonfara I, Hauer M, Doudna JA, Charpentier E. 2012. A programmable dual-RNA-guided DNA endonuclease in adaptive bacterial immunity. *Science* **339**: 816–821.

Jinek M, East A, Cheng A, Lin S, Ma E, Doudna J. 2013. RNA-programmed genome editing in human cells. *Elife* **2**: e00471.

Kawamura Y, Saito K, Kin T, Ono Y, Asai K, Sunohara T, Okada TN, Siomi MC, Siomi H. 2008. *Drosophila* endogenous small RNAs bind to Argonaute 2 in somatic cells. *Nature* **453**: 793-797.

Kawaoka S, Hayashi N, Suzuki Y, Abe H, Sugano S, Tomari Y, Shimada T, Katsuma S. 2009. The *Bombyx* ovary-derived cell line endogenously expresses PIWI/PIWI-interacting RNA complexes. *RNA* **15**: 1258-1264.

Kirino Y, Kim N, de Planell-Saguer M, Khandros E, Chiorean S, Klein PS, Rigoutsos I, Jongens TA, Mourelatos Z. 2009 *Nat Cell Biol.* **11**:652-658.

Klattenhoff C, Xi H, Li C, Lee S, Xu J, Khurana JS, Zhang F, Schultz N, Koppetsch BS, Nowosielska A, Seitz H, Zamore PD, Weng Z, Theurkauf WE. 2009 The *Drosophila* HP1 homolog Rhino is required for transposon silencing and piRNA production by dual-strand clusters. *Cell* **138**: 1137-1149.

Lasko PF, Ashburner M. 1988 The product of the *Drosophila* gene vasa is very similar to eukaryotic initiation factor-4A. *Nature* **335**: 611-617.

Le Thomas A, Stuwe, Li S, Du J, Marinov G, Rozhkov N, Chen YC, Luo Y, Sachidanandam R, Toth KF, Patel D, Aravin AA. 2014 Transgenerationally inherited piRNAs trigger piRNA biogenesis by changing the chromatin of piRNA clusters and inducing precursor processing. *Genes Dev.* **28**: 1667-1680.

Lewis PW, Beall EL, Fleischer TC, Georgette D, Link AJ, Botchan MR. 2004 Identification of a *Drosophila* Myb-E2F2/RBF transcriptional repressor complex. *Genes Dev* **18**: 2929-40.

Li C, Vagin VV, Lee S, Xu J, Ma S, Xi H, Seitz H, Horwich MD, Syrzycka M, Honda BM, et al. 2009. Collapse of germline piRNAs in the absence of Argonaute3 reveals somatic piRNAs in flies. *Cell* **137**: 509–521.

Lim AK, Kai T. 2007. Unique germ-line organelle, nuage, functions to repress selfish genetic elements in *Drosophila melanogaster*. *Proc Natl Acad Sci USA* **104**: 6714–6719.

Ma S, Chang J, Wang X, Liu Y, Zhang J, Lu W, Gao J, Shi R, Zhao P, Xia Q. 2014 CRISPR/Cas9 mediated multiplex genome editing and heritable mutagenesis of BmKu70 in *Bombyx mori*. *Sci Rep.* **4**:4489.

Mali P, Yang L, Esvelt KM, Aach J, Guell M, DiCarlo JE, Norville JE, Church GM. 2013. RNA-guided human genome engineering via Cas9. *Science* **339**: 823–826

Malone CD, Brennecke J, Dus M, Stark A, McCombie WR, Sachidanandam R, Hannon GJ. 2009. Specialized piRNA pathways act in germline and somatic tissues of the *Drosophila* ovary. *Cell* **137**: 522–535.

Meier K, Mathieu EL, Finkernagel F, Reuter LM, Scharfe M, Doehlemann G, Jarek M, Brehm A. 2012 LINT, a novel dL(3)mbt-containing complex, represses malignant brain tumour signature genes. *PLoS Genet.* **8**: e1002676.

Mohn F, Sienski G, Handler D, Brennecke J, 2014. The rhino-deadlock-cutoff complex licenses noncanonical transcription of dual-strand piRNA clusters in *Drosophila*. *Cell* **157**: 1364–1379.

Mohn F, Handler D, Brennecke J. 2015. piRNA-guided slicing specifies transcripts for Zucchini-dependent, phased piRNA biogenesis. *Science* **348**: 812–817.

Murota Y, Ishizu H, Nakagawa S, Iwasaki YW, Shibata S, Kamatani MK, Saito K, Okano H, Siomi H, Siomi MC. 2014. Yb integrates piRNA intermediates and processing factors into perinuclear bodies to enhance piRISC assembly. *Cell Rep* **8**: 103–113.

Nagao A, Sato K, Nishida KM, Siomi H, Siomi MC. 2011. Gender-specific hierarchy in nuage localization of PIWI-interacting RNA factors in *Drosophila*. *Front Genet* **2**: 55.

Niki Y, Yamaguchi T, Mahowald AP. 2006. Establishment of stable cell lines of *Drosophila* germ-line stem cells. *Proc Natl Acad Sci U S A* **103**, 16325- 6330.

Nishida KM, Saito K, Mori T, Kawamura Y, Nagami-Okada T, Inagaki S, Siomi H, Siomi MC. 2007. Gene silencing mechanisms mediated by Aubergine piRNA complexes in *Drosophila* male gonad. *RNA* **13**: 1911–1922.

Nishida KM, Okada TN, Kawamura T, Mituyama T, Kawamura Y, Inagaki S, Huang H, Chen D, Kodama T, Siomi H, et al. 2009. Functional involvement of Tudor and dPRMT5 in the piRNA processing pathway in *Drosophila* germlines. *EMBO J* **28**: 3820–3831.

Nishida KM, Iwasaki YW, Murota Y, Nagao A, Mannen T, Kato Y, Siomi H, Siomi MC. 2015. Respective functions of two distinct Siwi complexes assembled during PIWI-interacting RNA biogenesis in *Bombyx* germ cells. *Cell Rep* **10**: 193–203.

Nishimasu H, Ishizu H, Saito K, Fukuhara S, Kamatani MK, Bonnefond L, Matsumoto N, Nishizawa T, Nakanaga K, Aoki J, Ishitani R, Siomi H, Siomi MC, Nureki O. 2012. Structure and function of Zucchini endoribonuclease in piRNA biogenesis. *Nature* **491**: 284–287.

Nott TJ, Petsalaki E, Farber P, Jervis D, Fussner E, Plochowietz A, Craggs TD, Bazett-Jones DP, Pawson T, Forman-Kay JD, Baldwin AJ. 2015. Phase

transition of a disordered nuage protein generates environmentally responsive membraneless organelles. *Mol Cell*. **57**: 936-947.

Ohtani H, Iwasaki YW, Shibuya A, Siomi H, Siomi MC, Saito K. 2013. DmGTSF1 is necessary for Piwi-piRISC-mediated transcriptional transposon silencing in the *Drosophila* ovary. *Genes Dev* **27**: 1656–1661.

Olivieri D, Senti KA, Subramanian S, Sachidanandam R, Brennecke J. 2012. The cochaperone shutdown defines a group of biogenesis factors essential for all piRNA populations in *Drosophila*. *Mol Cell* **47**: 954-969.

Pane A, Jiang P, Zhao DY, Singh M, Schüpbach T. 2011 The Cutoff protein regulates piRNA cluster expression and piRNA production in the *Drosophila* germline. *EMBO J*. **30**: 4601-4615.

Patil VS, Anand A, Chakrabarti A, Kai T. 2014. The Tudor domain protein Tapas, a homolog of the vertebrate Tdrd7, functions in the piRNA pathway to regulate retrotransposons in germline of *Drosophila melanogaster*. *BMC Biol* **12**: 61.

Ran FA, Hsu PD, Wright J, Agarwala V, Scott DA, Zhang F. 2013. Genome engineering using the CRISPR-Cas9 system. *Nat. Protoc*. **11**: 2281– 2308.

Robine N, Lau NC, Balla S, Jin Z, Okamura K, Kuramochi-Miyagawa S, Blower MD, Lai EC. 2009. A broadly conserved pathway generates 3'UTR-directed primary piRNAs. *Curr Biol*. **19**: 2066-2076.

Saito K, Nishida KM, Mori T, Kawamura Y, Miyoshi K, Nagami T, Siomi H, Siomi MC. 2006. Specific association of Piwi with rasiRNAs derived from

retrotransposon and heterochromatic regions in the *Drosophila* genome. *Genes Dev* **20**: 2214–2222.

Saito K, Inagaki S, Mituyama T, Kawamura Y, Ono Y, Sakota E, Kotani H, Asai K, Siomi H, Siomi MC. 2009. A regulatory circuit for piwi by the large *Maf* gene *traffic jam* in *Drosophila*. *Nature* **461**: 1296–1299.

Saito K, Ishizu H, Komai M, Kotani H, Kawamura Y, Nishida KM, Siomi H, Siomi MC. 2010. Roles for the Yb body components Armitage and Yb in primary piRNA biogenesis in *Drosophila*. *Genes Dev* **24**: 2493–2498.

Sander JD, Joung JK. 2014. CRISPR-Cas systems for editing, regulating and targeting genomes. *Nat. Biotechnol.* **32**: 347–355.

Sato K, Nishida KM, Shibuya A, Siomi MC, Siomi H. 2011. Maelstrom coordinates microtubule organization during *Drosophila* oogenesis through interaction with components of the MTOC. *Genes Dev* **25**: 2361–2373.

Sato K, Iwasaki YW, Shibuya A, Carninci P, Tsuchizawa Y, Ishizu H, Siomi MC, Siomi H. 2015. Krimper enforces an antisense bias on piRNA pools by binding AGO3 in the *Drosophila* germline. *Mol Cell* **59**: 553–563.

Schneider I. 1972 Cell lines derived from late embryonic stages of *Drosophila melanogaster*. *J Embryol Exp Morphol.* **27**: 353–365.

Senti KA, Jurczak D, Sachidanandam R, Brennecke J. 2015. piRNA-guided slicing of transposon transcripts enforces their transcriptional silencing via specifying the nuclear piRNA repertoire. *Genes Dev* **29**: 1747–1762.

Sengoku T, Nureki O, Nakamura A, Kobayashi S, Yokoyama S. 2006. Structural basis for RNA unwinding by the DEAD-box protein *Drosophila* Vasa. *Cell* **125**: 287-300.

Sienski G, Dönertas D, Brennecke J. 2012 Transcriptional silencing of transposons by Piwi and maelstrom and its impact on chromatin state and gene expression. *Cell* **151**: 964-980.

Sienski G, Batki J, Senti KA, Dönertas D, Tirian L, Meixner K, Brennecke J. 2015 Silencio/CG9754 connects the Piwi-piRNA complex to the cellular heterochromatin machinery. *Genes Dev.* **29**: 2258-2271.

Siomi MC, Sato K, Pezic D, Aravin AA. 2011 PIWI-interacting small RNAs: the vanguard of genome defence. *Nat Rev Mol Cell Biol.* **12**: 246-258.

Specchia V, Piacentini L, Tritto P, Fanti L, D'Alessandro R, Palumbo G, Pimpinelli S, Bozzetti MP. 2010. Hsp90 prevents phenotypic variation by suppressing the mutagenic activity of transposons. *Nature* **463**: 662–665.

Sumiyoshi T, Sato K, Yamamoto H, Iwasaki YW, Siomi H, Siomi MC. 2016 Loss of *I(3)mbt* leads to acquisition of the ping-pong cycle in *Drosophila* ovarian somatic cells. *Genes Dev.* **30**: 1617-1622. *Genes Dev.* 2016 Jul 15;30(14):1617-22.

Vagin VV, Sigova A, Li C, Seitz H, Gvozdev V, Zamore PD. 2006. A distinct small RNA pathway silences selfish genetic elements in the germline. *Science* **313**:320-324.

Wang W, Han BW, Tipping C, Ge DT, Zhang Z, Weng Z, Zamore PD. 2015 Slicing and Binding by Ago3 or Aub Trigger Piwi-Bound piRNA Production by Distinct Mechanisms. *Mol Cell*. **59**: 819-830.

Webster A, Li S, Hur JK, Wachsmuth M, Bois JS, Perkins EM, Patel DJ, Aravin AA. Aub and Ago3 Are Recruited to Nuage through Two Mechanisms to Form a Ping-Pong Complex Assembled by Krimper. 2015. *Mol Cell* **59**: 564–575.

Wismar J, Löffler T, Habtemichael N, Vef O, Geissen M, Zirwes R, Altmeyer W, Sass H, Gateff E. 1995. The *Drosophila melanogaster* tumor suppressor gene *lethal(3)malignant brain tumor* encodes a proline-rich protein with a novel zinc finger. *Mech Dev* **53**: 141–154.

Xiol J, Spinelli P, Laussmann MA, Homolka D, Yang Z, Cora E, Couté Y, Conn S, Kadlec J, Sachidanandam R, et al. 2014. RNA clamping by Vasa assembles a piRNA amplifier complex on transposon transcripts. *Cell* **157**: 1698–1711.

Yamashiro H, Siomi MC. 2018 PIWI-Interacting RNA in *Drosophila*: Biogenesis, Transposon Regulation, and Beyond. *Chem Rev*. **118**: 4404-4421.

Yohn CB, Pusateri L, Barbosa V, Lehmann R. 2003. *l(3)malignant brain tumor* and three novel genes are required for *Drosophila* germ-cell formation. *Genetics* **165**: 1889–1900.

Yu B, Cassani M, Wang M, Liu M, Ma J, Li G, Zhang Z, Huang Y. 2015a Structural insights into Rhino-mediated germline piRNA cluster formation. *Cell Res*. **25**: 525-528.

Yu Y, Gu J, Jin Y, Luo Y, Preall JB, Ma J, Czech B, Hannon GJ. 2015b
Panoramix enforces piRNA-dependent cotranscriptional silencing. *Science* **350**:
339-342

Zhang F, Wang J, Xu J, Zhang Z, Koppetsch BS, Schultz N, Vreven T, Meignin
C, Davis I, Zamore PD, Weng Z, Theurkauf WE. 2012 UAP56 couples piRNA
clusters to the perinuclear transposon silencing machinery. *Cell* **151**: 871-884.

Zhang Z, Wang J, Schultz N, Zhang F, Parhad SS, Tu S, Vreven T, Zamore PD,
Weng Z, Theurkauf WE. 2014. The HP1 homolog rhino anchors a nuclear
complex that suppresses piRNA precursor splicing. *Cell* **157**: 1353–1363.

Figures

Figure 1

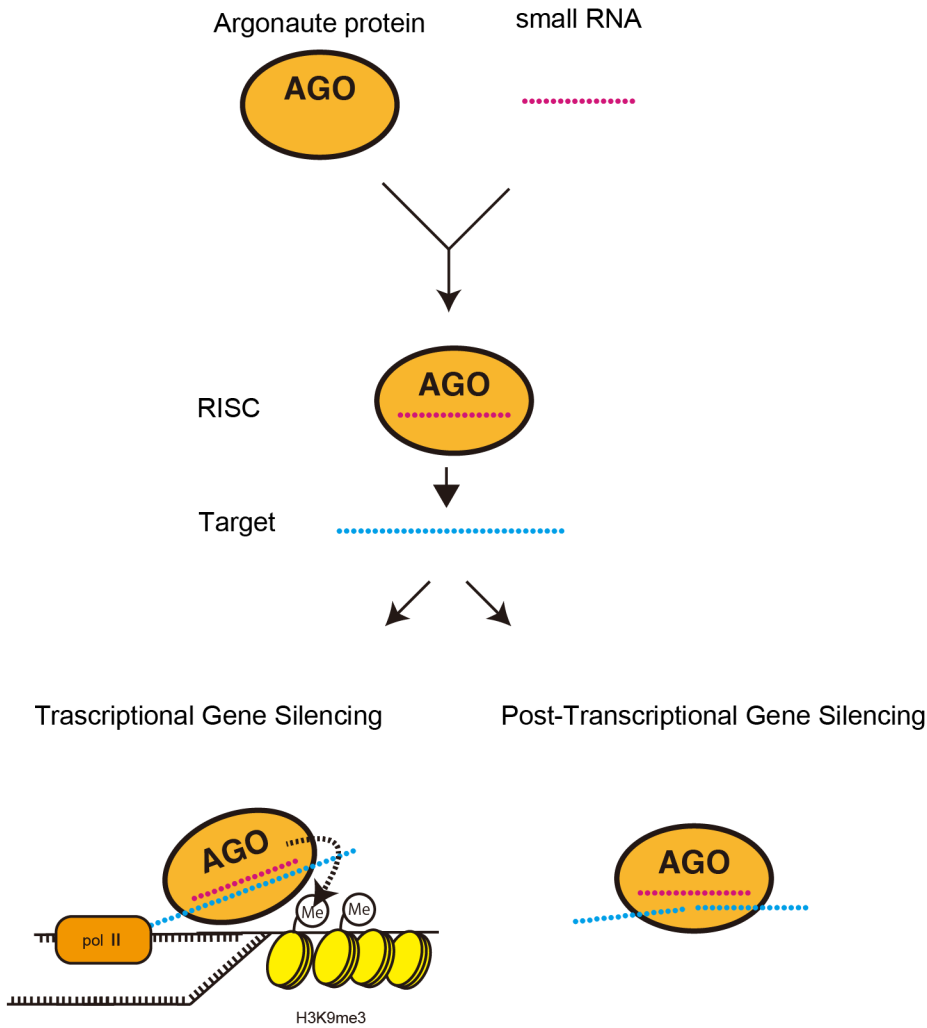


Figure 1. The small RNA biogenesis and function. Small RNAs bind Argonaute proteins. The complex termed RISC represses their targets in transcriptional or post-transcriptional levels.

Figure 2

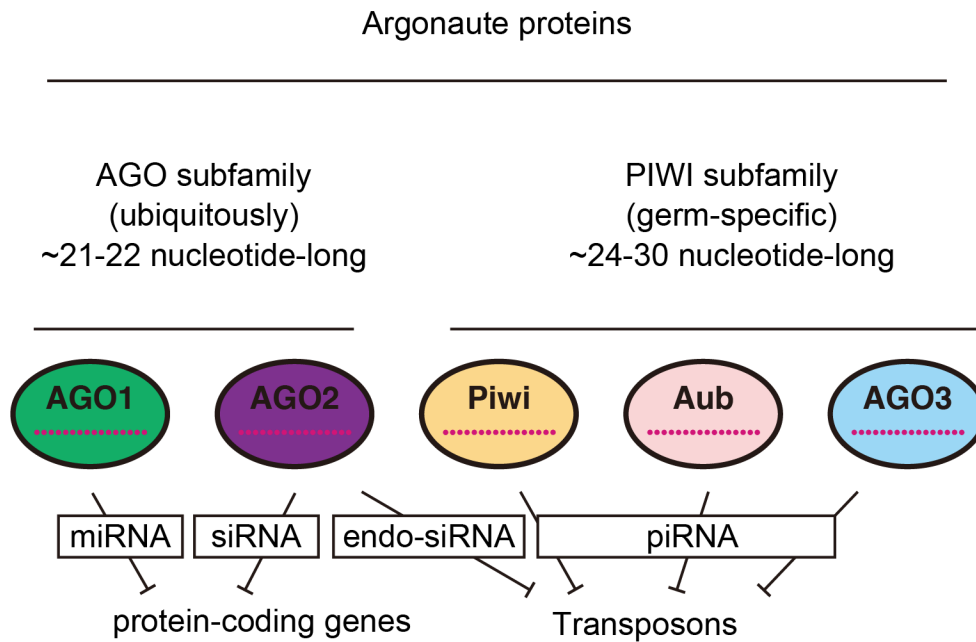
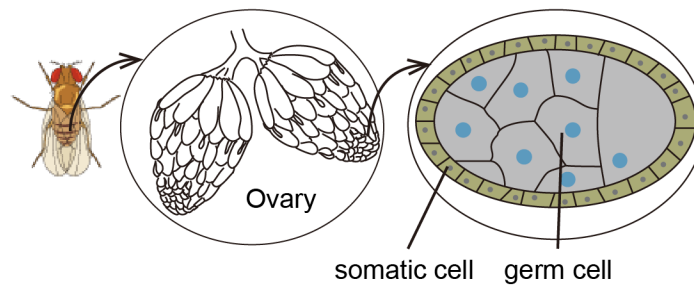


Figure 2. *Drosophila* has five Argonaute proteins. The Argonaute proteins are divided into two subfamilies; AGO subfamily and PIWI subfamily. Their binding the small RNAs bound to them and their functions are different each type.

Figure 3

A



B

somatic cells

germ cells

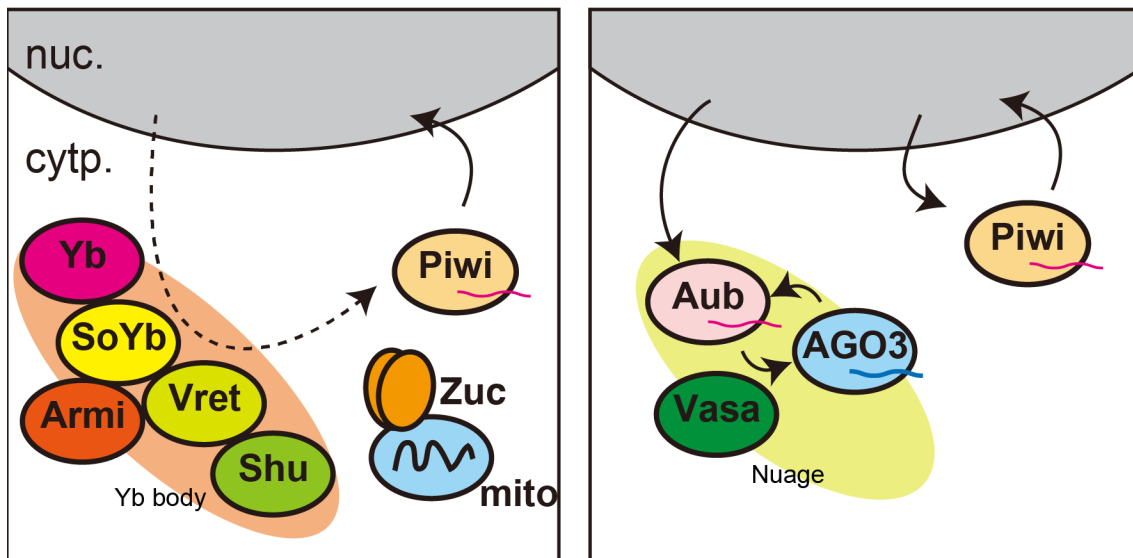


Figure 3. The expression of PIWI proteins in *Drosophila*. (A) *Drosophila* ovary contains germ cells and somatic cells surrounding the germ cells. (B) In germ cells not only Piwi but also Aub and AGO3 are expressed and the ping-pong pathway is activated, while Piwi is expressed in somatic cells.

Figure 4

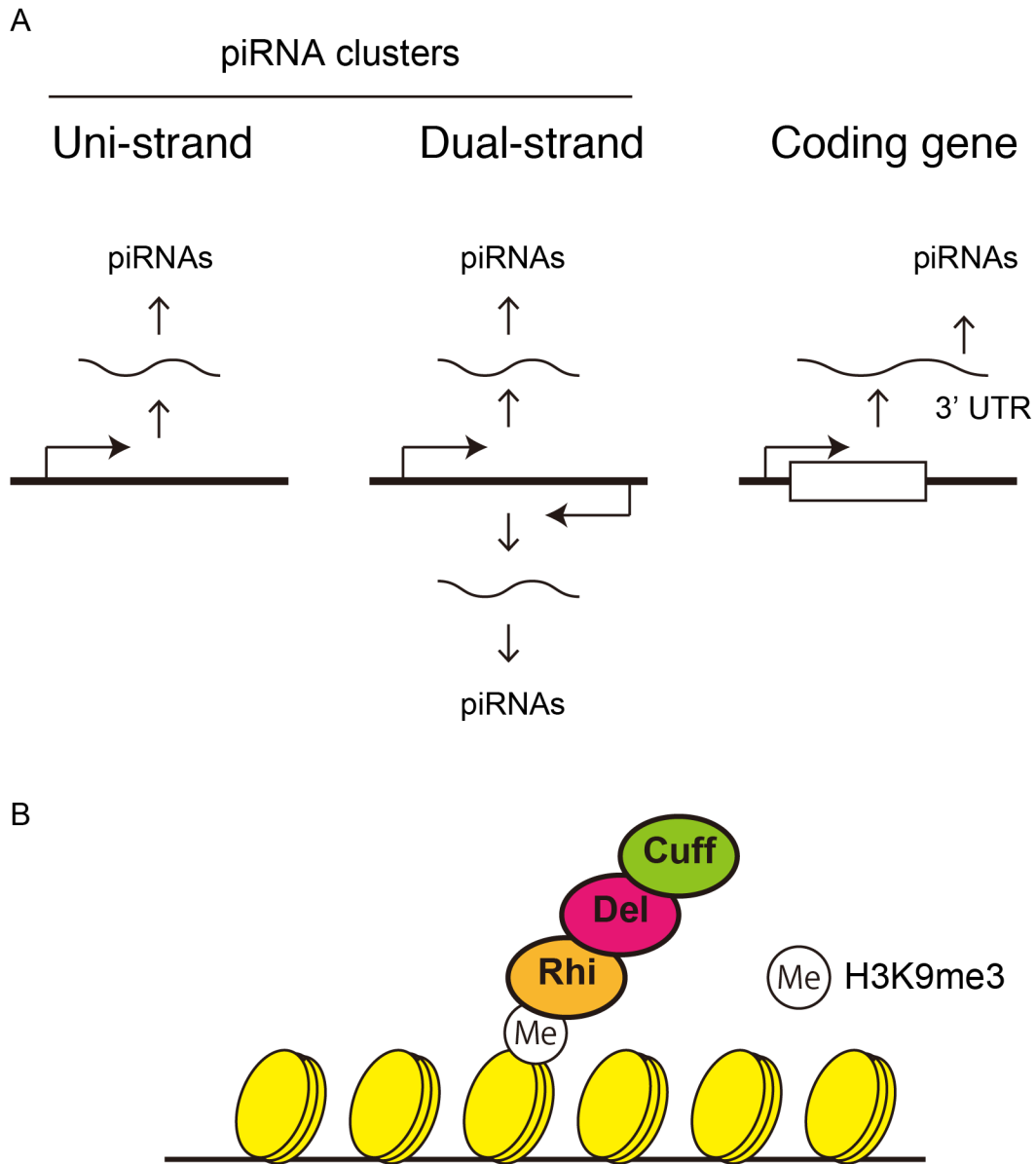


Figure 4. The piRNA transcription. (A) Uni-strand clusters are transcribed in one fixed direction, while dual-strand clusters are transcribed in both directions. Genic piRNAs are derived from UTR of some protein coding gene. (B) The rhino-deadlock-cutoff (RDC) complex is accumulated in the dual strand cluster. Rhi/Del/Cuff indicates Rhino/Deadlock/Cutoff each.

Figure 5

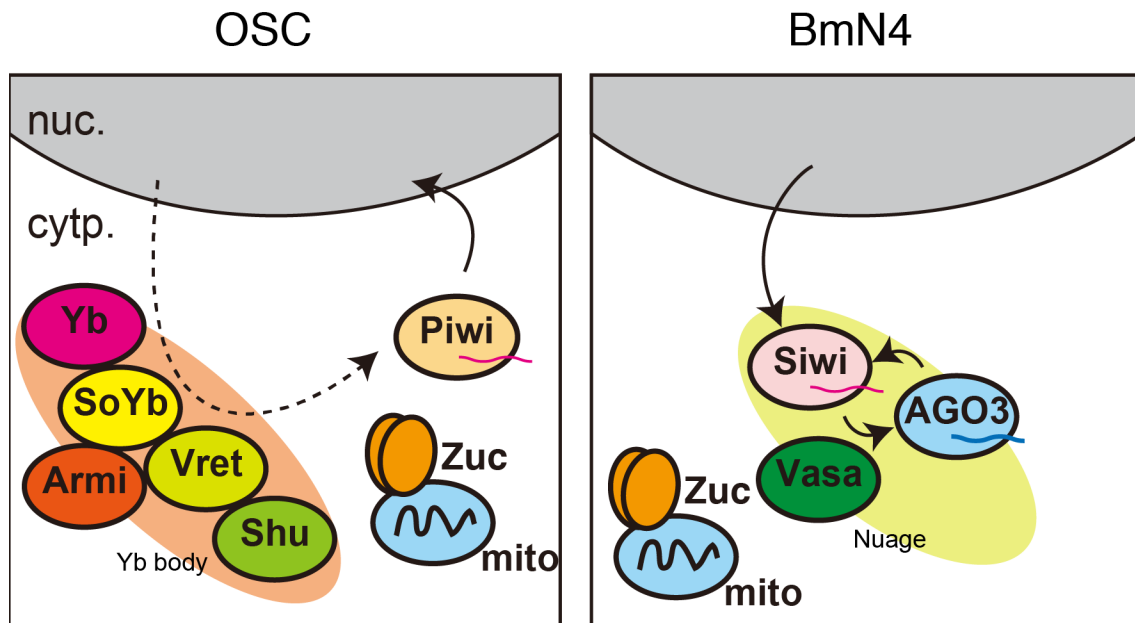


Figure 5. The available stable cell lines for piRNA biogenesis studies. OSCs are derived from *Drosophila* ovarian somatic cell, which have only somatic primary pathway. Also, BmN4 cells are derived from *Bombyx mori* germ cells, which have ping-pong pathway. In BmN4 cells, PIWI protein translocating to nucleus (e.g. Piwi in *Drosophila*) is absent.

Figure 6

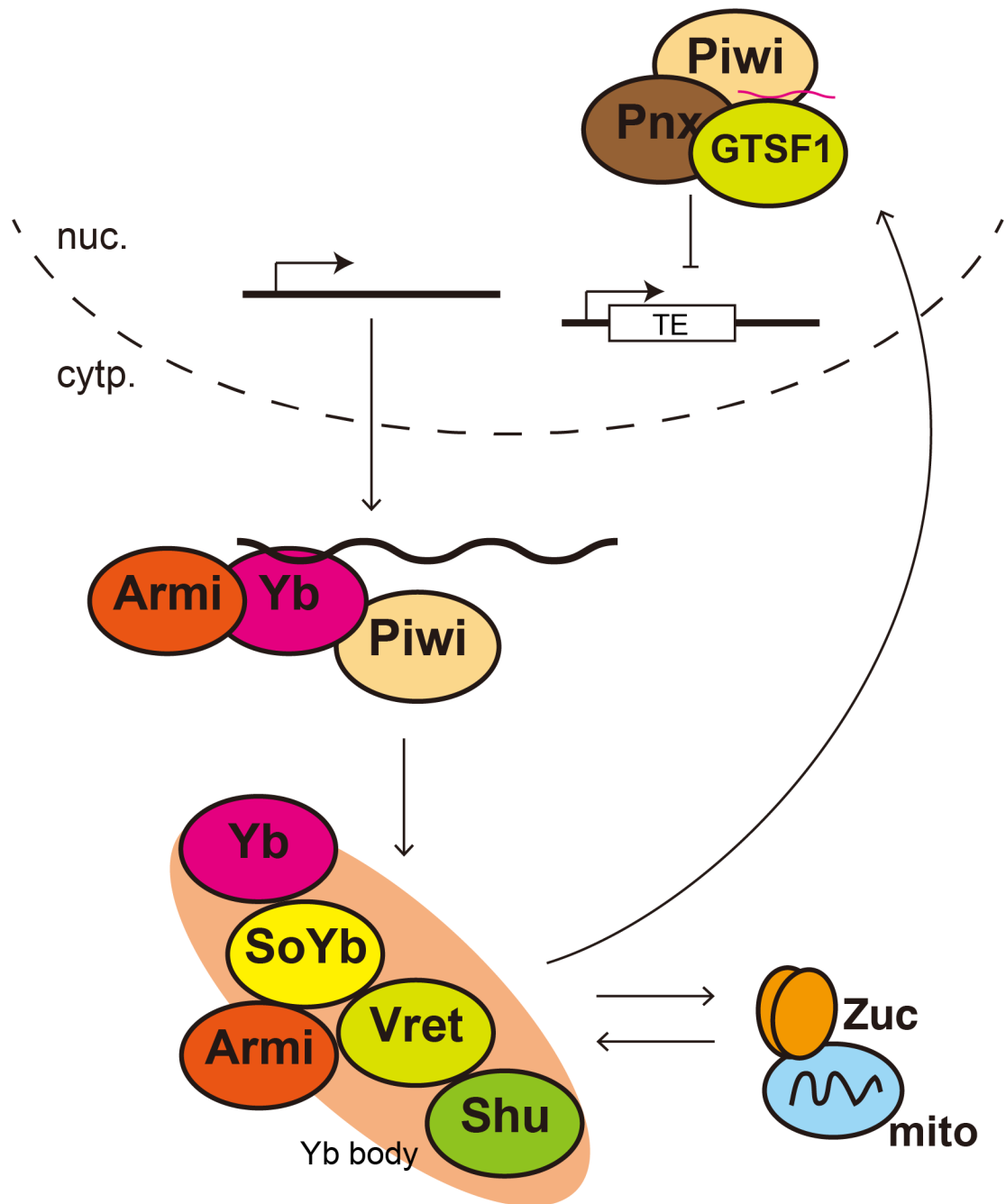


Figure 6. The mechanism of primary pathway in somatic cells. Piwi-piRNAs are processed by Yb body and mitochondrion components. The piRNA RISCs (piRISCs) are translocated to the nucleus and repress transposons together with nuclear factors.

Figure 7

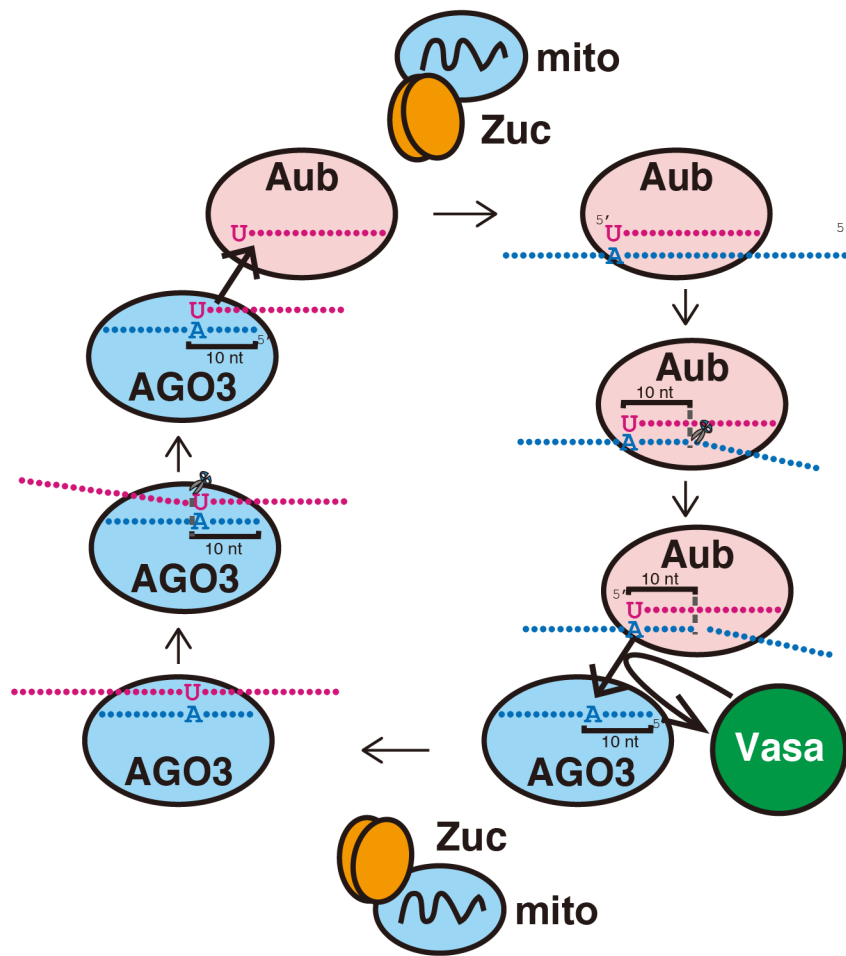


Figure 7. The mechanism of ping-pong pathway. The pathway represses transposon with cleaving it and processes cleavage product to piRNA. The red lines indicate antisense piRNAs. The blue lines indicate sense piRNAs.

Figure 8

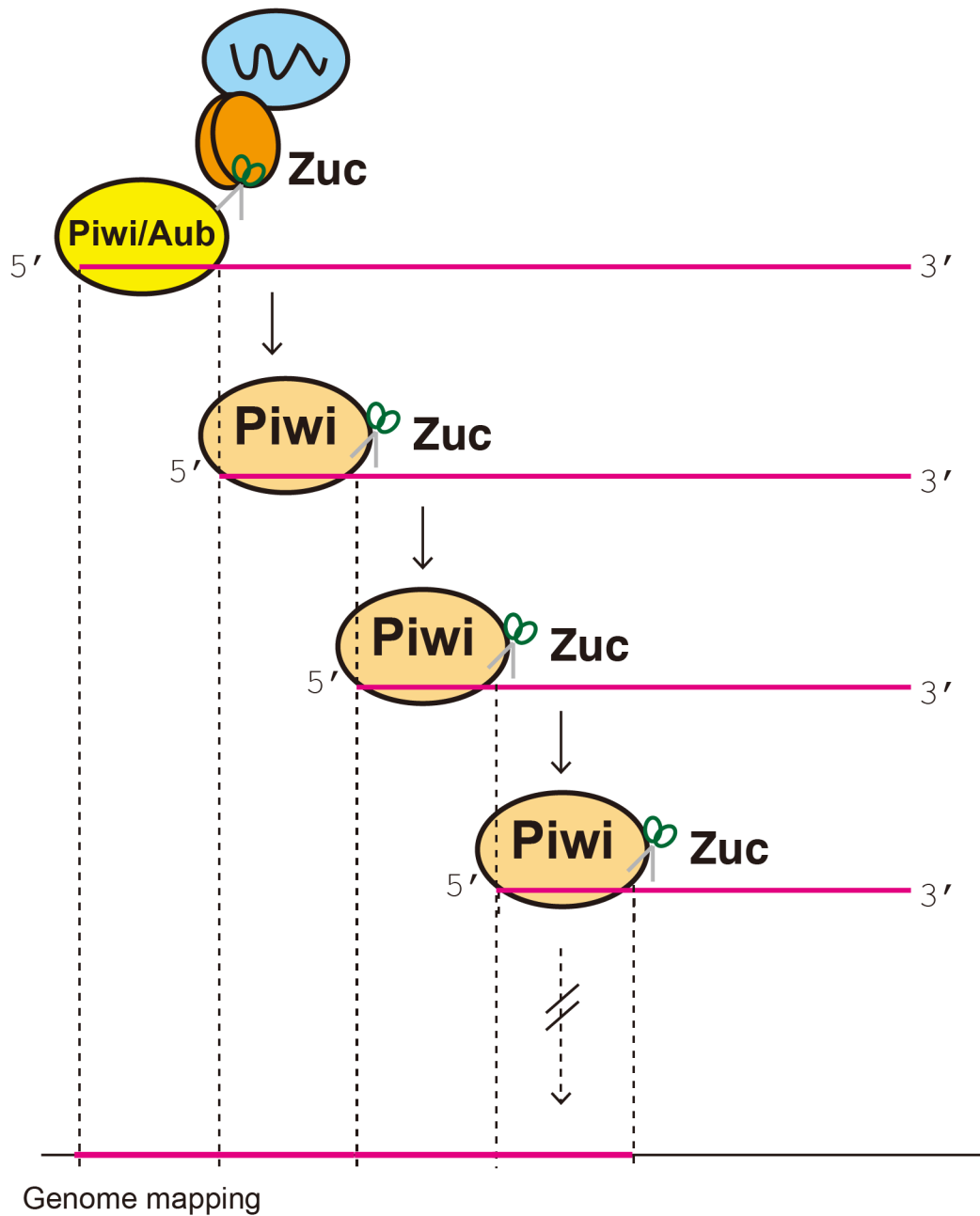


Figure 8. The mechanism of phased piRNA biogenesis pathway. Piwi- and Aub-piRNAs are cleaved by Zuc. The 3' end side of product is processed to a new Piwi-piRNA. This system is continued for a few times.

Figure 9

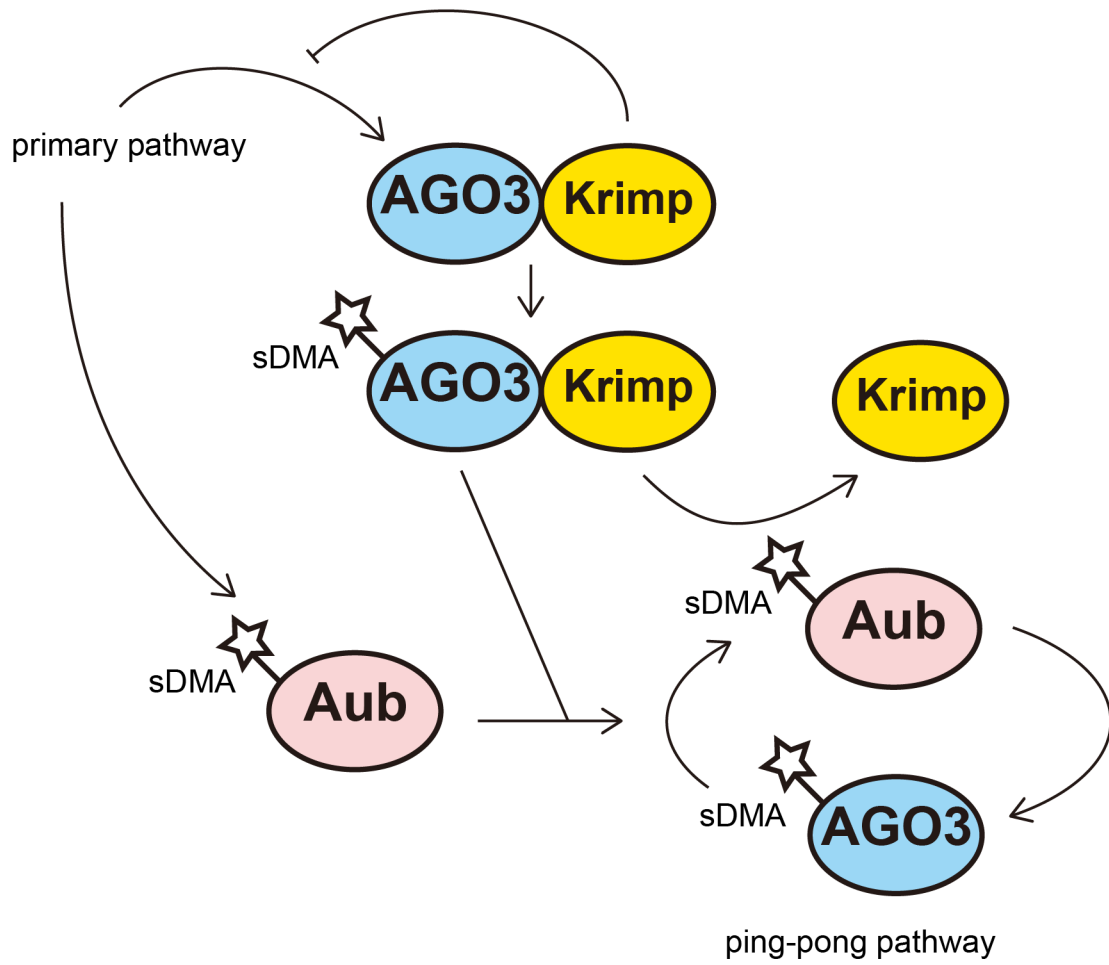


Figure 9. The model of Krimp activities. Krimp promotes its binding AGO3's sDMA modification and AGO3 localization to nuage.

Figure 10

Vasa-PA

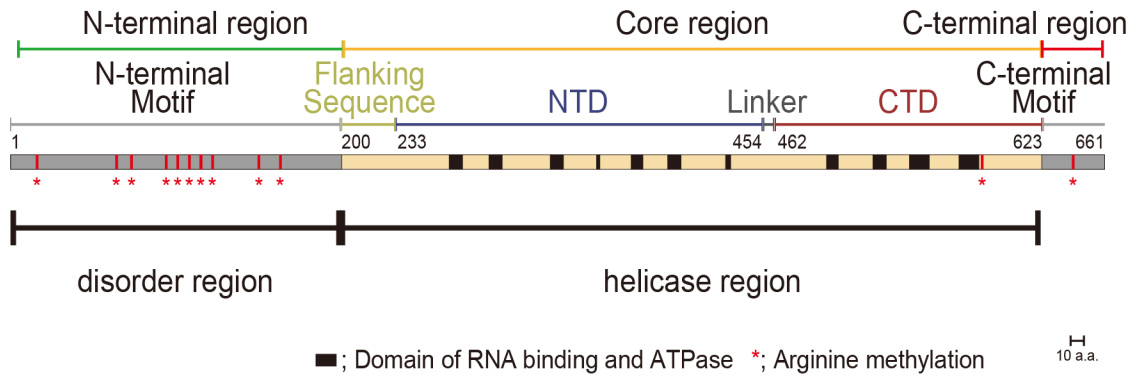


Figure 10. Vasa domain mapping. The N-terminal region contains disorder region and the region is methylated. Previously report showed that the region played important role to form granules. The Core region contains DEAD-box helicase region. The crystal structure was revealed in only the Core region. Black boxes indicate the domain of RNA binding and ATPase. Red asterisks indicate the methylated arginine.

Figure 11

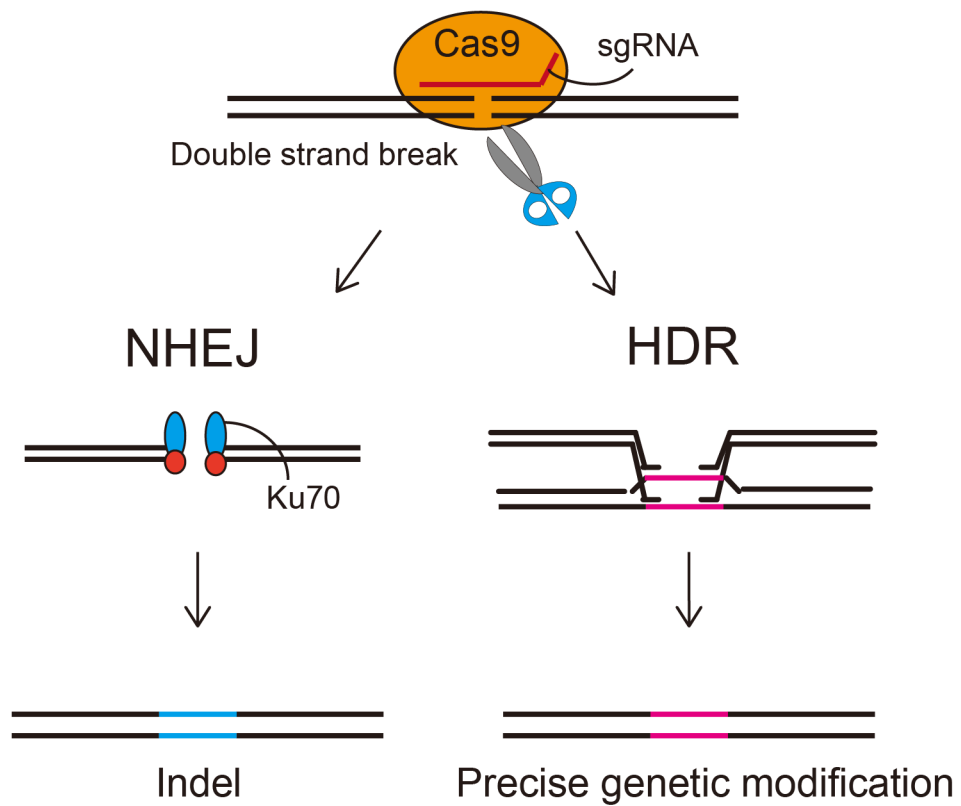


Figure 11. Genome editing by CRISPR/Cas9 system. Cas9-sgRNA complex cleaves genome DNAs, then endogenous repair systems, non-homologous end-joining (NHEJ) and homology-directed repair (HDR) are activated. These systems sometimes lead to genome editing.

Figure 12

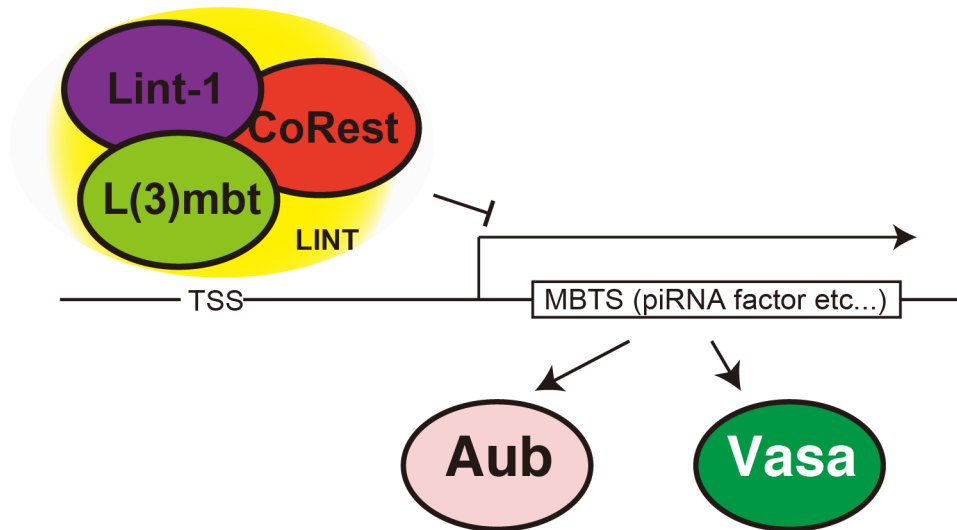


Figure 12. The current model of gene expression regulated by L(3)mbt. L(3)mbt forms LINT complex which regulates expression of MBTS genes.

Figure 13

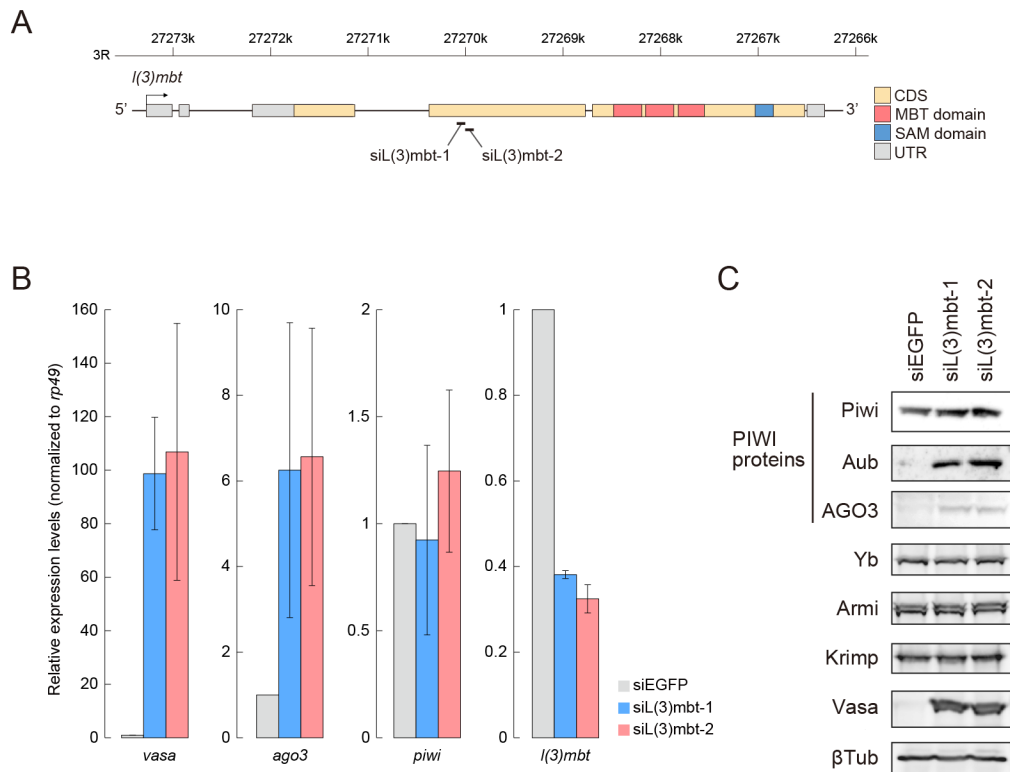


Figure 13. Ectopic expression of piRNA factors in *I(3)mbt*-depleted OSCs. (A) Genomic structure of the *I(3)mbt* locus and siRNA target sites. (B) qRT-PCR shows that *vasa* and *ago3* were up-regulated in OSCs by *I(3)mbt* depletion. In contrast, the *piwi* mRNA expression was unchanged by *I(3)mbt* depletion. *rp49* was used as an internal control. N = 3; error bars indicate SEM. (C) Western blotting shows up-regulation of Aub, AGO3, and Vasa by *I(3)mbt* depletion in OSCs. β Tubulin (β Tub) was employed as a loading control.

Figure 14

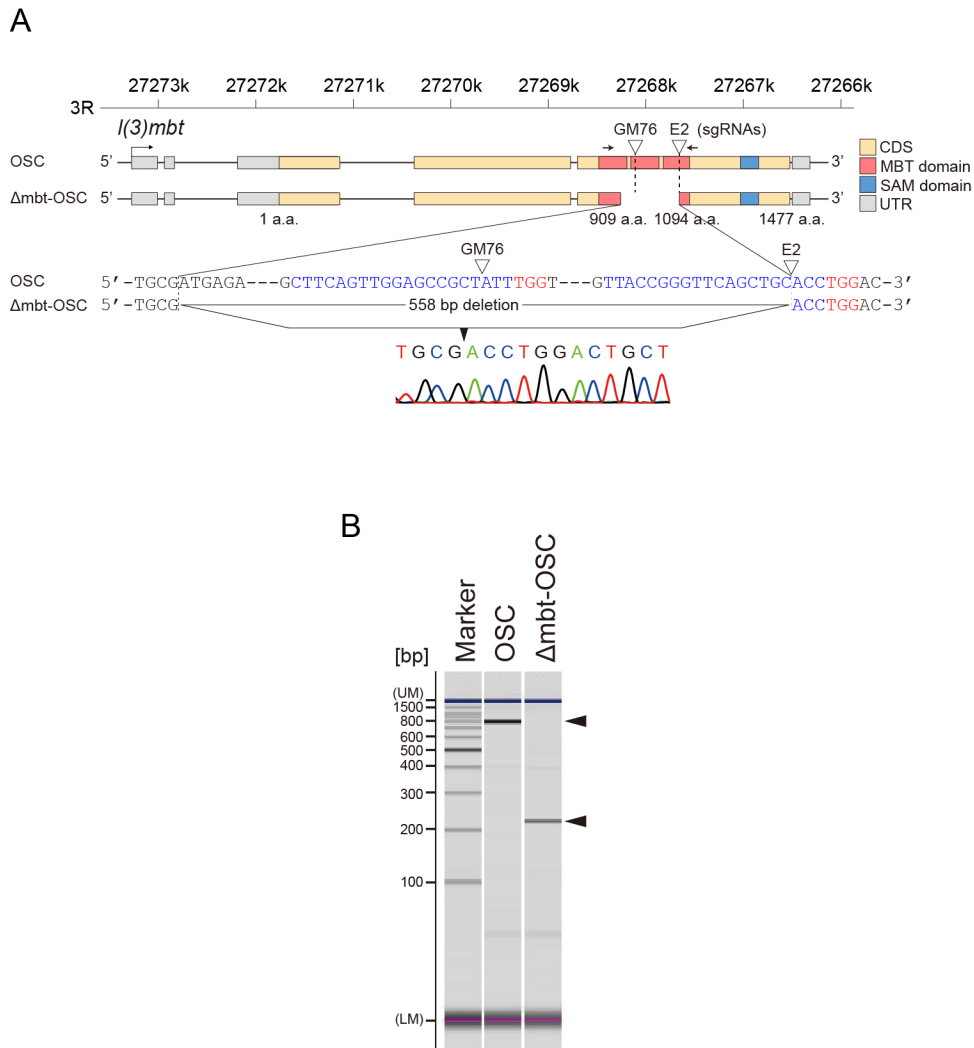
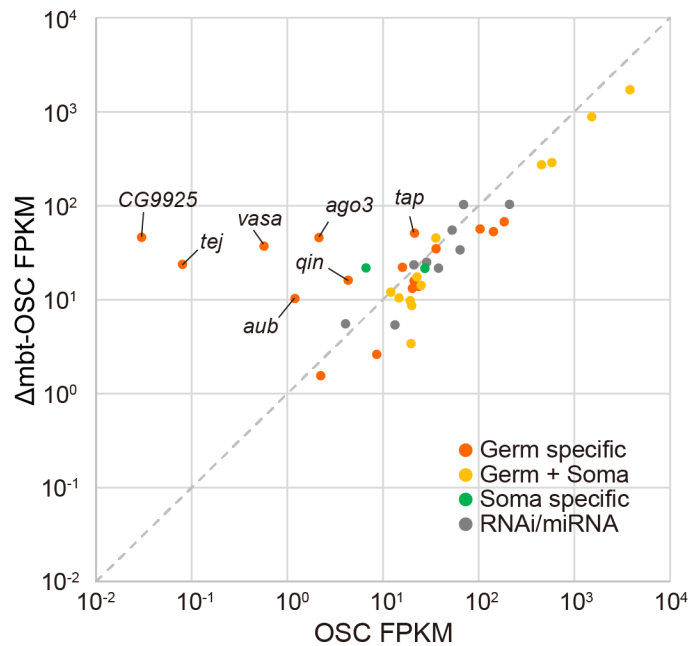


Figure 14. CRISPR-mediated generation of Δ mbt-OSCs. (A) Genomic structure of *I(3)mbt* locus in OSCs and Δ mbt-OSCs. SgRNAs E2 and GM76 targeting *I(3)mbt* exon 5 are indicated by arrowheads. Sequences at the *I(3)mbt* locus in OSCs and Δ mbt-OSCs are also shown (sgRNA and PAM sequences are shown in blue and red, respectively). CDS, protein coding DNA sequence; MBT domain, malignant brain tumor domain; SAM domain, sterile alpha motif domain; UTR, untranslated region. (B) Genomic PCR fragments amplified using a primer set shown by arrows in (A) are indicated by arrowheads (OSC, 772 nt; Δ mbt-OSC, 214 nt). UM and LM indicate Upper Marker and Lower Marker, respectively.

Figure 15



	OSC [FPKM]	Δmbt-OSC [FPKM]		OSC [FPKM]	Δmbt-OSC [FPKM]
Germ specific			Germ + Soma		
<i>UAP56</i>	184.58	67.59	<i>shu</i>	3798.68	1721.88
<i>spn-E</i>	142.42	53.02	<i>hsp83</i>	1516.88	884.65
<i>krimp</i>	102.93	56.68	<i>armi</i>	582.34	289.24
<i>tud</i>	35.75	34.89	<i>piwi</i>	454.98	273.26
<i>csul</i>	23.63	13.86	<i>mael</i>	35.66	45.46
<i>tap</i>	21.34	51.13	<i>minotaur</i>	25	14.29
<i>papi</i>	21.14	15.88	<i>vreteno</i>	22.56	17.52
<i>vls</i>	20.24	13.22	<i>zuc</i>	19.88	8.69
<i>del</i>	15.94	22.25	<i>gasz</i>	19.6	3.42
<i>BoYb</i>	8.58	2.62	<i>CG9754</i>	19.17	9.77
<i>qin</i>	4.31	16.15	<i>gtsf1</i>	14.63	10.5
<i>rhi</i>	2.23	1.56	<i>egg</i>	12.06	12.05
<i>ago3</i>	2.14	45.96	<i>Pimet</i>	0	12.46
<i>aub</i>	1.20	10.30			
<i>vasa</i>	0.57	37.22	Soma specific		
<i>tej</i>	0.08	23.84	<i>SoYb</i>	27.33	21.64
<i>CG9925</i>	0.03	46.27	<i>fs(1)Yb</i>	6.64	21.79
<i>squ</i>	0	0			
<i>cuff</i>	0	0			

Figure 15. mRNA expression of piRNA factors in Δmbt-OSC. (upper) Scatter plot comparing transcript abundance (mRNA-seq) of small RNA biogenesis genes in OSCs and Δmbt-OSCs. Classification of the factors to four clades, Germ specific, Germ + Soma, Soma specific, and RNAi/miRNA was carried out with reference to Handler et al. (Handler et al. 2013). (lower) Transcript abundance of small RNA biogenesis factors (germ specific, germ + soma, and soma specific) (Handler et al. 2013) in OSCs and Δmbt-OSCs counted by mRNA-seq. FPKM: Fragments per kilobase of exon per million mapped sequence reads.

Figure 16

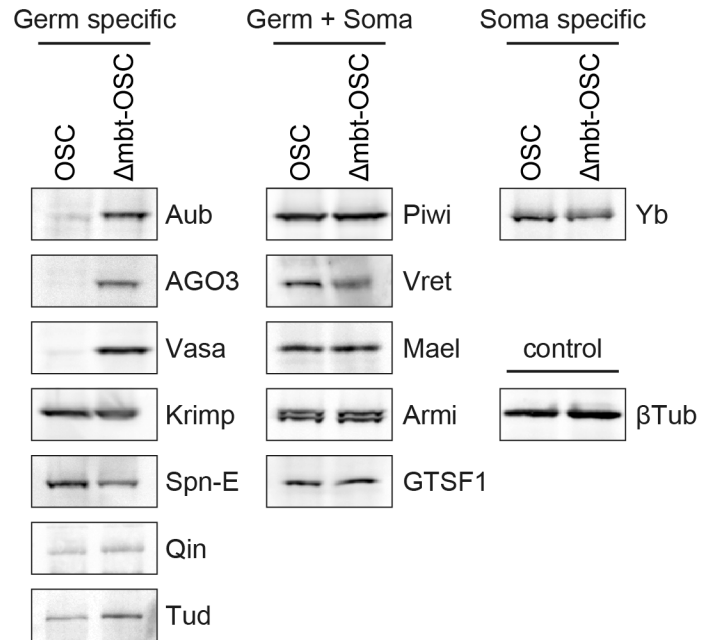


Figure 16. Protein expression of piRNA factors in Δ mbt-OSC. Western blotting shows protein expression of piRNA factors in OSCs and Δ mbt-OSCs. β Tubulin (β Tub) was detected as a loading control.

Figure 17

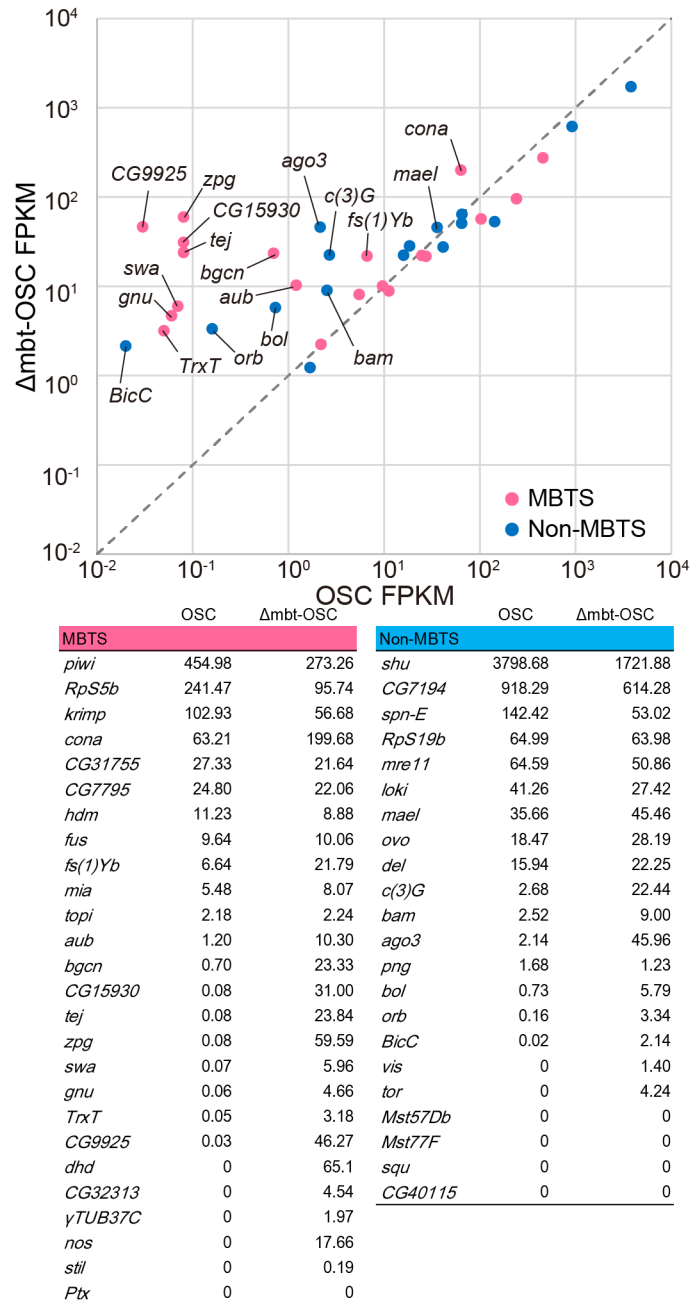


Figure 17. mRNA expression of MBTS in Δ mbt-OSC. (upper) Scatter plot comparing transcript abundance (mRNA-seq) of MBTS and non-MBTS genes in OSCs and Δ mbt-OSCs. Classification of MBTS and non-MBTS genes was carried out with reference to Janic et al. (Janic et al. 2010). (lower) Transcript abundance of MBTS and non-MBTS genes in OSCs and Δ mbt-OSCs counted by mRNA-seq. FPKM: fragments per kilobase of exon per million mapped sequence reads.

Figure 18

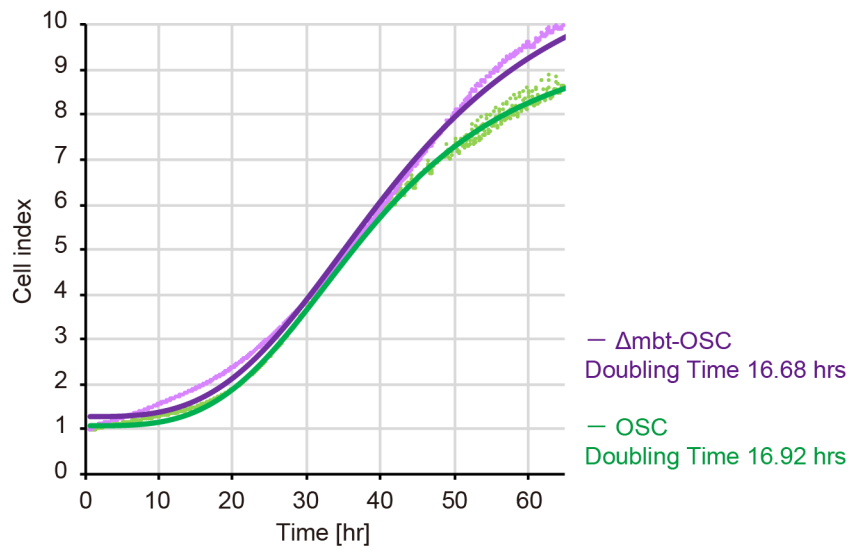


Figure 18. Real-time monitoring of cell proliferation speed. Cell-sensor impedance was expressed as an arbitrary unit called the Cell index. The Cell index values were plotted against time.

Figure 19

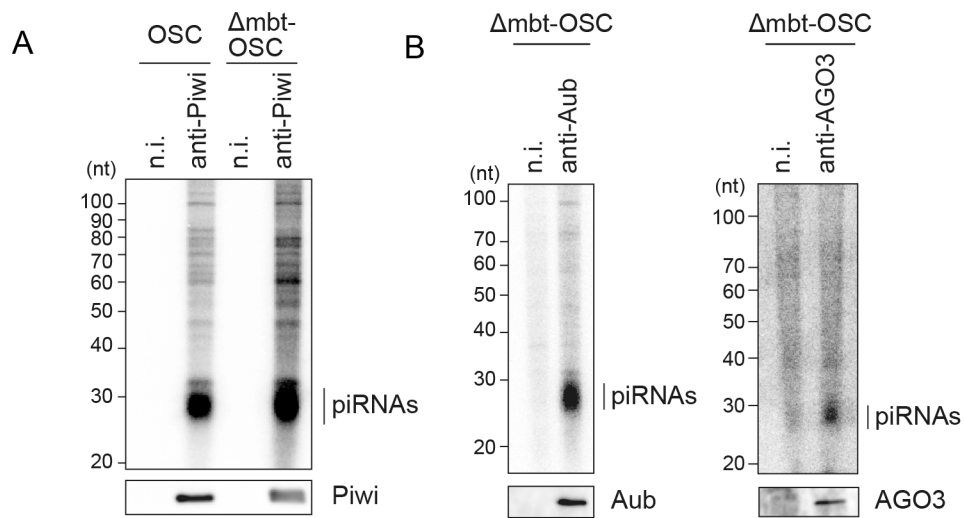


Figure 19. PIWI proteins bound piRNAs. (A) 32P-labeled piRNAs (upper panel) associated with Piwi (lower panel) in OSCs and Δ mbt-OSCs. (B) 32P-labeled piRNAs (upper panel) associated with Aub and AGO3 (lower panel) in Δ mbt-OSCs. n.i., nonimmune IgG.

Figure 20

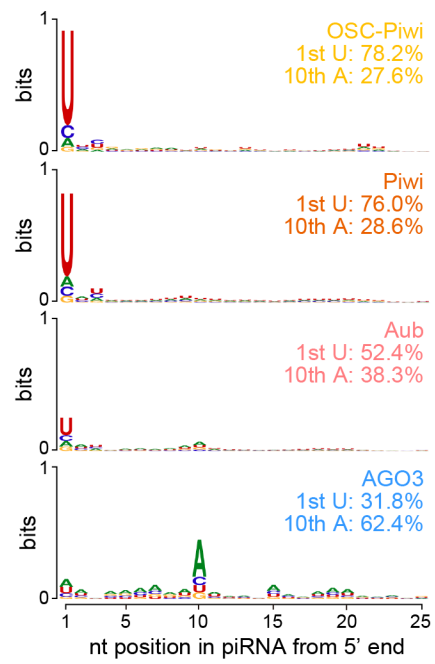


Figure 20. Sequence logos of Piwi/Aub/AGO3-bound piRNAs in Δ mbt-OSCs and Piwi-bound piRNAs (top: OSC-Piwi) in OSCs (Ishizu et al. 2015) mapped to transposons.

Figure 21

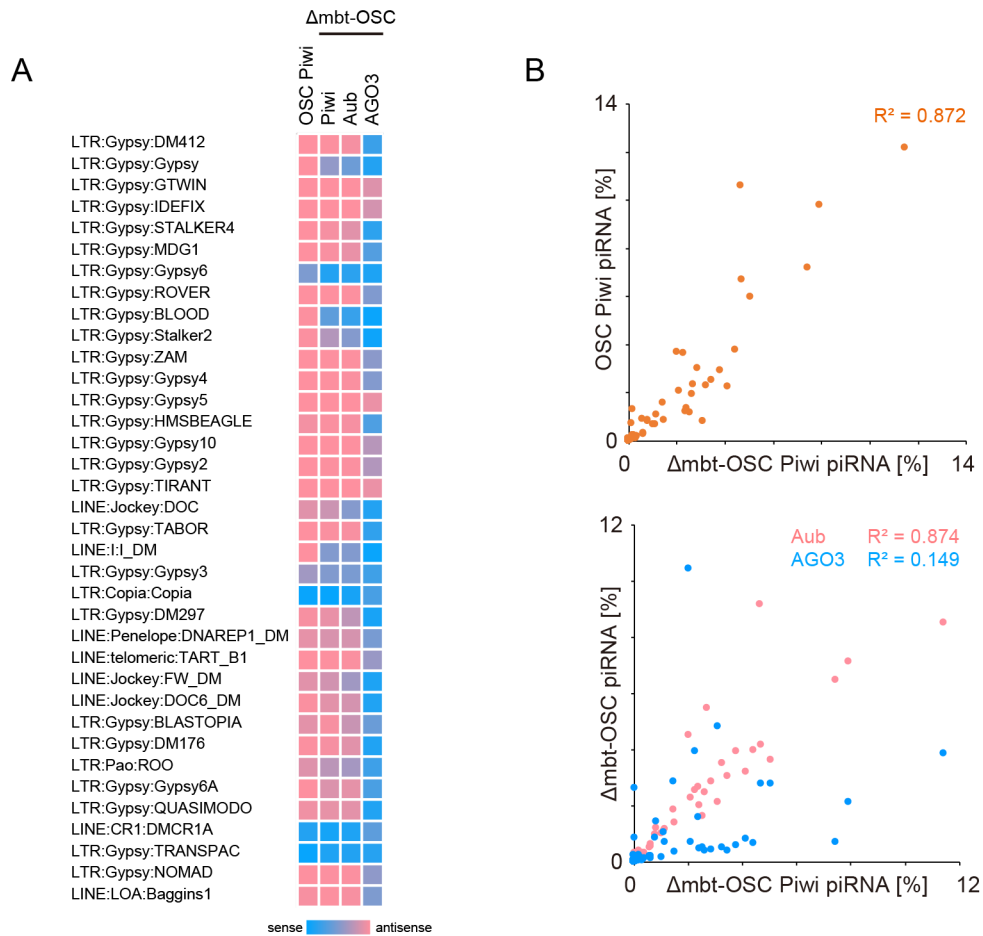


Figure 21 piRNAs for transposon in $\Delta mbt\text{-OSC}$. (A) Heatmaps of piRNA strand bias. Strand bias of transposon-derived piRNAs in Piwi/Aub/AGO3 bound RNA libraries from $\Delta mbt\text{-OSC}$ s is shown. Strand bias of Piwi-bound piRNAs in OSCs (Ishizu et al. 2015) is also shown. (B) (upper) Scatter plot showing correlation of antisense Piwi-bound piRNA reads in OSCs (%) (y axis) with those in $\Delta mbt\text{-OSC}$ s (%) (x axis). (lower) Correlation of antisense Aub- (pink dots) and antisense AGO3- (blue dots) bound piRNA reads in $\Delta mbt\text{-OSC}$ s (%) (y axis) with antisense Piwi-bound piRNA reads in $\Delta mbt\text{-OSC}$ s (%) (x axis) is also shown. Each dot corresponds to the ratio of piRNAs mapped to transposons (A).

Figure 22

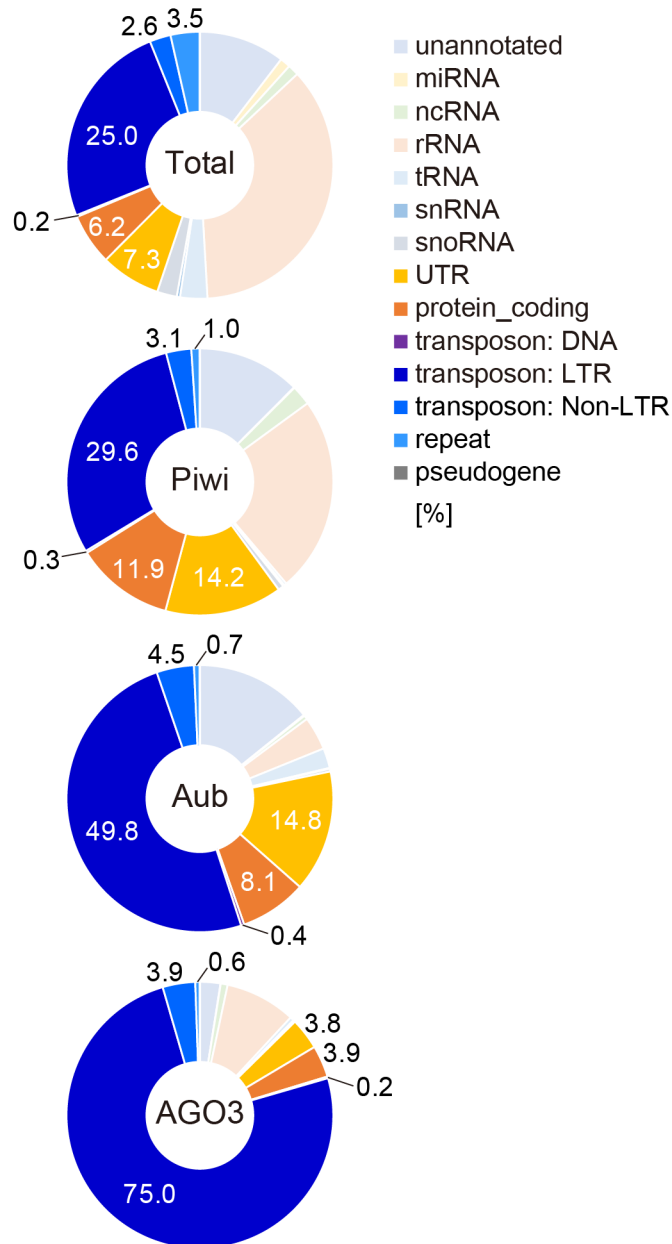


Figure 22. Pie charts summarizing the annotation of small RNA populations in total small RNAs, and Piwi/Aub/Ago3-bound piRNAs.

Figure 23

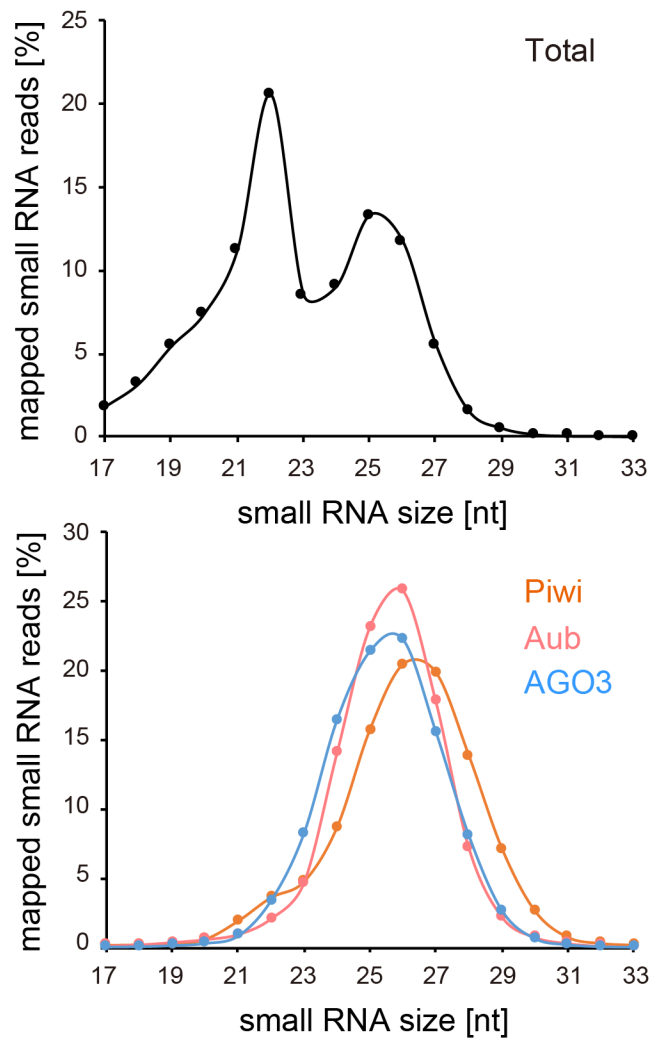


Figure 23. Small RNA size profiles for total small RNAs, and Piwi/Aub/Ago3-bound piRNAs. Sequences corresponding to rRNA, tRNA, snRNA, and snoRNA were omitted before analysis.

Figure 24

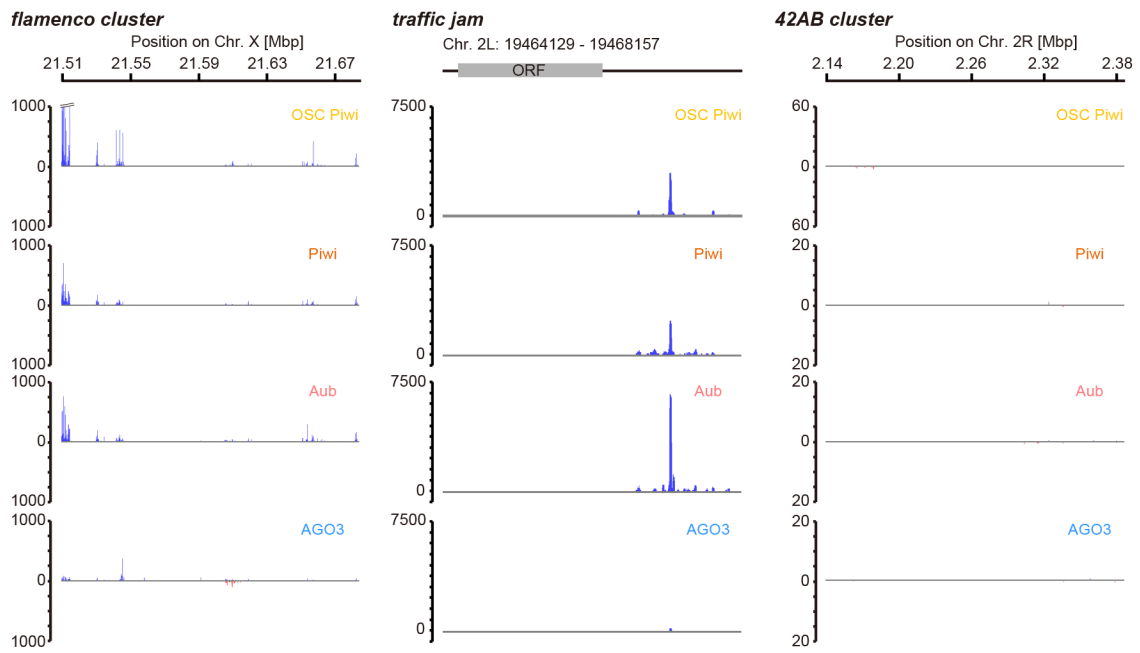


Figure 24. Mapping of Piwi/Aub/AGO3-bound piRNAs in Δ mbt-OSCs and Piwi-bound piRNAs in OSCs (Ishizu et al. 2015) to *flam*, *tj*, and *42AB*.

Figure 25

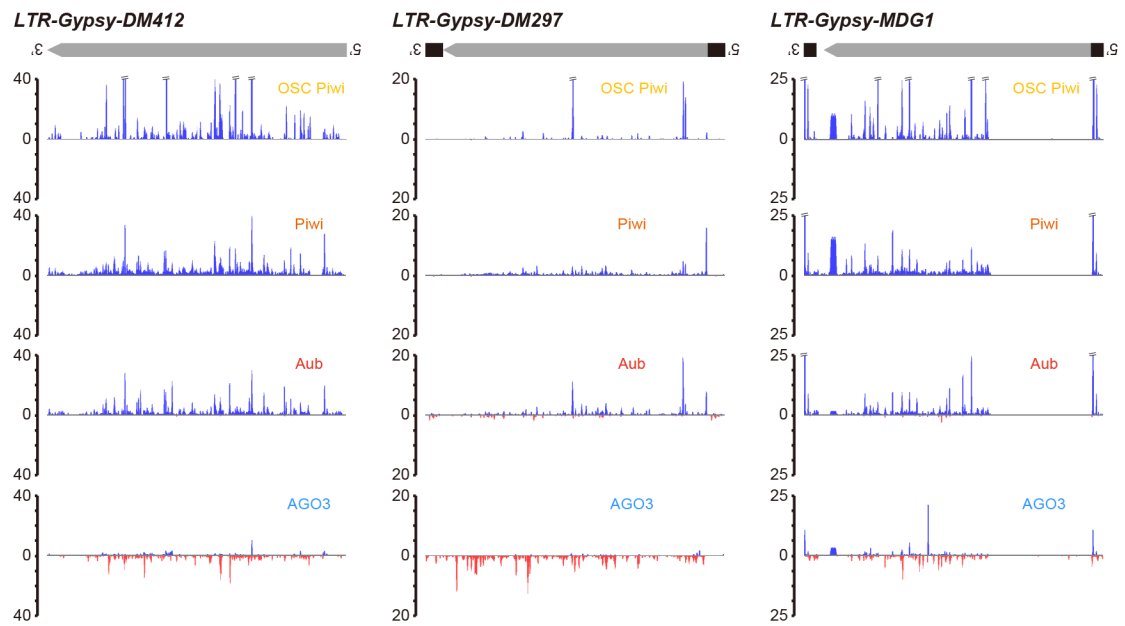


Figure 25. Mapping of Piwi/Aub/Ago3-bound piRNAs in Δ mbt-OSCs and Piwi-bound piRNAs in OSCs (Ishizu et al. 2015) to *DM412*, *DM297*, and *mdg1* transposons.

Figure 26

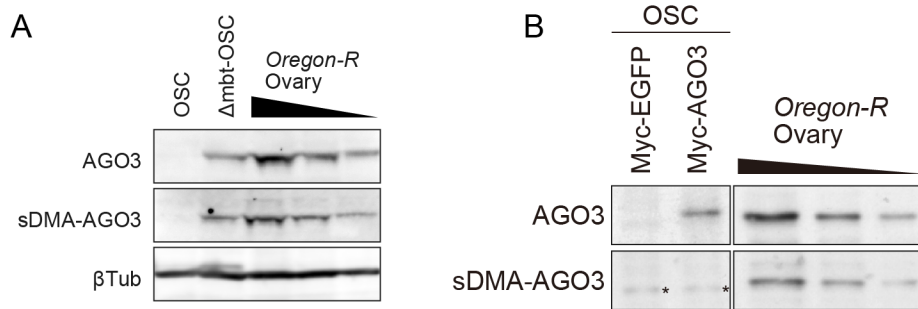


Figure 26. sDMA modification in Δ mbt-OSC. (A) Western blotting shows that AGO3 in Δ mbt-OSCs is symmetrical dimethylated, as in ovaries. (B) Myc-AGO3 overexpressed in OSCs by transfection is sDMA free. Asterisks indicate background signals.

Figure 27

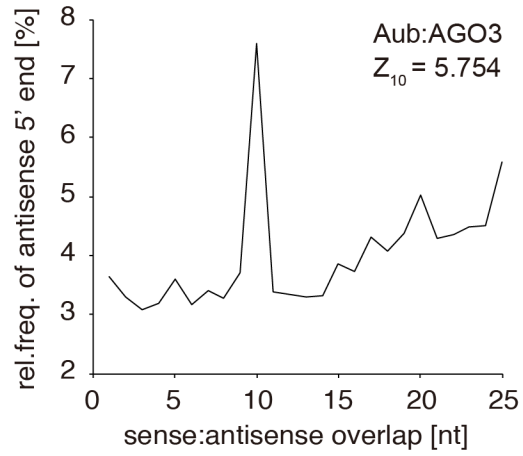


Figure 27. Depiction of the ping-pong signature between antisense Aub-bound piRNAs and sense AGO3-bound piRNAs defined as the value at position 10 nt. Graphs indicate the relative frequency that a complementary piRNA exists with a 5' end (y axis) at the indicated distance (x axis).

Figure 28

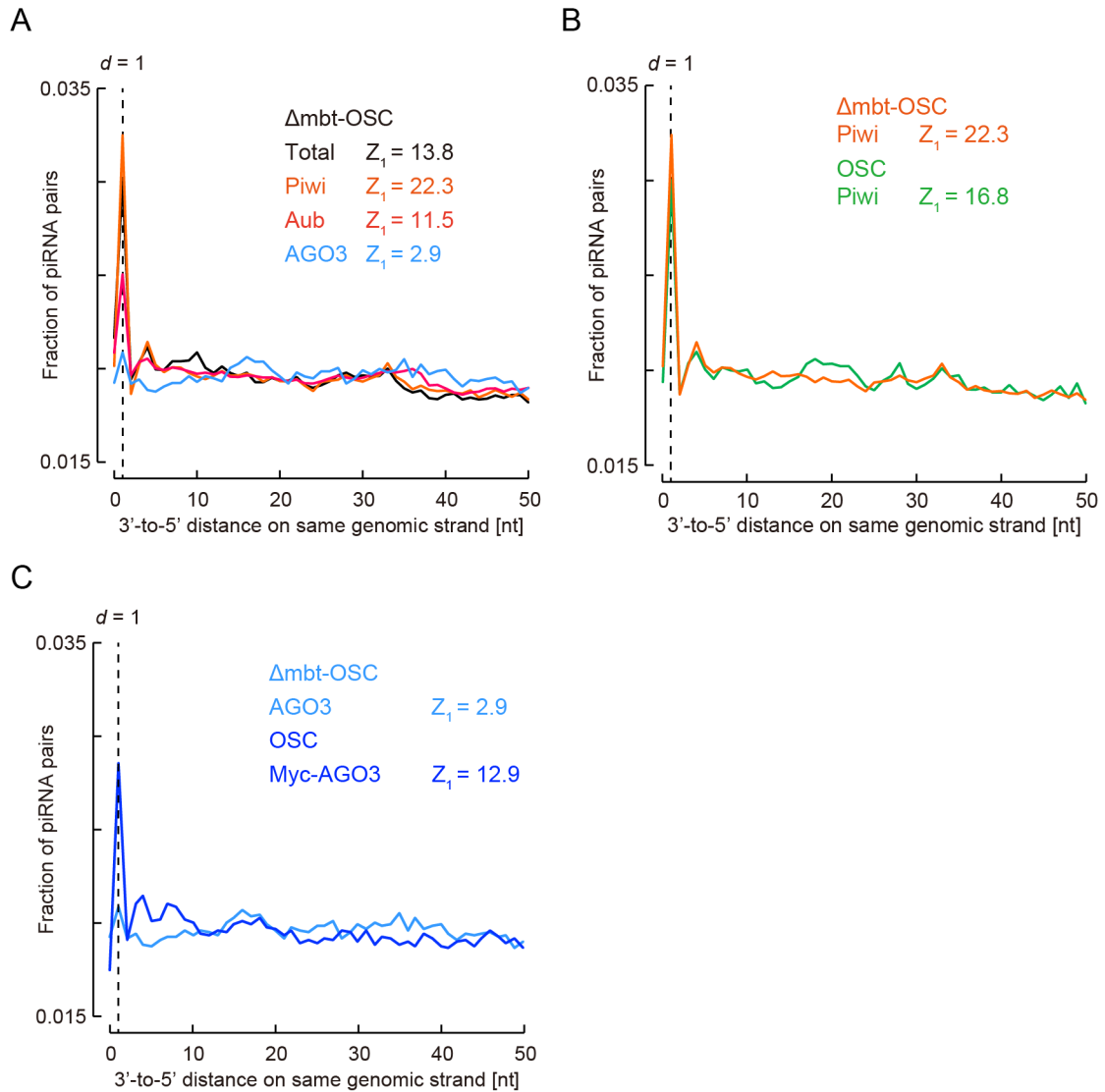


Figure 28. Characterization of phased piRNAs in Δ mbt-OSCs. (A) Analyses of phased piRNAs in total small RNAs, and Piwi/Aub/AGO3-bound piRNAs in Δ mbt-OSCs. The distance between the 3' end of the upstream piRNA and the 5' end of downstream piRNAs on the same genomic strand was analyzed. (B) Comparison of phased piRNAs in Piwi-bound piRNAs in OSCs (Ishizu et al. 2015) and Δ mbt-OSCs. (C) Analyses of phased piRNAs in AGO3-bound piRNAs in Δ mbt-OSCs and Myc-AGO3-bound piRNAs in OSCs (Sato et al. 2015).

Figure 29

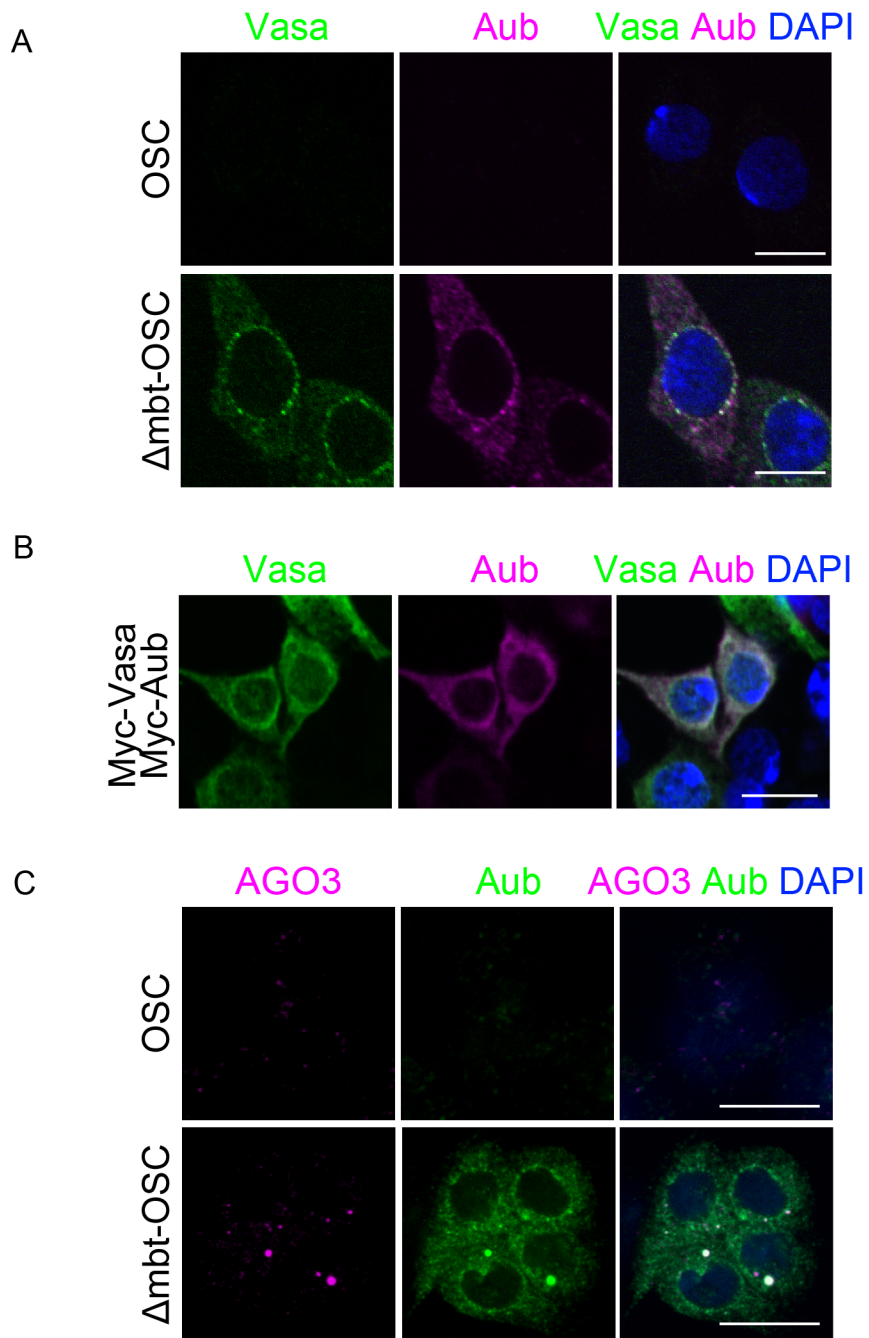


Figure 29. Nuage-like granules in Δ mbt-OSCs. (A) Immunostaining shows that Aub and Vasa coincide at nuage-like granules in Δ mbt-OSCs. (B) Co-expression of Myc-Aub with Myc-Vasa exogenously in OSCs by transfection. Immunostaining was performed using anti-Vasa and anti-Aub antibodies. (C) AGO3 colocalizes with Aub in Δ mbt-OSCs at nuage-like granules. Scale bars indicate 10 μ m.

Figure 30

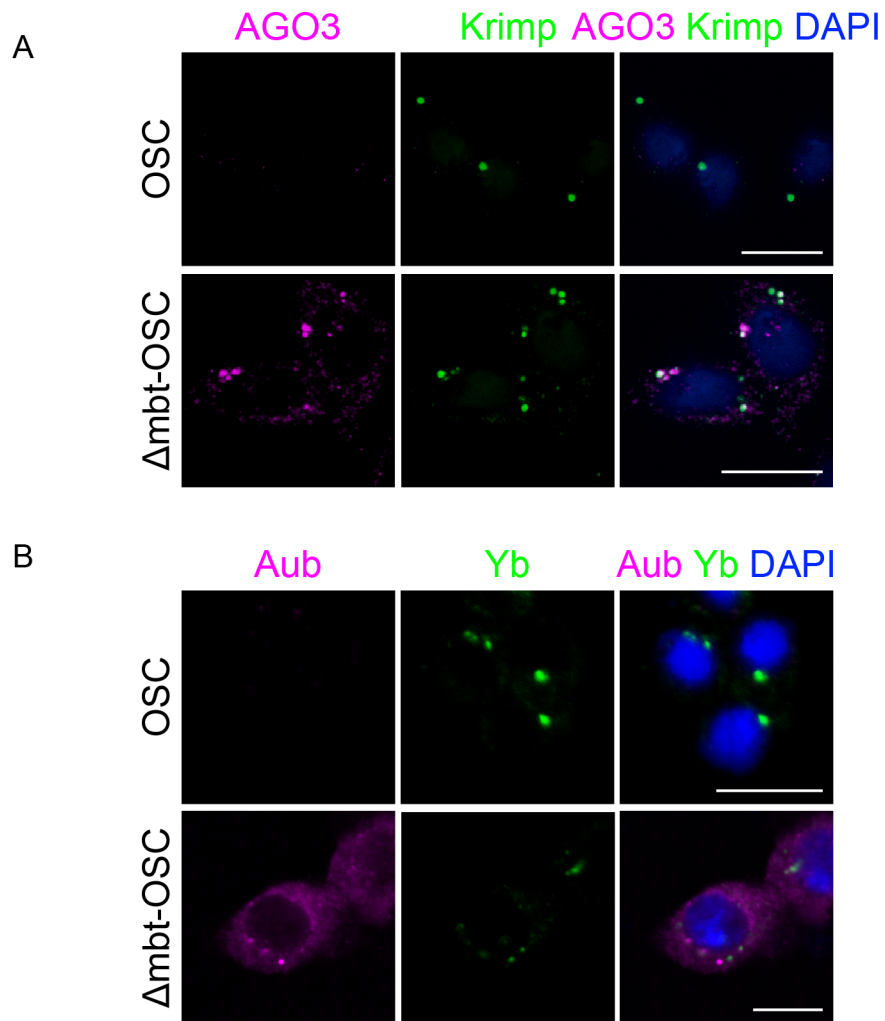


Figure 30. Nuage-like granules in Δ mbt-OSCs. (A) AGO3 partially colocalizes with Krimp in Δ mbt-OSCs at nuage-like granules. (B) Aub and Yb only occasionally coincide in Δ mbt-OSCs at granules. Scale bars indicate 10 μ m.

Figure 31

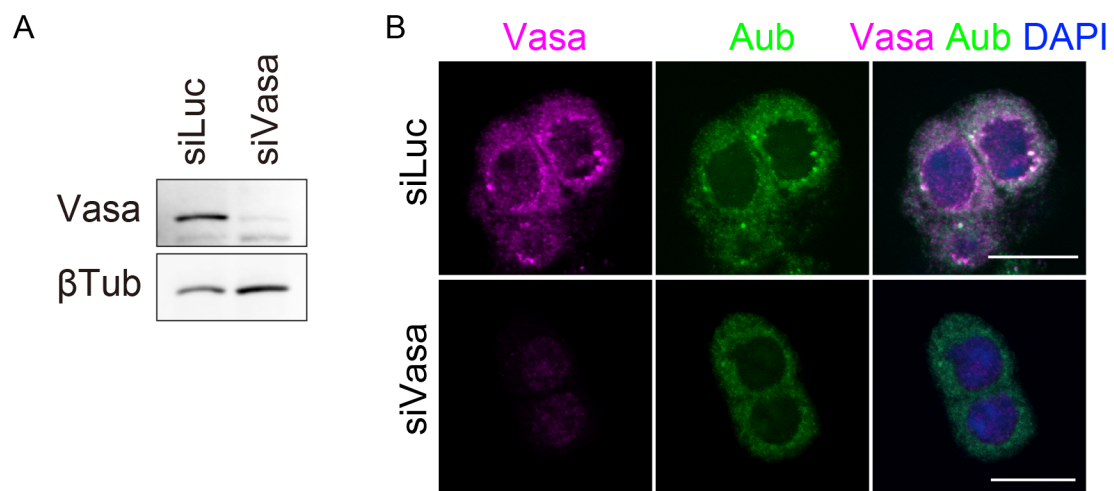


Figure 31. Localization effect of Vasa depletion in Δ mbt-OSCs. (A) RNAi efficiently reduced the amount of Vasa in Δ mbt-OSCs. siLuc was used as a negative control. (B) Depletion of Vasa in Δ mbt-OSCs caused Aub to be scattered in the cytoplasm in Δ mbt-OSCs. Scale bars indicate 10 μ m.

Figure 32

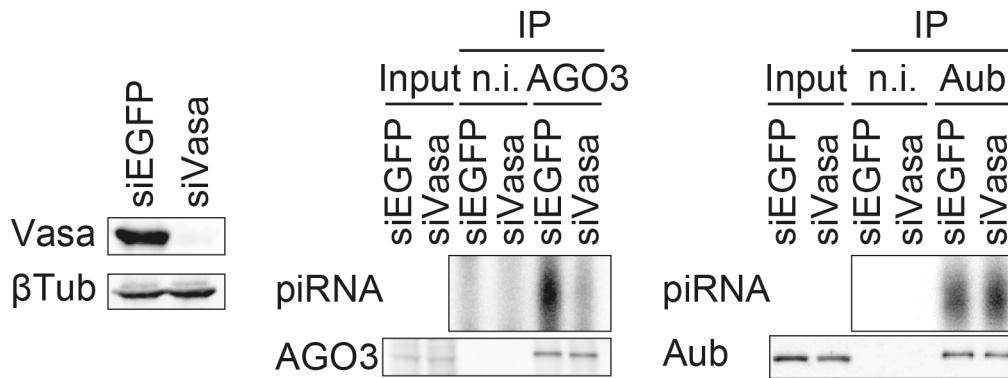


Figure 32. piRNA biogenesis effect of Vasa depletion in Δ mbt-OSCs. AGO3, but not Aub, associates with fewer secondary piRNAs in Δ mbt-OSCs upon Vasa depletion. siEGFP was used as a negative control. n.i., nonimmune IgG.

Figure 33

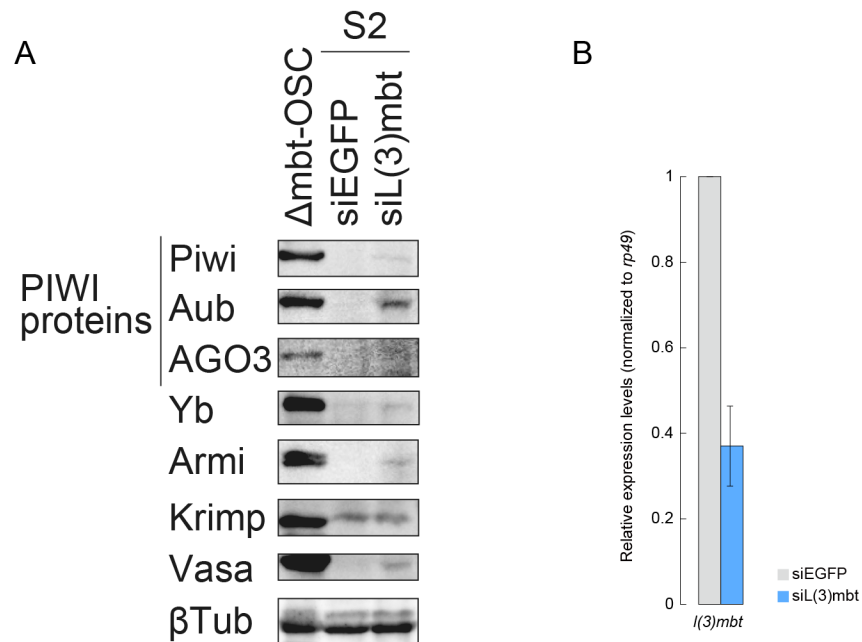


Figure 33. Expression levels of piRNA factors in S2 cells upon *l(3)mbt* depletion by RNAi. (A) Western blotting showed some factors up-regulation (B) qRT-PCR shows that RNAi treatment repressed *l(3)mbt* expression in S2 cells. *rp49* was used as an internal control. N = 2; error bars indicate SEM. dsEGFP (siEGFP) was used as a negative control.

Figure 34

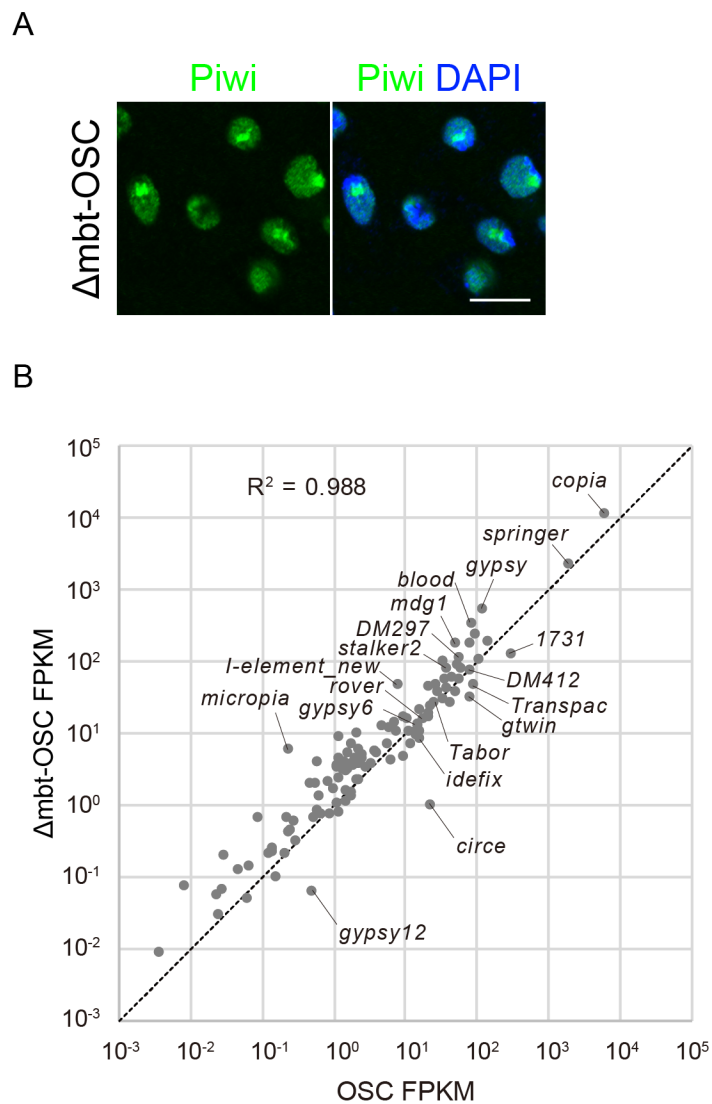


Figure 34. Piwi maintains its transposon silencing functions in Δ mbt-OSCs. (A) Immunofluorescence reveals that Piwi is localized in the nucleus of Δ mbt-OSCs. Scale bar indicates 10 μ m. (B) Scatter plot comparing transcript abundance (mRNA-seq) of transposons in OSCs and Δ mbt-OSCs.

Figure 35

第2章

本章については5年以内に雑誌等で刊行予定のため
非公開

Figure 36

第2章

本章については5年以内に雑誌等で刊行予定のため
非公開

Figure 37

第2章

本章については5年以内に雑誌等で刊行予定のため
非公開

Figure 38

第2章

本章については5年以内に雑誌等で刊行予定のため
非公開

Figure 39

第2章

本章については5年以内に雑誌等で刊行予定のため
非公開

Figure 40

第2章

本章については5年以内に雑誌等で刊行予定のため
非公開

Figure 41

第2章

本章については5年以内に雑誌等で刊行予定のため
非公開

Figure 42

第2章

本章については5年以内に雑誌等で刊行予定のため
非公開

Figure 43

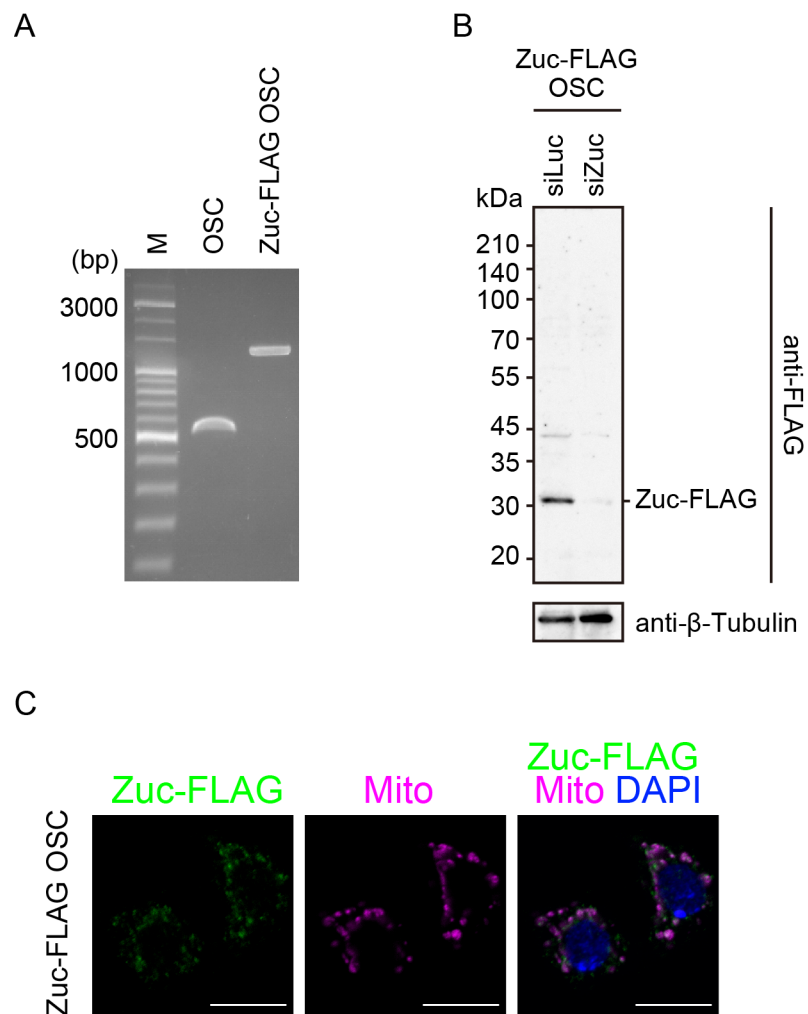


Figure 43. Zuc detectable OSC was established. (A) Genomic PCR fragments amplified with a primer set flanking of sgRNA target. (B) Western blot analysis of Zuc-FLAG OSC with anti-FLAG and anti- β -Tubulin after transfection with siRNA targeting luciferase or zuc. Correct integration of FLAG tag was confirmed by significant reduction of signal after zuc knockdown. (C) Localization of Zuc in Zuc-FLAG OSC. Scale bars indicate 10 μ m.

Figure 44

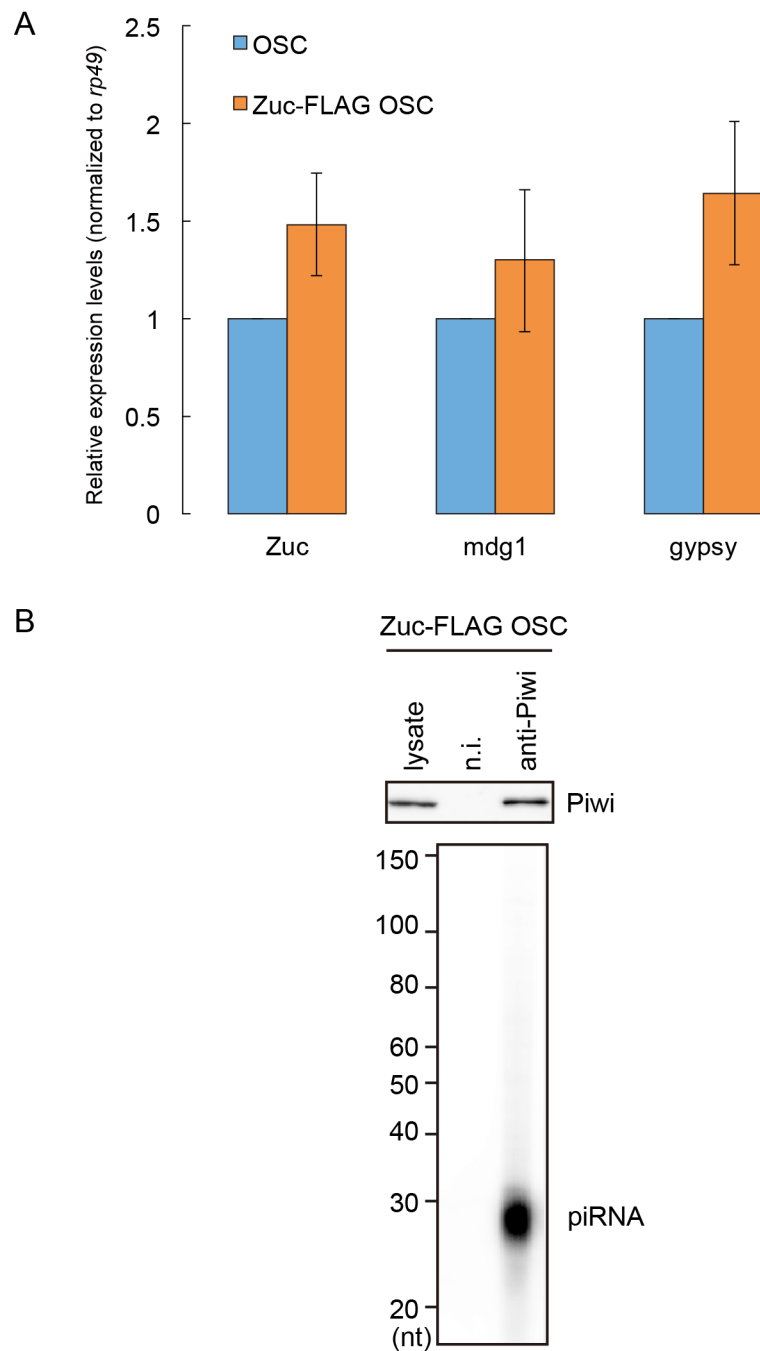


Figure 44. Effect of FLAG insertion to *zuc* locus. (A) *Zuc* and transposon expression analysis by RT-qPCR. These expression levels were unchanged. *rp49* was used as an internal control. N = 3; error bars indicate SEM. (B) Piwi binds mature piRNA in *Zuc*-FLAG OSC. n.i., nonimmune IgG.

Figure 45

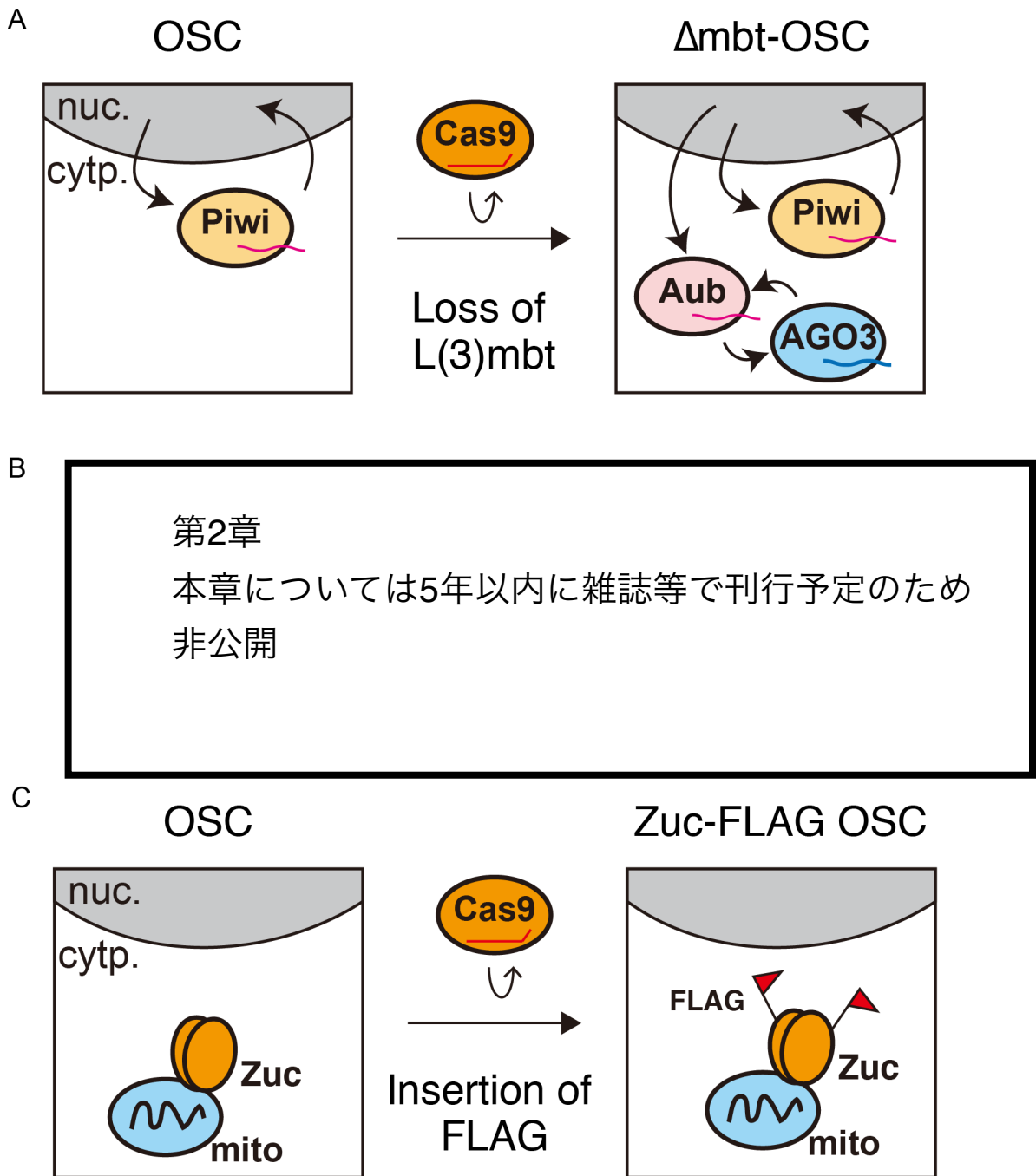


Figure 45. The new cell lines are established. (A) Establishment of Δ mbt-OSC. (B) The model of Vasa activity in the ping-pong pathway. (C) Establishment of Zuc-FLAG OSC.

Tables

Table 1

Table 1. List of primers and siRNAs. RNA is shown in *italics*.

Experiment	Sequence	Description	
Cas9 vector	TCTAGAGATCTCCATCCTACC	inverse PCR forward primer	
	CTTTTTCTTTTTGCCTGGCC	inverse PCR reverse primer	
	<i>GGCGGCCACGAAAAAGGCCGGCCAGG CAAAAAGAAAAGAAAGGACGGGGAT CGTTGCTCAATGCGCCGATGTGAGG AGAATCCCGGACCTATGCGCAAGCCTT TGCTCAAGAAATCCACCCCTCATTGA AAGAGCAACGGCTACAATCAACAGCAT CCCCATCTGAAAGACTACAGGTGGC CAGCGCAGCTCTCTAGCAGCGGCC GCATCTCACTGGTGTCAATGTATATCAT TTTTACTGGGGACCTTGGCGAGAACTC GTGGTGTGGCACTGCTGCTGCTGCG GGCAGCTGGCAACCTGACTTGTATCGT CGCGATCGGAATGAGAAGAGGGGCAT CTTGAAGCCCTGGGACGGTGGCGGAC AGGTTCTTCTGATCTGATCCTGGGAT CAAAGCCATAGTGAAGGACAGTGAAG ACAGCCGACGGCAGTTGGGATTCGTGA ATTGCTGCCCTCTGTTTATGTGGGA GGGCTAATAGAGATCTCCATACCTA CCAGTTCTGCGCTGCGACG</i>	<i>gBlock, TZA:Blasticidin resistance gene</i>	
	CAGCTGACCCGTTTAGAGCTAGAAATA GC	L(3)mbt sgRNA E2 forward primer	
	AAACCGGTAAACAGTATTGAGG	L(3)mbt sgRNA E2 reverse primer	
	AGCCCTATTTGTTTAGAGCTAGAAATA GC	L(3)mbt sgRNA GM76 forward primer	
	CCAACCTGAAGCAGTATTGAGG	L(3)mbt sgRNA GM76 reverse primer	
	CTTGGAGCTGGATTTGGCTCCCGCT	Zuc sense for Zuc knockin	
	AAACAGGGGAGCCAAATCCAGCTC	sgRNA antisense for Zuc knockin	
	TTTTGGCGGATCAATAAAGC	Zuc forward primer	
GGCACTCCTTTGTGTGTGA	Zuc reverse primer		
TACGACTCTGGGTGAACGC	l(3)mbt forward primer		
GACATCCCTCCACATCGCA	l(3)mbt reverse primer		
pAcM-EGFP vector	GGGCCCTTGAAGGTAAGCC	pAcE-F	
	GGTACCAAGCTCTTGTACAGCTC	pAcE-R	
EGFP-Vasa	<i>GACGAGCTGTACAAGAGCTTGGTACC ATGCTCGACGACTGGGATGATGA ACCTTCCAAAGGCGCTTAATCCATTGC TCTCTTCTCCGACATTGGTG</i>	EGFP-Vasa-F EGFP-Vasa-R	
	CAGGCCGATCGATGCTAGTA	inverse PCR forward primer for E400Q Vasa	
E400Q Vasa inverted PCR	ATCCAGCACACGAATCGAGTGT	inverse PCR reverse primer for E400Q Vasa	
	GCCGAGCAGGCTTGC	inverse PCR forward primer for R528A Vasa	
R528A Vasa inverted PCR	TTGACTGTGAGACGATCGCC	inverse PCR reverse primer for R528A Vasa	
	<i>TACAAGAAGCTTGGTACCATGATACCC CTAATCATTTCAAAGAATTCCT TCTTACCTTCCAAAGGCGCTTAATCCATTGC AATATTGAAATGTTGGCCACA TGATATTGATACAAGAAGCATGACGATA AGAACAAGCTTGGTACCGAAT TGAATCTGTAGCTTCCGCTGCTGCTCCT TATAGCTTCCCATGGTGGCTAG</i>	EGFP-CG7194-F EGFP-CG7194-R	
pAcF inverted PCR	<i>CGCTCGAGTCTAGAGGGCCCATTTTA CAACCGAAAAGAAGTGG GGGTTACTCTGAAAGGGCCCTTATGAS CTCGCTGCTCC</i>	pAcF-F pAcF-R	
	CGCTCGAGTCTAGAGGGCCCATTTTA CAACCGAAAAGAAGTGG GGGTTACTCTGAAAGGGCCCTTATGAS CTCGCTGCTCC	Nup358-F Nup358-R	
qRT-PCR	AGCCGCTCAACGATGCA	vasa forward primer	
	AACATCGCTGCCGTCA	vasa reverse primer	
	CTGCAATTTGGCCTCCATA	ago3 forward primer	
	GGGGAGTTGCAATCCTTT	ago3 reverse primer	
	CAAGGCCGATAATTGGACA	<i>piwi</i> forward primer	
	CCATCGCTGGAGTGGTAAG	<i>piwi</i> reverse primer	
	GCCCCGAGAATATCAGACG	l(3)mbt forward primer	
	AGGAGACGCTTTTCGCTTGG	l(3)mbt reverse primer	
	HDR vector	TAAAGCGCTAGAGAAAACG	5' homology arm, genome PCR forward primer
		CTTGAGCTGGATTTGGCTCC	5' homology arm, genome PCR reverse primer
AAATCAATTGATTAATGATGACT		3' homology arm, genome PCR forward primer	
TTTTGTTTTGCCATTCACCA		3' homology arm, genome PCR reverse primer	
<i>TAACGACGGCCAGTGAAATTCGAGCTCG GTACCCGGGATCAAAGCGCGCTAGA GAAACG</i>		5' homology arm, 2nd PCR forward primer with homologous overlap region	
<i>TGTCATGATCTTATAATCACCCTCATGG TCTTTGTAGTCTTGGAGCTGGATTTGGC TCC</i>		5' homology arm, 2nd PCR reverse primer with homologous overlap region	
<i>CGCCGCGGGATCACTTCGGGATGGA CGAGCTGACTAGAAATCAATTGATTA TGTATGACT</i>		3' homology arm, 2nd PCR forward primer with homologous overlap region	
<i>ACCCCAAGCTTGCATGCCTGAGGCTCG ACTCTAGAGGATCTTTGTTTTGCCATT CACC</i>		3' homology arm, 2nd PCR reverse primer with homologous overlap region	
<i>TCGTACAAACCATGACGGTATATA AAGATCATGACATGATTACAAAGATGA CGATGACAAGGAAGCGGGATCGTT GCTCAGATCGCGGATGTGAGGAGAA TCCCGGACCTGTGAGCAAGCGCGAG AGCTGTTACCCGGGGTGGCCCATCC TGCTGAGCTGACGGCGGAGCAATAAC GGCCACAGTTCAGGGTCTCCGGCGA GGCAACTGAAAGCGGCGCTACGCGA AGCTGACCCCTGAAGTTCATCTGCCA CCGGCAAGCTGCCCTGCCCTGGCCC ACCTCTGTACCACCCCTGACCTACGGC GTCCAGTGTTCACCGCTACCCAGGAC CACATGAAGCAGCAGCCTTCTTCAAG TCCGCCATCCCGAAGGCTACGCTCAG GAGCGACCATCTTCTTCAAGGACGAG GGCAACTGAAAGCGGCGCTACGCGA GAAGTTCGAGGGGACACCCCTGGTA ACCGCATCGAGCTGAAGGGCATCGACT TCAAGGAGGACCGCAACATCCTGGGG CAACAAGTGAAGTGAACATCAAGAGC CAACAAGCTTATATGCGCGACAGC AGAAGAAGCGCATCAAGGTGAATCTCA AGATCCCGCACACATCGAGGACCGCA GGTGTGAGCTGCGGACACATCGAGG CAGAAACCCCATCGGCGACCGCCC CGTGTGCTGCCCGCAACCACTCCT GAGCACCAAGTCCGCTGAGCAAG ACCCCAAGCAGAAAGCGGATCAACATG TCTGCTGGAGTCTGTGACCCGCGCC GGGATCACTCTCGCATGACGAGCTG TAGTAG</i>		<i>gBlock, 3xFLAG:TZA-EGFP</i>	
GGAGGGGAGCCAAATCCAGCT		PAM silent mutation, inverse PCR forward primer	
GTCTTCGAAAAGCCCGCA	PAM silent mutation, inverse PCR reverse primer		
RNAi	<i>GGCAAGCUGACCCUGAAGU</i>	siRNA sense for EGFP	
	<i>TUUAUCAGGGUACGCUUGCCT</i>	siRNA antisense for EGFP	
	<i>CCUCUGGAGAUUGCCGUAATT</i>	siRNA sense for L(3)mbt-1	
	<i>UUACGGACAUCUCAGAGGTT</i>	siRNA antisense for L(3)mbt-1	
	<i>CCACCUGGUGUAAGGAAAT</i>	siRNA sense for L(3)mbt-2	
	<i>UUUCUUGACACCAGGUGTT</i>	siRNA antisense for L(3)mbt-2	
	<i>CGUACGCGAAUUCUGGATT</i>	siRNA sense for Luc	
	<i>UCGAAGUAUUCGGUACGTT</i>	siRNA antisense for Luc	
	<i>GCAUUGCCGUCAGCUGUTT</i>	siRNA sense for Vasa	
	<i>AACUUCGUUUGUCUGCTT</i>	siRNA antisense for Vasa	
<i>GCCAGUCAUUGGACAACTT</i>	siRNA sense for Ku70		
<i>UGUUGCCAUGCAGUGGCTT</i>	siRNA antisense for Ku70		
<i>UGUCUGAGCAUACAAGCTT</i>	siRNA sense for CG7194		
<i>GCUUUGUAUUGCUCAGACTT</i>	siRNA antisense for CG7194		
<i>GCAUUGCCGUCAGCUGUTT</i>	siRNA sense for Zuc		
<i>ACAGUCGUCAGCCGUAUGCTT</i>	siRNA antisense for Zuc		
RNAi in S2	<i>TAATACGACTCACTATAGGGAGAGGTTC GAGCTGATGAG</i>	dsRNA against l(3)mbt forward primer	
	<i>TAATACGACTCACTATAGGGAGAGATCT CGAAGCAGTTGG</i>	dsRNA against l(3)mbt reverse primer	

Table 2

Table 2. List of Gene Ontology terms of the biological process category associated with differentially expressed genes in OSCs and Δ mbt-OSCs.

OSC < Δ mbt-OSC

Term	PValue
GO:0055114~oxidation reduction	1.41E-04
GO:0007155~cell adhesion	0.004
GO:0045727~positive regulation of translation	0.006
GO:0006026~aminoglycan catabolic process	0.008
GO:0022610~biological adhesion	0.009
GO:0046012~positive regulation of oskar mRNA translation	0.009
GO:0000272~polysaccharide catabolic process	0.010
GO:0006928~cell motion	0.011
GO:0042461~photoreceptor cell development	0.013
GO:0060429~epithelium development	0.014
GO:0009792~embryonic development ending in birth or egg hatching	0.019
GO:0007398~ectoderm development	0.019
GO:0042462~eye photoreceptor cell development	0.021
GO:0048729~tissue morphogenesis	0.022
GO:0010648~negative regulation of cell communication	0.023
GO:0007422~peripheral nervous system development	0.025
GO:0001700~embryonic development via the syncytial blastoderm	0.026
GO:0007354~zygotic determination of anterior/posterior axis, embryo	0.028
GO:0034329~cell junction assembly	0.031
GO:0046530~photoreceptor cell differentiation	0.034
GO:0007127~meiosis I	0.034
GO:0006032~chitin catabolic process	0.034
GO:0032270~positive regulation of cellular protein metabolic process	0.034
GO:0051247~positive regulation of protein metabolic process	0.034
GO:0042067~establishment of ommatidial polarity	0.037
GO:0007164~establishment of tissue polarity	0.038
GO:0002009~morphogenesis of an epithelium	0.038
GO:0007561~imaginal disc eversion	0.039
GO:0048598~embryonic morphogenesis	0.039
GO:0009952~anterior/posterior pattern formation	0.042
GO:0008544~epidermis development	0.043
GO:0001754~eye photoreceptor cell differentiation	0.044
GO:0030178~negative regulation of Wnt receptor signaling pathway	0.045
GO:0001745~compound eye morphogenesis	0.045
GO:0009880~embryonic pattern specification	0.046
GO:0048610~reproductive cellular process	0.047
GO:0007411~axon guidance	0.048
GO:0016477~cell migration	0.050
GO:0048134~germ-line cyst formation	0.050

OSC > Δ mbt-OSC

Term	PValue
GO:0000022~mitotic spindle elongation	0.010
GO:0051231~spindle elongation	0.011
GO:0006412~translation	0.015
GO:0007052~mitotic spindle organization	0.017
GO:0007051~spindle organization	0.038
GO:0000278~mitotic cell cycle	0.041
GO:0006350~transcription	0.048
GO:0009303~rRNA transcription	0.050
GO:0008272~sulfate transport	0.050

Acknowledgement

I first would like to thank Professor Dr. Mikiko C. Siomi. Although I was Tokyo University of Science student, she kindly gave me a chance studying in her laboratory 6 years ago. Thanks to her I experience great science in the perfect study environment. Also, she planned the research and experiments and advised me. I thank also Professor Dr. Haruhiko Siomi and Assistant Professors Dr. Yuka W. Iwasaki, Dr. Hirotsugu Ishizu, Dr. Kaoru Sato, Dr. Ryo Murakami and Dr. Kazumichi M. Nishida. They always kindly advised me. Especially, Dr. Yuka W. Iwasaki, Dr. Hirotsugu Ishizu and Dr. Kaoru Sato helped my research. I would like to say greatly thank you for them. I must thank my co-workers, Hitomi Yamamoto, Shogo Kuriyama, and Yutaka Miyazaki. Without their help, my research would have not been progress. Of course, I thank my colleagues and my family.

Thank you very much.